Cell architecture and flagella of hyperthermophilic Archaea

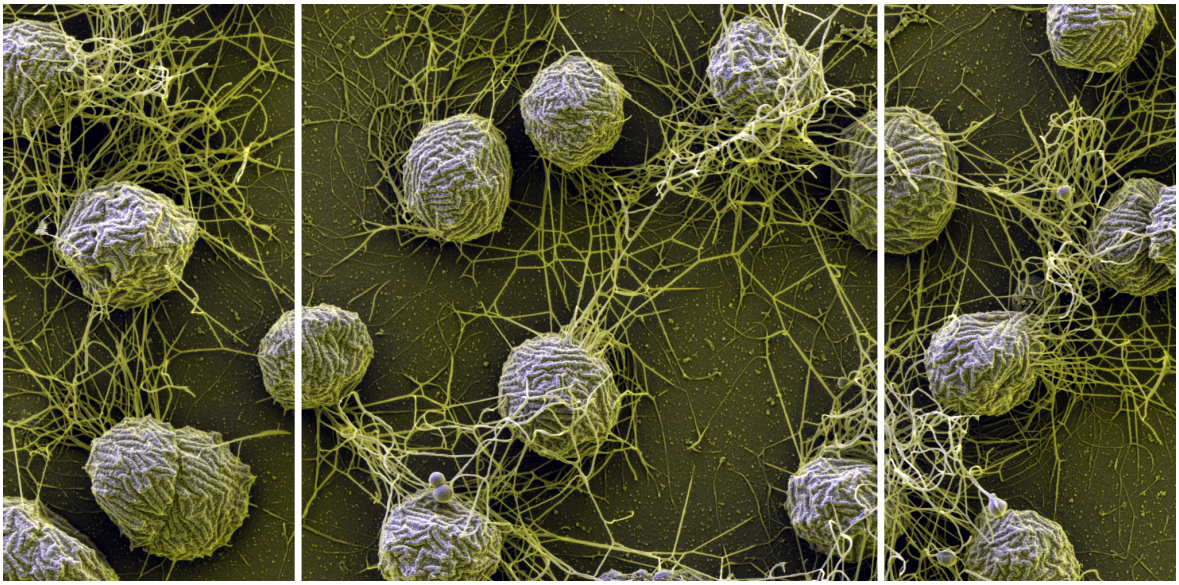

DISSERTATION

zur Erlangung des Doktorgrades der Naturwissenschaften (Dr. rer. nat.)
der Fakultät für Biologie und Vorklinische Medizin der
Universität Regensburg

vorgelegt von

Annett Bellack

aus

Wilhelm-Pieck-Stadt Guben

November 2011

Scanning electron micrograph on the cover visualizes *M. villosus* grown on glassy carbon (composite image of in-lens SE- and EsB-signals).

Image courtesy of Gerhard Wanner
LMU Munich, Germany

Das Promotionsgesuch wurde eingereicht am: 22.11.2011

Diese Arbeit wurde angeleitet von: Prof. Dr. Reinhard Wirth

Prüfungsausschuss:	Vorsitzender:	Prof. Dr. Thomas Dresselhaus
	1. Gutachter:	Prof. Dr. Reinhard Wirth
	2. Gutachter:	apl. Prof. Dr. Reinhard Rachel
	3. Prüfer:	Prof. Dr. Reinhard Sterner

Table of contents

List of figures

List of tables

Publications in peer-reviewed journals and book chapter

Bellack, A., Huber, H., Rachel, R., Wanner, G., and Wirth, R. (2011). *Methanocaldococcus villosus* sp. nov., a heavily flagellated Archaeon that adheres to surfaces and forms cell–cell contacts. *Int J Syst Evol Microbiol* **61**, 1239−1245.

Wirth, R., Bellack, A., Bertl, M., Bilek, Y., Heimerl, T., Herzog, B., Leisner, M., Probst, A., Rachel, R., and Sarbu, C., Schopf, S. and Wanner, G. (2011). The mode of cell wall growth in selected archaea follows the general mode of cell wall growth in bacteria - An analysis using fluorescent dyes. *Appl Environ Microbiol* **77**, 1556−1562.

Rachel, R., Meyer, C., Klingl, A., Gürster, S., Heimerl, T., Wasserburger, N., Burghardt, T., Küper, U., Bellack, A., and Schopf, S., Wirth, R., Huber, H. and Wanner, G. (2010). Analysis of the ultrastructure of Archaea by electron microscopy. *In* Methods in cell biology: Electron microscopy of model systems 96, ed. T. Möller-Reichert. Academic Press: New York, NY, pp. 47–69.

Müller, D.W., Meyer, C., Gürster, S., Küper, U., Huber, H., Rachel, R., Wanner, G., Wirth, R., and Bellack, A. (2009). The Iho670 fibers of *Ignicoccus hospitalis*: A new type of archaeal cell surface appendage. *J Bacteriol* **191**, 6465−6468.

1 Introduction

Over the past three decades, Archaea were scientifically accepted as third domain of life based on physiological, biochemical, sequence and whole-genome analyses. Nevertheless, their introduction by Carl R. Woese and George E. Fox (1977) was initially rigorously attacked because it violated a central dogma, the eukaryote-prokaryote dichotomy. Since the discovery of Prokaryotes 350 years ago, they have been described as a single group of microorganisms, which was classified in accordance with morphological and metabolic properties. The impact of evolution was not considered until the 1960s, when molecular criteria started to replace the old phenotypic characterization. With Sanger's radioactive oligonucleotide cataloging approach (Sanger et al., 1965), ribosomal RNA was accessible for the construction of a universal phylogenetic tree. Woese and coworkers adapted this method and, to cover the full range of microorganisms, collaborated with different experts in the field of cultivation, of which Ralph Wolfe was the most important one (Woese, 2007). His PhD student William Balch developed an efficient technique for growing methanogens in pressurized serum bottles (Balch and Wolfe, 1976) and thus, the first non-bacterial 16S rRNA oligonucleotide sequences were generated for *Methanothermobacter thermoautotrophicus* (formerly *Methanobacterium thermoautotrophicum*) in July 1976. The stunning result, an rRNA catalog that possessed neither 'prokaryotic' nor 'eukaryotic' signatures, was firstly believed to be an experimental error (Woese, 2004). However, repeating the tests and comparing them with datasets from other methanogens showed that they grouped far apart from all other sequenced organisms and the concept of three primary kingdoms – the Eubacteria, the Archaeabacteria, and the Urkaryotes – was proposed (Woese and Fox, 1977). Published in Proceedings of the National Academy of Sciences (PNAS), the publication was not widely read and not well received by the scientific community. The vehement opponents, among them the Nobel laureate Salvador E. Luria, faced Woese and also Wolfe with extreme hostility (Woese, 2004) and consequently, they did not get a chance by the scientific commuminty to present and defend the 'third form of life'. Against all odds, Woese continued his work and, rapidly, found with *Halobacterium*, *Halococcus*, *Sulfolobus*, and *Thermoplasma* other organisms that had the same new type of 16S rRNA (Woese et al., 1978). In this study, also some unique characteristics of Archaeabacteria were presented justifying the reclassification and definition of the three domain system of Archaea, Bacteria, and Eukarya (Woese et al., 1990). Even in 1998, this concept was opposed by the evolutionary biologist Ernst Mayr

who stated that the physicist Woese "quite naturally does not have an extensive familiarity with the principles of classification" (Mayr, 1998).

In contrast to this refusal, a small group of scientists supported the idea of the three-branched phylogenetic tree of life from the beginning, whereof the Germans Otto Kandler, Karl O. Stetter, and Wolfram Zillig substantially participated in its establishment. Zillig had encountered certain anomalies when analyzing DNA-dependent RNA polymerases that could be easily explained based on the new concept. The complex archaeal enzymes were shown to resemble those of the Eukaryotes and were therewith clearly distinct from the 'prokaryotic' type (Huet et al., 1983). Beside this molecular evidence, Zillig and his young colleague Stetter started in 1980 their first field trip to investigate boiling springs and mud pools of Iceland to analyze their microbial diversity (Stetter, 2006). From their anaerobic samples Stetter succeeded in isolating *Methanothermus fervidus*, which exhibited with 97°C a much higher upper temperature limit than assumed for methanogenesis (Stetter et al., 1981). Another hyperthermophilic species, *Thermoproteus tenax* was isolated from these samples (Zillig et al., 1981a), followed by the proposal of the *Thermoproteales* as new branch within the Archaeabacteria (Zillig et al., 1981b). Especially Stetter continued these microbiology field studies, confirming the new tree of life with the discovery of about 50 species mostly belonging to the Archaea (Stetter, 2006). Instead, Kandler has directly accompanied Woese since early 1977, when he was among the first scientists introduced to the three-kingdom concept before publishing, and was "the only one to understand and accept it upon first hearing" (Woese, 2007). Working on the field of (bacterial) cell walls, he detected neither glucosamine and muramic acid nor typical amino acids of peptidoglycan in *Methanosarcina barkeri* although the cells possess a thick and rigid cell wall like Gram-positive Bacteria. Hence, methanogens were proposed as divergent systematic group differing considerably from Bacteria (Kandler and Hippe, 1977). Three years earlier, the presence of a "subunit-structured" cell wall and the concomitant lack of a peptidoglycan layer were described for *Sulfolobus acidocaldarius* supporting the concept of a new major division distinct from Gram-positive and Gram-negative Bacteria (Weiss, 1974).

Already in the 1950's, a first hint to the uniqueness of archaeal cell walls was detected when analyzing *Halobacterium salinarum* (formerly *H. halobium*) by electron microscopy. Its cell wall was shown to consist of only one layer of globular particles arranged in a hexagonal pattern (Houwink, 1956), a structure initially believed to be a curiosity. Ongoing structural and biochemical analyses revealed other unusual cell envelope types,

all confirming the three-domain concept of Woese. Archaea lack muramic acid and bacterial cell wall polymers and possess only a single membrane (König et al., 2007); the only known exception are cells of the genus *Ignicoccus* with their second, outermost membrane (Rachel et al., 2002). Archaeal cytoplasmic membranes are in fact enclosed by a large diversity of complex polymers such as e.g. (glyco-)proteins, pseudomurein, or methanochondroitin (Figure I).

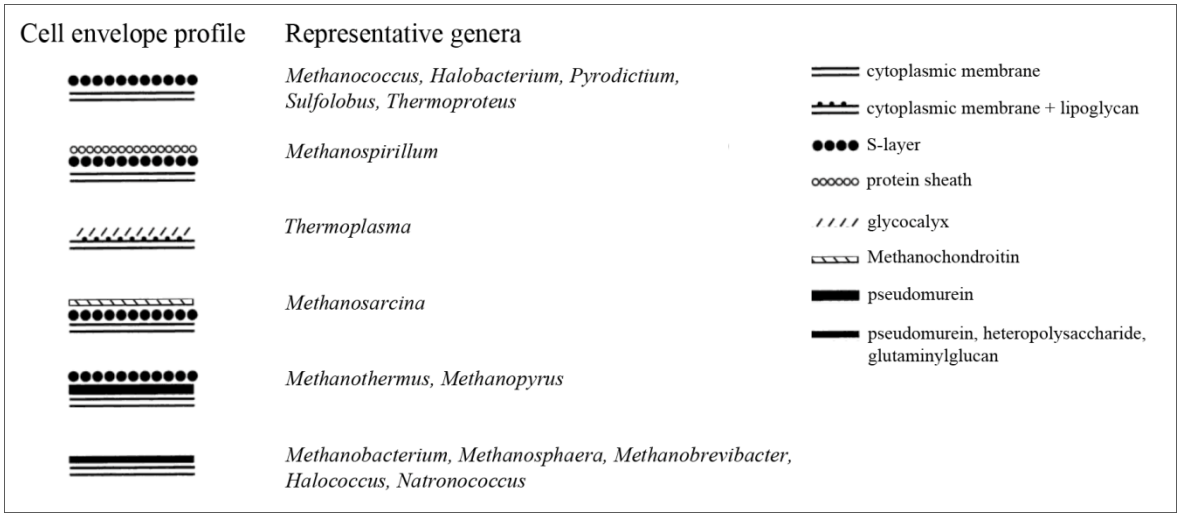

Figure I: Cell wall profiles of Archaea. Modified from König et al., 2007.

Most Archaea, including almost all Crenarchaeota, possess a proteinaceous surface layer (S-layer) as sole outermost component that forms a two-dimensional regularly structured array (Kandler and König, 1985; Beveridge and Graham, 1991; Baumeister and Lembcke, 1992). These arrays consist of morphological building blocks of two, three, four, or six subunits corresponding to a p2, p3, p4, or p6 symmetry, whereof the latter predominates among Archaea. Complementary electron microscopic studies have shown that the symmetry is identical or similar within a genus, or even within a family (e.g. the *Thermococcaceae*) or within an order (e.g. the *Thermoproteales* or the *Methanococcales*). In other cases, the arrangement of subunits helps to distinguish between closely related genera, e.g. *Pyrodictium* versus *Pyrolobus* or *Archaeoglobus* versus *Ferroglobus* (König et al., 2007). Besides the symmetry, S-layers are characterized by the center-to-center spacing of the (glyco)protein subunits varying between 9 nm in the SM1 Euryarchaeon (Moissl, 2004) and 35 nm in *Staphylothermus marinus* (Peters, 1995). Filamentous protrusions of protein domains anchor the S-layer in the cytoplasmic membrane, suggesting to also act in the immobilization of membrane lipids and proteins (Baumeister and Lembcke, 1992). Since no viable S-layer-less mutants have been detected in Archaea, its pivotal role in

shape maintaining and mechanical, osmotic, and (probably) thermal stabilization of cells seems to be obvious (Engelhardt, 2007).

A suitable model system for studying thermal adaption of S-layers is represented by the order *Methanococcales*, which includes mesophilic, thermophilic, and hyperthermophilic species. Comparison of the S-layer genes revealed a high overall homology but noteworthy differences were displayed in the amino acid composition. In mesophilic S-layer proteins a reduction in charged residues and an increase in polar residues were found compared to the thermophilic and hyperthermophilic counterparts. Database analyses identified multiple N-glycosylation sites and the existence of an almost identical 28 amino acid signal peptide in all analyzed species (Akça et al., 2002).

N-linked glycosylation and signal peptide removal are the most common posttranslational modifications found in archaeal proteins, of which S-layer proteins and flagellins are the best studied ones. N-terminal signal peptides act as sorting signals for recognition and targeting and are cleaved by their corresponding signal peptidase. Up to now, two different signal peptidases are known in Archaea, the signal peptidase I (SPI) and type IV prepilin peptidase (TFPP)-like enzymes (Jarrell et al., 2010b). The first identified and characterized SPI enzyme was found in *Methanococcus voltae* possessing its active site on the external face of the cytoplasmic membrane (Ng and Jarrell, 2003). The enzyme processes the majority of secreted preproteins all containing a class I signal peptide that is made of a basic n-region followed by a hydrophobic core (h-region) and ends in a carboxyl-terminal region (c-region) including the cleavage site (Ng et al., 2007). The much better studied TFPP-like enzymes include different peptidases all cleaving class III signal peptides. The flagellin processing enzyme FlaK was initially characterized from *Methanococcus maripaludis* and *M. voltae* (Bardy and Jarrell, 2002, 2003) and acts in a more stringent manner, compared to its equivalent in *S. solfataricus*, PibD, which cleaves not only flagellins but also some sugar-binding proteins (Albers et al., 2003). Most recently, a novel euryarchaeal peptidase, EppA, was detected that specifically cleaves proteins with a similar amino acid motif upstream of the cleavage site. This varied domain of unknown function DUF361 was found among others in the pilins of *M. maripaludis* (Szabó et al., 2007b). The essential role of signal peptidases in Archaea was demonstrated by deletion mutant analyses revealing e.g. *flaK*$^-$ transformants to be non-flagellated (Bardy and Jarrell, 2003).

Besides signal peptide cleavage, N-glycosylation plays an important role in the cells: The absence of N-glycosylation in *Haloferax volcanii* compromised S-layer stability (Abu-

Qarn et al., 2007), whereas in *M. voltae*, absent or partial N-glycosylation was shown to result in flagella-less or flagella-deficient mutants with obvious defects in motility (Chaban et al., 2006). Already in the 1970's, the occurrence of glycoproteins was shown on the cell surface of *H. salinarum* (Mescher et al., 1974). Further studies demonstrated that oligosaccharides are sequentially assembled on a dolichyl phosphate carrier on the cytoplasmic site of the membrane, translocated across the membrane and then transferred to the target protein (Yurist-Doutsch et al., 2008).

Archaea have been shown to possess a variety of different types of cell surface structures that are structurally and biochemically distinct from those of Bacteria (e.g. reviewed by Ng et al., 2008). In times of the prokaryote-eukaryote dichotomy, these differences were not recognized and hence, based on superficial similarities, equal terms were introduced for bacterial and archaeal cell appendages. In general, flagella are defined as rotating motility organelles whereas pili and/or fimbriae name cell surface appendages primarily involved in adhesion. Even though being far from a uniform nomenclature, this concept is still valid and is complemented by newly discovered archaeal cell surface structures. Contrary to flagella and pili/fimbriae, these highly specialized cell appendages are restricted to single organisms or genera.

Most recently, the fibers of *Ignicoccus hospitalis* were described as new kind of archaeal cell surface appendages being 14 nm in diameter and up to 20 µm in length. They are mainly composed of the 33 kDa protein Iho670, for which no clear data are available concerning its glycosylation (Müller et al., 2009). Fibers were also found in *I. islandicus* and *I. pacificus*; for the latter organism, the N-terminus of the major protein (39 kDa) was homologous to that of Iho670 (Meyer, 2010). Although found in planktonic cells, a function of fibers as motility organelles is unlikely since swimming of *I. hospitalis* was never observed, and therefore the organism is assumed to be non-motile (Herzog, 2009). In contrast, cells expressed far more fibers when grown on carbon-coated gold grids suggesting they may play a role in adhesion (Meyer, 2010).

When studying the ultrastructure of *Pyrodictium abyssi* by transmission and scanning electron microscopy, its cells were identified to be enmeshed in a three-dimensional, regular-arrayed network of tubules, the cannulae (Latin: *little reeds*). The hollow cylindrical cannulae with an outer diameter of 25 nm (Rieger et al., 1995) are made of (at least) three glycoproteins and can withstand temperatures of up to 130°C without loss of secondary structure. Tomographic reconstructions of a cell conjunct with two cannulae

showed that they enter the periplasmic space only, but not the cytoplasm, thus interconnecting two cells with each other (Nickell et al., 2003). The formation of these cell-cell contacts and therewith the growth of cannulae is directly linked to cell division; their dynamics were observed with aid of high intensity dark-field light microscopy (Horn et al., 1999). Based on these findings, *Pyrodictium* was suggested to be a primitive, multicellular Prokaryote, which could possibly use cannulae for intercellular transport of e.g. metabolites, signaling molecules, or even genetic material (Nickell et al., 2003).

A third type of very special archaeal cell surface appendages are the hami (singular hamus; Latin: *hook*) of the SM1 Euryarchaeon, a cold-loving Archaeon discovered in sulfidic springs of the Sippenauer Moor, near Regensburg, Germany (Rudolph et al., 2001). Hami are characterized by their very complex ultrastructure exhibiting a well-defined base-to-top organization. The central part of the 7−8 nm thin filament is made of barbwire-like structures with prickles 4 nm in diameter that emanate in regular intervals. Distally, the hamus ends in a prickle-free segment capped by a tripartite grappling hook. Each cell possesses about 100 of these 1−3 µm long nanosized 'anchors', which were shown to mediate strong adhesion among single cells and also to various chemically different materials. On molecular level, hami are mainly composed of a 120 kDa protein reacting negatively in glycoprotein assays (Moissl et al., 2005).

In Archaea, the term fimbriae is restricted to cell appendages expressed by members of the order *Methanobacteriales*, which are up to 10 µm in length and 4−5 µm in diameter (Doddema et al., 1979). In a recent study of *M. thermoautotrophicus* fimbriae, it has been revealed that, in contrast to non-motile planktonic cells, adherent cells express a multitude of fimbriae. Immunological studies identified the cell appendages as functional adhesins, and hence their involvement in biofilm formation was discussed. The authors showed that fimbriae are built (mainly) of Mth60, a 16 kDa glycoprotein. Although no homologues of Mth60 were detected in the database (Thoma et al., 2008), recent studies grouped the fimbriae together with one of the most common archaeal cell appendages, the pili (Jarrell et al., 2010a; Ng et al., 2011).

Already in 1973, it was reported that *Sulfolobus* cultures attach by means of numerous pili 5 nm in width to sulfur deposited in flowing springs (Weiss, 1973). More recent studies found that the formation of 10-nm pili in *S. solfataricus* can also be induced by use of high doses of UV irradiation (Fröls et al., 2007; Fröls et al., 2008). The so-called Ups pili (UV-inducible pili of *Sulfolobus*) not only mediate cellular aggregation (Fröls et al., 2008) but also the attachment of cells to surfaces (Zolghadr et al., 2010). In the genus

Methanococcus, pili are clearly outnumbered by flagella (Koval and Jarrell, 1987), whereby their analysis was restricted until genetic techniques allowed the generation of flagella-less mutants (Moore and Leigh, 2005). Pili isolated from these mutants were 6 nm in diameter and apparently possessed no hook or anchoring structure. The major pilin, MMP1685, with an intact molecular mass of 9.7 kDa, was identified by mass spectrometry (Ng et al., 2011).

Archaeal flagella, the best characterized archaeal surface appendages, are found in nearly all major taxa of Crenarchaeota and Euryarchaeota, including methanogens, halophiles, and thermoacidophiles. Despite that at a first glance some similarities to bacterial flagella seem to exist, biochemical and ultrastructural analyses identified them as unique motility apparatus. Electron microscopic studies revealed archaeal flagella to be 10−15 nm in diameter (Typke et al., 1988; Cruden et al., 1989) forming a right-handed helix with no central channel, suggesting assembly of the filaments by adding subunits to their base (Alam and Oesterhelt, 1984; Szabó et al., 2007a; Cohen-Krausz and Trachtenberg, 2008). Although isolated flagella of many different Archaea have been analyzed to date, a detailed characterization of their ultrastructure at high resolution or of the anchoring mechanism is missing in most cases. Cruden et al. (1989) demonstrated that flagella of *Methanospirillum hungatei* and *Methanothermococcus thermolithotrophicus* consist of a filament, a hook, and a basal body with two rings. First insights into anchoring of archaeal flagella inside the cell were obtained so far for Halobacteria only. Solubilization of *H. salinarum* cell envelopes has shown that the flagellar bundle is inserted in a distinct ‘polar cap’ (Kupper et al., 1994), which is located as a polar membrane below the cytoplasmic membrane (Kireev et al., 2006).

Analyses of archaeal genomes identified 2−6 flagellin genes with the exceptions of *Metallosphaera sedula*, *M. barkeri*, and three *Sulfolobus* species, carrying only a single flagellin gene (Ng et al., 2006; Auernik et al., 2008). These genes named *flaA* and/or *flaB* are located in a major gene cluster together with flagella-associated genes *flaC−flaJ*. Their function is mostly hypothetically but was demonstrated to be necessary for proper flagellar assembly (Chaban et al., 2007). From the data obtained, a model for the assembly of archaeal flagella was proposed (Figure II; Jarrell and McBride, 2008).

Initially, archaeal flagella were identified as motility structures and their rotation as driving force for swimming was extensively studied in the model organism *H. salinarum* (Alam and Oesterhelt, 1984; Marwan et al., 1991). By contrast, flagella-dependent motility in *S. solfataricus* was investigated by swarming assay analysis of a flagella-less mutant

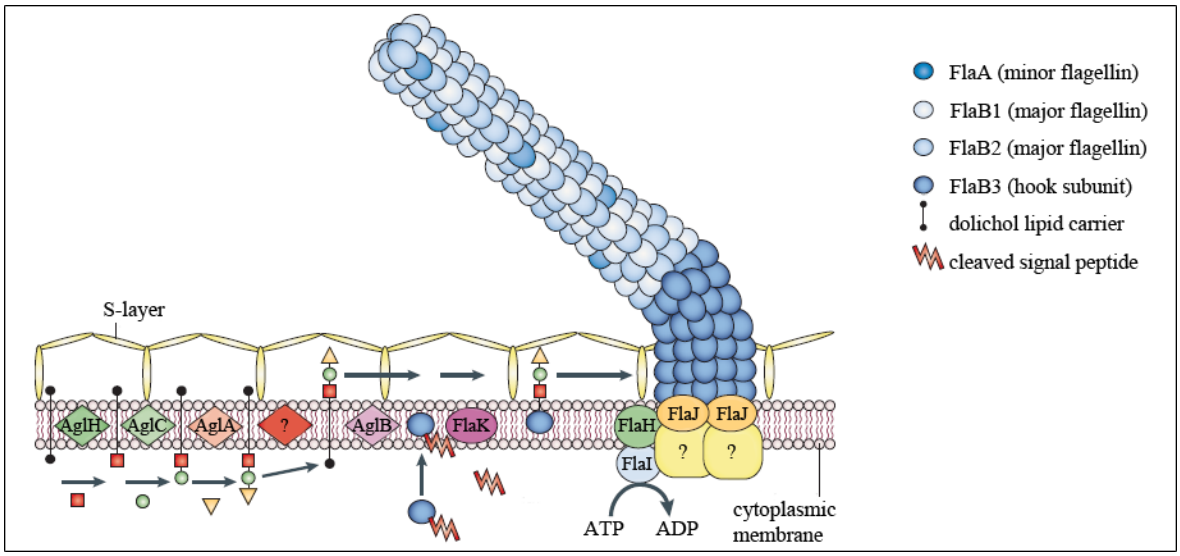

Figure II: The assembly of archaeal flagella. Model showing the posttranslational modification of flagellins and their assembly into the growing flagellum using the example of *Methanococcus voltae*. Modified from Jarrell and McBride, 2008.

(Szabó et al., 2007a). First evidence that archaeal flagella are multifunctional organelles was demonstrated for the hyperthermophilic model organism *Pyrococcus furiosus*. Here, flagella mediate swimming motility, the formation of cell-cell contacts and the attachment to abiotic surfaces. Electron microscopic studies of cells attached to these surfaces identified them growing in (micro)colonies or in a biofilm-like manner (Näther et al., 2006). Aside from this monospecies biofilm, *P. furiosus* can colonize unfavorable materials, when grown in coculture with *Methanopyrus kandleri*, whilst adhering to the methanogenic partner which initially attaches to the surface. The resulting layered 'fried egg colonies' represent the first known cultured archaeal bispecies biofilm (Schopf et al., 2008).

Nowadays, biofilms are commonly accepted as the natural living form of microorganisms. Up to 90% of the dry mass of biofilms is built from a self-produced matrix of hydrated extracellular polymeric substances (EPS). Mainly composed of polysaccharides, proteins, nucleic acids and lipids, EPS provide, among others, the mechanical stability of biofilms, and enable intense interactions of cells including cell-cell communication, horizontal gene transfer or the generation of a external digestive system (Flemming and Wingender, 2010).

In contrast to the well-studied bacterial biofilms, the formation of archaeal biofilms has sparsely been studied. The first monospecies biofilms in laboratory cultures were investigated for *Thermococcus litoralis* (Rinker and Kelly, 1996) and *Archaeoglobus fulgidus* (Lapaglia and Hartzell, 1997). *T. litoralis* developed biofilms on hydrophilic surfaces such as glass slides and polycarbonate filters particularly after adding organic compounds to the medium. On these surfaces and also in batch cultures with defined or

complex medium, the produced EPS contained mannose as the only monosaccharide constituent (Rinker and Kelly, 1996). In *A. fulgidus*, production of heterogeneous, morphologically variable biofilms was induced by different conditions of stress, e.g. treatment with chemicals or changes in temperature or pH. A comparison of phenol- and ethanol-extracted fractions of *A. fulgidus* biofilms and cells identified proteins, polysaccharides and metals as biofilm components (Lapaglia and Hartzell, 1997). Compared to these early data on euryarchaeal biofilms, a first study dealing with crenarchaeal biofilms was published very recently. Comprehensive analyses of three *Sulfolobus* species in static systems have shown that they differ in their initial attachment to surfaces and that the resulting biofilm varied from simple carpet-like to high density tower-like structures. After initiation of biofilm formation, all three organisms were proven to produce EPS composed of glucose, galactose, mannose, and N-acetylglucosamine (Koerdt et al., 2010). Similar EPS compositions were described previously for *S. solfataricus* grown in fermentors and batch cultures (Nicolaus et al., 1993) or surface-attached (Zolghadr et al., 2010).

In contrast to these cultured biofilms, Henneberger et al. (2006) have given first insights into a naturally occurring archaeal monospecies biofilm. Submersing a biofilm-trapping system made of polyethylene nets into the drilling hole of the sulfidic Islinger Muehlbach spring (Regensburg, Germany), slime-like, milky droplets sticking strongly to the nets were observed after exposure of only 10 min. Analysis of the drops identified at least 95% of the cells to be the SM1 Euryarchaeon, whereas the other up to 5% were morphologically different Bacteria. Cells in the biofilm were enclosed by EPS, the biochemical investigation of which indicates the presence of carbohydrates and proteins in a total ratio of 1:1.5. EPS and especially the hami maintained a constant distance of approximately 4 µm between the cells resulting in regular three-dimensional arrangement of the cells inside the biofilm (Henneberger et al., 2006).

Understanding the ultrastructure of archaeal cells and cell appendages with regard to functionality is highly desirable but can be only performed under laboratory conditions and with suitable model organisms. As described above, the present body of literature answers this query partially for different models belonging either to the Crenarchaeota (*Sulfolobus* and *Ignicoccus*) or the Euryarchaeota (*Halobacterium*, *Methanococcus*, and *Pyrococcus*). But what is missing in the current research is a comprehensive study of all aspects for one organism.

To address this topic in the present thesis, two hyperthermophilic species, *Pyrococcus furiosus* and *Methanocaldococcus* sp. KIN24-T80, are in the focus of interest since both possess multiple multifunctional flagella.

Pyrococcus furiosus was isolated from geothermally heated marine sediments of the beach of Porto di Levante (Vulcano Island, Italy). Enrichment of the samples revealed regular to slightly irregular cocci with a diameter of 0.8−2.5 µm. The cells were described to be strictly anaerobic heterotrophs metabolizing maltose, starch, peptone, and complex organic substrates. CO_2 and H_2 were detected as sole metabolic products, and the inhibitory effect on growth by high concentrations of the hydrogen can be prevented by addition of elemental sulfur to the medium. Beside the short doubling time of 37 min at its optimal growth temperature of 100°C, *P. furiosus* was named due to its strong motility (Fiala and Stetter, 1986). Swimming of cells was observed directly at 95°C (Herzog, 2009) using a high-temperature light microscope equipped with electrically heated slide holder and objectives (Horn et al., 1999). Electron microscopic studies revealed the cells to possess about 50 monopolar peritrichous flagella (Fiala and Stetter, 1986), which were shown to be necessary for swimming since cells after removal of flagella by shearing were non-motile (Näther, 2007). In a recent study on *P. furiosus*, it has been shown that the function of its flagella is not restricted to motility: Cells can grow on different natural and synthetic materials, on which they are embedded in a dense network of flagella mediating the contact to the surface and to other cells (Figure IIIa). Addition of antibodies generated against native purified flagella detached the cells from the surfaces allowing the conclusion that flagella also are functional adhesins. Adhesion was suggested to be specific since different types of interaction with surfaces, ranging from no or single cells to microcolonies of a few thousand cells, were detected (Näther et al., 2006).

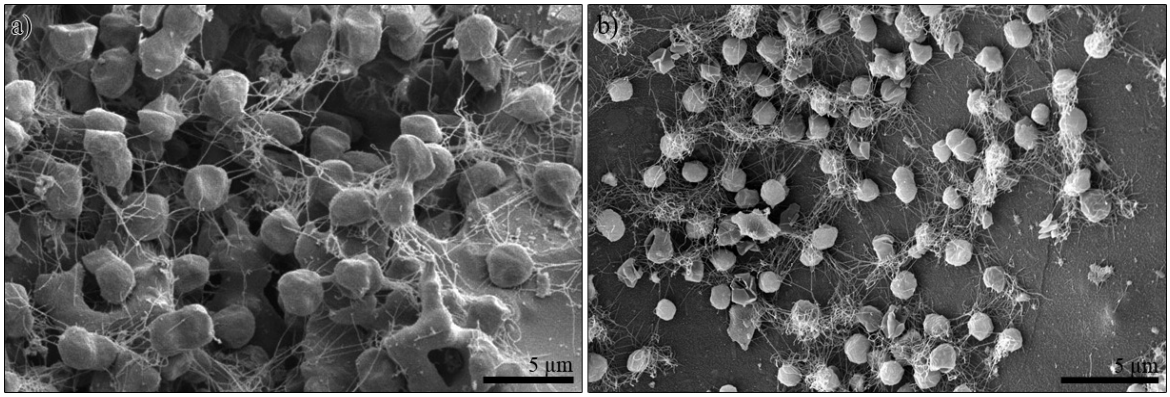

Figure III: *Pyrococcus furiosus* and *Methanocaldococcus* sp. KIN24-T80. Cells of a) *P. furiosus* and b) *Methanocaldococcus* sp. KIN24-T80 were grown on quartz and visualized by scanning electron microscopy. Modified from a) Näther et al., 2006 and b) Janker, 2008.

Similar to *P. furiosus*, flagella of another, newly discovered species were also identified to be involved in adhesion and formation of cell-cell contacts (Bellack, 2007).

Methanocaldococcus sp. KIN24-T80 was isolated during a laboratory microbial diversity course ("Organismische Mikrobiologie I/II") at the University of Regensburg in 2005. The original sample consisted of pulverized rocky sediments originating from a shallow active hydrothermal system at Kolbeinsey Ridge, north of Iceland. Cells of the new isolate were identified as regular to irregular cocci showing an intense green-blue fluorescence under UV-exposure. They had an average diameter of 1 µm and occurred singly or in pairs. The chemolithoautotrophic cells gained their energy exclusively by reduction of CO_2 with H_2 and grew optimally at 80°C. Based on a neighbour-joining analysis of the 16S rRNA gene sequence along with other archaeal sequences, the new isolate represents a deep branch within the genus *Methanocaldococcus* with approximately 95% sequence similarity to *M. jannaschii* as its closest relative (Bellack, 2007).

All validly described species of this genus are characterized by multiple flagella (Jones et al., 1983; Jeanthon et al., 1998; Jeanthon et al., 1999; L'Haridon et al., 2003), whereas the two species of the second genus within the *Methanocaldococcaceae*, *Methanotorris*, possess only a few cell appendages (Burggraf et al., 1990; Takai et al., 2004). Moreover, flagellation seems to correlate with motility as *Methanocaldococci* are highly motile in contrast to the *Methanotorris* species (Whitman et al., 2001). In accordance with this concept, recent studies revealed that *Methanocaldococcus* sp. KIN24-T80 is a very fast swimmer (Herzog, 2009) and has about 50 polarly inserted flagella (Bellack, 2007). Initial adhesion studies demonstrated that cells of this organism were able to adhere to different materials (Bellack, 2007; Janker, 2008) and that flagella form the contact to the surface and to other cells (Figure IIIb).

Therewith, *Methanocaldococcus* sp. KIN24-T80 would be a suitable model organism to study the function of its flagella in more detail.

2 Objectives

The present thesis attempts to contribute to the existing body of archaeal research on ultrastructure of flagella, cell architecture, and adhesion and biofilm formation.

Therefore, the study aimed to identify flagellar-associated proteins and adhesion structures in membrane fractions of *Pyrococcus furiosus* by analysis of cell envelopes with aid of SDS-PAGE and transmission electron microscopy. To gain insights into the subcellular localization of those proteins, different immuno-labeling techniques were compared. In a second project, the characterization of the isolate *Methanocaldococcus* sp. KIN24-T80 was completed to provide a novel suitable model organism for the analysis of archaeal cell appendages with respect to their ultrastructure and their function in adhesion.

Furthermore, this study involved the investigation and comparison of the cell architecture of both organisms. Different preparation techniques and various (electron) microscopic methods were utilized to address this query.

3 Material

1 Chemicals, biochemicals and gases

Chemicals not listed here were purchased from VWR, Darmstadt, Germany.

Table I: List of (bio-)chemicals.

Chemical	Supplier	City (country[a])
3-amino-9-ethylcarbazole	Sigma-Aldrich Chemie GmbH	Munich (DE)
Agar (Bacto™)	Becton, Dickinson and Company	Heidelberg (DE)
Agarose (Broad Range for PFGE)	Carl Roth GmbH + Co. KG	Karlsruhe (DE)
Agarose (peqGOLD Universal)	peqlab Biotechnologie GmbH	Erlangen (DE)
Alexa Fluor® 488 and 555, succinimidyl ester	Invitrogen (Life Technologies)	Karlsruhe (DE)
Ammonium persulfate	Serva	Heidelberg (DE)
Ampicillin, Na-salt	MP Biomedicals Germany GmbH	Eschwege (DE)
APS (ammonium persulfate)	Serva	Karlsruhe (DE)
Bromphenol blue (Na-salt)	Serva	Heidelberg (DE)
BSA (bovine serum albumin)	Sigma-Aldrich Chemie GmbH	Munich (DE)
Calcium chloride dihydrate	Riedel-de Haën (Sigma-Aldrich)	Munich (DE)
Calcofluor (Fluorescent Brightener 28)	Sigma-Aldrich Chemie GmbH	Munich (DE)
Cesium chloride	Biomol	Hamburg (DE)
Chloramphenicol	Serva	Heidelberg (DE)
Cobalt chloride hexahydrate	Acros (Thermo Scientific)	Nidderau (DE)
Coomassie Brilliant Blue G250	Serva	Heidelberg (DE)
CTAB (cetyltrimethylammonium bromide)	Serva	Heidelberg (DE)
D (+) Biotin	Calbiochem	Darmstadt (DE)
DAPI (4',6-diamidino-2-phenylindole)	AppliChem GmbH	Darmstadt (DE)
DDM (n-dodecyl-beta-D-maltoside)	Anatrace	Maumee,OH(US)
DDSA (dodecenylsuccinic anhydride)	Fluka (Sigma-Aldrich)	Munich (DE)
DMSO (dimethyl sulfoxide)	Serva	Heidelberg (DE)
DMP-30™ [2,4,6-tris(dimethylaminomethyl)phenol]	Fluka (Sigma-Aldrich)	Munich (DE)
DTT (dithiothreitol)	MP Biomedicals Germany GmbH	Eschwege (DE)
EDTA (ethylenediaminetetraacetic acid), Na-salt	MP Biomedicals Germany GmbH	Eschwege (DE)
Epoxy embedding medium	Fluka (Sigma-Aldrich)	Munich (DE)
Ethanol p.a.	J.T. Baker	Deventer (NL)
Ethidium bromide	Serva	Heidelberg (DE)
Glycerol	MP Biomedicals Germany GmbH	Eschwege (DE)
Glutardialdehyde (25%, EM-grade)	Sigma-Aldrich Chemie GmbH	Munich (DE)
HEPES [4-(2-Hydroxyethyl)piperazine-1-ethane-sulfonic acid], titr.	Sigma-Aldrich Chemie GmbH	Munich (DE)
IPTG (isopropyl-β-D-thiogalactopyranoside)	Peqlab Biotechnologie GmbH	Erlangen (DE)
Lead citrate	Serva	Heidelberg (DE)
Methanol p.a.	Sigma-Aldrich Chemie GmbH	Munich (DE)
MNA (methyl nadic anhydride)	Fluka (Sigma-Aldrich)	Munich (DE)
MOPS [3-(N-morpholino)propanesulfonic acid], titr.	Sigma-Aldrich Chemie GmbH	Munich (DE)
N-Lauroylsarcosine, Na-salt	Sigma-Aldrich Chemie GmbH	Munich (DE)
Nickel ammonium sulfate hexahydrate	Fluka (Sigma-Aldrich)	Munich (DE)
PEG (polyethylene glycol) 6000	Serva	Heidelberg (DE)
Peptone (Bacto™)	Becton, Dickinson and Company	Heidelberg (DE)
Periodic acid	Sigma-Aldrich Chemie GmbH	Munich (DE)
Phenol	Carl Roth GmbH + Co. KG	Karlsruhe (DE)
Phenol-Chloroform-Isopropanol (25:24:1)	Biomol	Hamburg (DE)
PMSF (phenylmethylsulfonyl fluoride)	Serva	Heidelberg (DE)
Resazurin, Na-salt	Serva	Heidelberg (DE)
Schiff's reagent	Carl Roth GmbH + Co. KG	Karlsruhe (DE)
Silver nitrate	Carl Roth GmbH + Co. KG	Karlsruhe (DE)

titr. titration (Sigma pH buffers for titration)
[a] DE Germany, NL Netherlands, US United States of America

Table I: List of (bio-)chemicals - continued

Chemical	Supplier	City (country[a])
Skimmed milk powder	Milchwerke Regensburg	Regensburg (DE)
Sodium carbonate	Carl Roth GmbH + Co. KG	Karlsruhe (DE)
Sodium metabisulfite	Sigma-Aldrich Chemie GmbH	Munich (DE)
Sodium selenate	Sigma-Aldrich Chemie GmbH	Munich (DE)
Sodium sulfide × 7–9 H_2O	Fluka (Sigma-Aldrich)	Munich (DE)
Sodium thiosulfate	Fluka (Sigma-Aldrich)	Munich (DE)
Taurodeoxycholate, Na-salt	Sigma-Aldrich Chemie GmbH	Munich (DE)
TEMED (tetramethylethylenediamine)	Carl Roth GmbH + Co. KG	Karlsruhe (DE)
Tris [tris(hydroxymethyl)aminomethane]	USB Corporation	Cleveland, OH (US)
Triton X-100	MP Biomedicals Germany GmbH	Eschwege (DE)
Triton X-114	Boehringer Mannheim GmbH	Mannheim (DE)
Tween® 20	Serva	Heidelberg (DE)
Tween® 80	Serva	Heidelberg (DE)
Uranyl acetate	Fluka (Sigma-Aldrich)	Munich (DE)
Urea	Fluka (Sigma-Aldrich)	Munich (DE)
Yeast extract (Bacto™)	Becton, Dickinson and Company	Heidelberg (DE)

titr. titration (Sigma pH buffers for titration)
[a] DE Germany, NL Netherlands, US United States of America

All gases used were purchased from Linde Technische Gase (Nuernberg, Germany).

2 Nucleic acids

Primers were purchased from Metabion (Martinsried, Germany).

Table II: List of primers, plasmids, and DNA size markers.

16S rRNA primer	Sequence (5'→3')	Reference
8af	TCYGGTTGATCCTGCC	(Eder et al., 1999)
1406ur	ACGGGCGGTGTGTRCAA	(Lane, 1991)

Cloning primer	Sequence (5'→3')[a]	Restriction enzyme
Gdh_pET21a_EcoRI_F	GGAGC**G▼AATTC**ATGGTTGAGCAAGACC	EcoRI
Gdh_pET21a_SalI_R	ACTT**G▼TCGAC**TCAGTGCTTGACCCATC	SalI

Plasmid primer	Sequence (5'→3')
T7 promoter	TAATACGACTCACTATAGGG
T7 terminator	GCTAGTTATTGCTCAGCGG

Plasmid	Function	Reference
pET21a	amp^R His•Tag® T7•Tag® T7 lac pBR322origin f1origin	Novagen®

DNA size marker	Supplier	City (country[b])
GeneRuler™ 1kb DNA Ladder, ready-to-use	Fermentas (Thermo Scientific)	St. Leon-Rot (DE)
GeneRuler™ 100bp DNA Ladder, ready-to-use	Fermentas (Thermo Scinetific)	St. Leon-Rot (DE)
Lambda DNA	New England Biolabs GmbH	Frankfurt (DE)
Lambda DNA/EcoRI+HindIII Marker, 3, ready-to-use	Fermentas (Thermo Scientific)	St. Leon-Rot (DE)
Lambda Ladder PFG Marker	New England Biolabs GmbH	Frankfurt (DE)
Yeast Chromosome PFG Marker	New England Biolabs GmbH	Frankfurt (DE)

[a] bold: recognition sequence, ▼ restriction site
[b] DE Germany

3 Enzymes and polypeptides

Table III: List of enzymes and polypeptides.

Enzyme[a]/polypeptide	Supplier	City (country[b])
Chymotrypsin (sequencing grade)	Roche Applied Science	Mannheim (DE)
DNaseI	Roche Applied Science	Mannheim (DE)
Lysozyme	Sigma-Aldrich Chemie GmbH	Munich (DE)
PageRuler™ Prestained Protein Ladder (10–170 kDa)	Fermentas (Thermo Fisher)	St. Leon-Rot (DE)
PageRuler™ Unstained Protein Ladder (10–200 kDa)	Fermentas (Thermo Fisher)	St. Leon-Rot (DE)
Prestained Protein Marker, Broad Range (7–175 kDa)	New England Biolabs GmbH	Frankfurt (DE)
Protein Marker, Broad Range (2–212 kDa)	New England Biolabs GmbH	Frankfurt (DE)
Proteinase K	Merck	Darmstadt (DE)
Restriction enzymes (with buffers)	New England Biolabs GmbH	Frankfurt (DE)
RNase, DNase-free (solution)	Roche Applied Science	Mannheim (DE)
RNaseA (powder)	Omni Life Sciences	Bremen (DE)
T4 DNA ligase	New England Biolabs GmbH	Frankfurt (DE)
Trypsin (sequencing grade)	Roche Applied Science	Mannheim (DE)

[a] Enzymes were used with provided buffers.
[b] DE Germany

4 Antibodies

All primary antibodies were supplied by Davids Biotechnologie (Regensburg, Germany).

Table IV: List of antibodies.

Primary antibodies	Source	Immunization by	Reference
Anti-Fla KIN	Polyclonal rabbit	Sheared and purified KIN flagella	Bellack, 2007
Anti-Fla Pfu	Polyclonal rabbit	Sheared and purified Pfu flagella	Näther et al., 2006
Anti-FlaB0-MT Pfu	Polyclonal rabbit	Recombinant middle part of Pfu FlaB0	Näther, 2007
Anti-FlaB1-MT Pfu	Polyclonal rabbit	Recombinant middle part of Pfu FlaB1	Näther, 2007
Anti-FlaB2-MT Pfu	Polyclonal rabbit	Recombinant middle part of Pfu FlaB2	Wimmer, 2007
Anti-FlaB2-CT Pfu	Polyclonal rabbit	Recombinant C-terminus of Pfu FlaB2	Wimmer, 2007
Anti-Gdh Pfu	Polyclonal rabbit	Recombinant Pfu Gdh	This study
Anti-OF Pfu	Polyclonal rabbit	Sheared whole cells of Pfu	Schopf, 2011

Secondary antibodies	Supplier	City (country)[a]
Goat anti-rabbit IgG (whole molecule)-Peroxidase	Sigma-Aldrich Chemie GmbH	Munich (DE)
Goat anti-rabbit (6 nm gold)	Aurion	Wageningen (NL)

CT C-terminus, Gdh glutamate dehydrogenase, KIN *M. villosus*, MT middle part, Pfu *P. furiosus*
[a] DE Germany, NL Netherlands

5 Glassware

All glassware used was manufactured by Schott Glas (Mainz, Germany), except 100 ml serum bottles (soda-lime glass; PPS Pharmapack Stute GmbH, Rheinbreitbach, Germany) and 1L-pressure bottles (borosilicate glass; Müller + Krempel AG, Bülach, Switzerland).

6 Consumables

Table V: List of consumables.

Material	Manufacturer	City (country[a])
Aluminium seals (Ø 20 mm, 10 mm hole)	WICOM	Heppenheim (DE)
Centrifuge tube (15.0 ml, 50.0 ml)	Carl Roth GmbH + Co. KG	Karlsruhe (DE)
Coverslips (20 mm × 20 mm)	Paul Marienfeld GmbH & Co. KG	Lauda-Koenigshofen (DE)
Cryovials (1.7 ml)	Sarstedt AG & Co.	Nuembrecht (DE)
Cuvettes	Bio-Rad	Munich (DE)
Dialysis membranes, ZelluTrans	Carl Roth GmbH + Co. KG	Karlsruhe (DE)
DryEase® mini cellophane	Invitrogen (Life technologies)	Darmstadt (DE)
Eppendorf tubes (0.5 ml, 1.5 ml, 2.0 ml)	Eppendorf	Hamburg (DE)
Folded filters (Ø 185 mm)	Schleicher & Schuell	Dassel (DE)
Filter discs (Ø 90 mm)	Sartorius AG	Goettingen (DE)
Glass capillaries	Hilgenberg GmbH	Malsfeld (DE)
Grids for electron microscopy		
Aperture discs, gold-coated, hole 100 µm	Plano GmbH	Wetzlar (DE)
Copper grids (400 mesh, 400 × 100 mesh)	Plano GmbH	Wetzlar (DE)
Copper grids, hexagonal (700 mesh)	Plano GmbH	Wetzlar (DE)
Gold grids (400 mesh)	Plano GmbH	Wetzlar (DE)
Nickel grids	Plano GmbH	Wetzlar (DE)
Immersion oil		
for standard microscopy	Zeiss	Munich (DE)
for CLSM (fluorescence-free)	Fluka (Sigma-Aldrich)	Exeter (UK)
Kits		
Alexa Fluor® 488 Protein Labeling Kit	Invitrogen (life technologies)	Darmstadt (DE)
Genomic DNA Buffer Set	QIAGEN GmbH	Hilden (DE)
MinElute PCR Purification Kit	QIAGEN GmbH	Hilden (DE)
PeqGOLD Plasmid Mini Kit I	Peqlab Biotechnologie GmbH	Erlangen (DE)
Phusion® High-Fidelity PCR Kit	New England Biolabs GmbH	Frankfurt (DE)
QIAGEN Genomic-tip (100/G and 500/G)	QIAGEN GmbH	Hilden (DE)
QIAGEN Plasmid Maxi Kit	QIAGEN GmbH	Hilden (DE)
QIAquick PCR Purification Kit	QIAGEN GmbH	Hilden (DE)
Taq-DNA-Polymerase (all inclusive)	Peqlab Biotechnologie GmbH	Erlangen (DE)
Taq PCR Master Mix Kit	QIAGEN GmbH	Hilden (DE)
Needles, disposable	Terumo Europa	Leuven (BE)
Parafilm "M"	Pechiney Plastic Packaging	Chicago, IL (US)
Pasteur pipets, wide opening, disposable (2.5 ml)	Carl Roth GmbH + Co. KG	Karlsruhe (DE)
PCR tubes, with attached claps (0.2 ml)	VWR	Darmstadt (DE)
Petri dishes (Ø 90 mm)	Sarstedt AG & Co.	Nuembrecht (DE)
pH-indicator stripes	VWR	Darmstadt (DE)
Roti®-PVDF (polyvinylidene fluoride) membrane	Carl Roth GmbH + Co. KG	Karlsruhe (DE)
Rubber stopper (for serum bottles)	Deutsch & Naumann	Berlin (DE)
Serological pipettes (25.0 ml)	Greiner Bio-one GmbH	Frickenhausen (DE)
Slides	Menzel GmbH und Co. KG	Braunschweig (DE)
Sterile filter		
Steritop™ Filter Units	Millipore	Schwalbach/Ts. (DE)
Syringe filters, Rotilabo® (0.22 µm; PVDF, CME)	Carl Roth GmbH + Co. KG	Karlsruhe (DE)
Surgical scalpels, disposable	Braun	Tuttlingen (DE)
Syringes, disposable (1.0 ml)	Ersta	Maersk (DK)
Tips		
Tips, for gel loading (200 µl)	VWR	Darmstadt (DE)
Tips, safeguard (10 µl)	Biozym Scientific GmbH	Hess. Oldendorf (DE)
Tips, safeguard (100 µl, 200 µl, 1,000 µl))	Peqlab Biotechnologie GmbH	Erlangen (DE)
Tips, universal (10 µl)	Gilson	
Tips, universal (200 µl, 1,000 µl)	Sarstedt AG & Co.	Nuembrecht (DE)
Ultracentrifuge tubes Ultra-Clear™ (4.0 ml)	Beckman Coulter	Krefeld (DE)
Whatman® chromatography paper 3 MM Chr	Whatman GmbH	Dassel (DE)

[a] BE Belgium, DK Denmark, DE Germany, UK United Kingdom, US United States of America

7 Instrumentation

Table VI: List of instruments.

Instrument	Supplier	City (country[a])
Anaerobic Chamber	Coy Laboratory Products Inc.	Grass Lake, MI (US)
Autoclaves		
SANOclav LaM-20-MCS-J	Adolf Wolf SANOclav	Bad Ueberkingen-Hausen (DE)
HST 32/25	Zirbus technology GmbH	Bad Grund/Harz (DE)
Cameras		
Canon PowerShot A620	Canon	Krefeld (DE)
Nikon CoolPix 995	Nikon	Duesseldorf (DE)
pco.pixelfly and pco.1600 CCD camera	PCO AG	Kelheim (DE)
Slow-Scan-CCD	TVIPS-Tietz GmbH	Gauting (DE)
Cell counting chamber (depth 0.02 mm)	Brand GmbH und Co. KG	Wertheim (DE)
Centrifuges		
Biofuge 13 (rotor 3757)	Heraeus Instruments	Hanau (DE)
Biofuge 28 RS (rotor 8575)	Heraeus Instruments	Hanau (DE)
Continuous flow centrifuge (rotor HCT22.300 8575)	Heraeus Instruments	Hanau (DE)
Cooling centrifuge 5402 (rotor F45-18-11)	Eppendorf	Hamburg (DE)
Labofuge GL (rotor 2159)	Heraeus Instruments	Hanau (DE)
Megafuge 1.0	Heraeus Instruments	Hanau (DE)
Sorvall RC 5C plus	DuPont	Bad Homburg (DE)
Ultracentrifuge Optima LE-80K	Beckman Coulter	Krefeld (DE)
Vacuum centrifuge DNAmini	Heto-Holten	Allerøed (DK)
Chromatography system Econo	Bio-Rad	Munich (DE)
Diamond knife	Diatome	Biel (CH)
Dispenser Dispensette®	Brand GmbH und Co. KG	Wertheim (DE)
Electrophoresis Power Supply ST305	GibcoBRL LifeTechnologies	Eggenstein
Electroporation apparatus Genepulser® II	Bio-Rad	Munich (DE)
Fermentor (16 L, 50 L, 100 L)	Bioengineering AG	Wald (CH)
Freeze-etch unit CFE-50	Cressington	Watford (UK)
Freeze substitution unit EM-AFS2	Leica	Wetzlar (DE)
High-pressure freezer EM-PACT 2 and HPM100	Leica	Wetzlar (DE)
Incubators		
Heraeus Typ T6 and T12	Heraeus Instruments	Hamburg (DE)
Kelvitron® t	Heraeus Instruments	Hamburg (DE)
Mytron WB 120	Mytron	Heiligenstadt (DE)
Imaging System BioDoc-It®	UVP	Cambridge (UK)
Magnetic stirrer MR2002, MR3002 (heatable)	Heidolph Elektro GmbH und Co. KG	Kelheim (DE)
Microflow® Biological Safety Cabinet	Nunc (Thermo Scientific)	Langenselbold (DE)
Microscopes		
Axiovert IM35	Zeiss	Munich (DE)
Confocal Laser Scanning Microscope LSM510 Meta	Zeiss	Munich (DE)
Nikon Labophot-2 and Mikrophot	Nikon	Duesseldorf (DE)
Olympus BX 50 and BX 60	Olympus	Hamburg (DE)
Transmission electron microscope CM12	FEI	Eindhoven (NE)
Mini-gel drying system DryEase®	Novex	San Diego, CA (US)
NanoDrop ND-1000	Peqlab BiotechnologieGmbH	Erlangen (DE)
PCR cycler		
MJ Mini™ Gradient Thermal Cycler	Bio-Rad	Munich (DE)
Perkin Elmer GeneAmp PCR System 9600	Perkin Elmer Inc.	Waltham (US)
pH meter	WTW	Weilheim (DE)
Plasma Cleaner/Sterilizer PDC-3XG	Harrick Plasma	Ithaca (USA)
Pulsed Field Electrophoresis System CHEF-DR® III	Bio-Rad	Munich (DE)
Rollerdrum™ Model TC7	New Brunswick Scientific	Edison, NJ (US)

[a] CH Switzerland, DK Denmark, DE Germany, UK United Kingdom, NE Netherlands, US United States of America

Table VI: List of instruments - continued.

Instrument	Supplier	City (country[a])
Scales		
MC1 Analytic AC 120 S	Satorius AG	Goettingen (DE)
Precision Standard TP400D	Ohaus	Cambridge (UK)
SemiDry Transfer Cell	Bio-Rad	Munich (DE)
Spectral photometer Spectronic Genesys 5	Milton Roy (Thermo Scient.)	Schwerte (DE)
Thermomixer compact 5350	Eppendorf	Hamburg (DE)
Ultra-Turrax T25	IKA-Werke	Staufen (DE)
Ultrasonic cell disruptor Sonifier® S-250A	Branson Ultrasonics	Danbury, CT (US)
UV Transilluminator (λ = 322 nm)	Herolab	Wiesloch (DE)
Vortex Genie 2	Scientific Industries	Bohemia (US)
Water bath	Memmert	Schwabach (DE)
Water bath shaker Gryotory® Model G76	New Brunswick Scientific	Edison, NJ (US)
Ultramicrotome UltracutE and EM UC6	Leica	Wetzlar (DE)
UV Chamber GS Gene Linker™	Biorad	Munich (DE)

[a] CH Switzerland, DK Denmark, DE Germany, UK United Kingdom, NE Netherlands, US United States of America

8 Buffers and (stock) solutions

Buffer compositions are given per liter of solution; smaller volumes are marked. If not indicated otherwise, the solvent is H_2O. The pH was measured at room temperature and adjusted with NaOH or HCl. By default, buffers were stored at room temperature.

Table VII: List of buffers and (stock) solutions.

Buffer/solution	Chemical agent	Amount	Concentration
Ampicillin stock	Ampicillin, Na-salt		20.0 mg/ml
	Filter sterilize and store at -20°C. Use within a month.		
Chloramphenicol stock	Chloramphenicol in ethanol		34.0 mg/ml
	Filter sterilize and store at -20°C.		
DAPI stock	DAPI		400.0 µg/ml
	Store aliquots at -20°C. Stable for at least six month.		
IPTG	IPTG in 100 ml LiChrosolve® water	2.38 g	100.0 mM
	Filter sterilize and store at -20°C. Use within four month.		
DNase	DNase in LiChrosolve® water		2.5 or 10.0 mg/ml
	Store at 2−8°C-		
Lysozyme	Lysozyme in LiChrosolve® water		100.0 mg/ml
	Store at -20°C in aliquots.		
Proteinase K	Proteinase K in LiChrosolve® water		20.0 mg/ml
	Store at 2–8°C.		
RNaseA	RNaseA in LiChrosolve® water		10 or 100 mg/ml
	Store at 2–8°C. Use within six month.		
PMFS	PMFS in pure isopropanol		7.0 mg/ml
	The solution is stable for at least nine month at room temperature.		

Table VII: List of buffers and (stock) solutions - continued.

Buffer/solution	Chemical agent	Amount	Concentration
PBS	NaCl	8.00 g	137.0 mM
	KCl	0.20 g	2.7 mM
	Na_2HPO_4	1.40 g	10.0 mM
	KH_2PO_4	0.24 g	1.76 mM
	Adjust pH 7.2 with 1 M NaOH.		
DAPI solution	3 M sodium acetate pH 4.7	200.00 µl	600.0 mM
	5 M Na_2-EDTA	100.00 µl	500.0 mM
	10% (w/v) SDS	1.00 µl/10.00 µl	0.01%/0.1% (w/v)
	DAPI stock solution	200.00 µl	200.0 µM
	Add H_2O to 1 ml. Store in the dark at 4°C. Solution by default with 0.1% (w/v) SDS, for methogens 0.01% (w/v) SDS.		
Calcofluor solution	Calcofluor		0.05% (w/v)
	Store protected from light.		
Alexa Fluor® dyes	Dissolve 1 mg of dye in 2 ml pure methanol and make aliquots of 166 µl. After incubation for 30 min at -80°C, sublimate the solvent in a vacuum centrifuge protected from light. Store at -20°C. Protect from light and moisture.		
Uranyl acetate solution pH 4.0	Uranyl acetate		2.0% (w/v)
	Acetic acid		0.1% (v/v)
Fixative buffer pH 7.0 (SEM)	Cacodylate		75.0 mM
	$MgCl_2$		2.0 mM
	NaCl		340.0/480.0 mM
	Osmolarity of the buffer has to be adapted to the growth medium of fixed cells.		
Substitution solution EGFU (TEM)	Ethanol	9.3 ml	93.0% (v/v)
	Glutardialdehyde	50.00 µl	0.5% (v/v)
	Formaldehyde	100.00 mg	1.0% (w/v)
	Uranyl acetate	50.00 mg	0.5% (w/v)
	Prepare formaldehyde freshly by depolymerization of paraformaldehyde. The EGFU solution contains 5.4% H_2O present in glutardi- and formaldehyde.		
Embedding medium Epon (TEM)	Epoxy embedding medium		46.0% (v/v)
	DDSA		28.5% (v/v)
	MNA		23.3% (w/v)
	DMP-30™		0.2% (w/v)
	Mix all chemicals except DMP-30™ under slow stirring, add DMP-30™ after 30 min and stir further for 30 min.		
Substitution solution AOUH (FIB-SEM)	Acetone		92.8% (v/v)
	Osmium tetroxide		2.0% (w/v)
	Uranyl acetate		0.2% (w/v)
	H_2O		5.0% (v/v)
Lead citrate solution	$Pb(NO_3)_2$		80.0 mM
	Na_3-citrate		100.0 mM
	NaOH (1N, free of CO_2)		16% (v/v)
	Use water free of CO_2. Adjust pH 11.5.		
PBS glycine	Glycine in 10 ml PBS	0.01 g	0.1% (w/v)
	Store at 4°C.		
PBS-BSA 1%	BSA in 10 ml PBS	0.10 g	1.0% (w/v)
	Store aliquots at -20°C.		
PBS-BSA 0.1%	PBS-BSA 1% in 10 ml PBS	1.00 ml	0.1% (w/v)
	Dilute immediately before use.		

Table VII: List of buffers and (stock) solutions - continued.

Buffer/solution	Chemical agent	Amount	Concentration
PBS-GA	Glutardialdehyde in 1 ml PBS	80.00 µl	2.0% (v/v)
	Prepare immediately before use.		
PBG	NaCl	8.00 g	137.0 mM
	KCl	0.20 g	2.7 mM
	Na_2HPO_4	1.40 g	10.0 mM
	KH_2PO_4	0.24 g	1.76 mM
	Gelatine	2.00 g	0.2% (w/v)
	BSA	5.00 g	0.5% (w/v)
	Adjust pH 7.4 with 1M NaOH.		
PBG-GA	Glutardialdehyde in 1 ml PBG	80.00 µl	2.0% (v/v)
	Prepare immediately before use.		
Dialysis membrane buffer	$NaHCO_3$	8.40 g	100.0 mM
	Na_2-EDTA	0.27 g	1.0 mM
	NaCl	0.88 g	15.0 mM
	Na_3-citrate	0.44 g	1.5 mM
	Cut dialysis membranes into pieces and stir for 15 min in $NaHCO_3$/Na_2-EDTA at 100°C. Rinse with water. Autoclave in NaCl/Na_3-citrate and store at 4°C.		
Basal salt solution	NaCl	14.00 g	239.5 mM
	$MgSO_4 \times 7\ H_2O$	7.00 g	28.4 mM
	KCl	0.35 g	4.7 mM
TE buffer pH 7.5	Tris/HCl	1.21 g	10.0 mM
	Na_2-EDTA	0.27 g	1.0 mM
TA buffer pH 6.0	Tris/Glacial acetic acid	2.42 g	20.0 mM
Lower Tris Buffer pH 8.8	Tris	181.71 g	1.5 M
	SDS	4.00 g	0.4% (w/v)
Upper Tris Buffer pH 6.8	Tris	60.57 g	500.0 mM
	SDS	4.00 g	0.4% (w/v)
Electrophoresis Buffer	Tris/HCl pH 8.5	3.03 g	25.0 mM
	Glycin	15.01 g	200.0 mM
	SDS	1.00 g	0.1% (w/v)
Loading dye (100 ml) 2-fold	Tris/HCl pH 7.5	0.73 g	60.0 mM
	Glycerol	10.00 ml	10.0% (v/v)
	SDS	2.00 g	2.0% (w/v)
	Bromphenol blue	10.00 mg	0.01% (w/v)
	2-mercaptoethanol	5.00 ml	5.0% (v/v)
	For long-term storage prepare loading without 2-mercaptoethanol.		
Coomassie staining	Coomassie Brilliant Blue G250	2.50 g	0.25% (w/v)
	Methanol	300.00 ml	30.0% (v/v)
	Acetic acid	100.00 ml	10.0% (v/v)
Coomassie destaining	Methanol	300.00 ml	30.0% (v/v)
	Acetic acid	100.00 ml	10.0% (v/v)
Silver fixation	Methanol	500.00 ml	50.0% (v/v)
	Acetic acid	100.00 ml	10.0% (v/v)
Silver washing I	Ethanol	500.00 ml	50.0% (v/v)
Silver washing II	Ethanol	100.00 ml	10.0% (v/v)

Table VII: List of buffers and (stock) solutions - continued.

Buffer/solution	Chemical agent	Amount	Concentration
Silver blocking (90 ml)	$Na_2S_2O_3 \times 5\ H_2O$	20.00 mg	0.022 % (w/v)
	Prepare immediately before use. 90 ml sufficient for two minigels.		
Silver staining (100 ml)	$AgNO_3$	0.10 g	0.1% (w/v)
	Formaldehyde, 37.0% (v/v)	75.00 µl	
	Prepare immediately before use. 100 ml sufficient for two minigels.		
Silver developing (100ml)	Na_2CO_3	6.00 g	6.0% (w/v)
	Formaldehyde, 37.0% (v/v)	50.00 µl	
	Prepare immediately before use. 100 ml sufficient for two minigels.		
Silver stopping	Acetic acid	100.00 ml	10.0% (v/v)
PAS fixation	Ethanol	400.00 ml	40.0% (v/v)
	Acetic acid	50.00 ml	5.0% (v/v)
PAS oxidation (100 ml)	Periodic acid	0.70 g	0.7% (w/v)
	Acetic acid	5.00 ml	5.0% (v/v)
PAS reduction (100 ml)	$Na_2S_2O_5$	0.20 g	0.2% (w/v)
	Acetic acid	5.00 ml	5.0% (v/v)
PAS destaining	$Na_2S_2O_5$	1.00 g	0.1% (w/v)
	Acetic acid	50.00 ml	5.0% (v/v)
Gel drying buffer	Ethanole	220.00 ml	22.0% (v/v)
	Glycerol	20.00 ml	2.0% (v/v)
	Isopropanol	10.00 ml	1.0% (v/v)
Semidry blotting buffer (Towbin et al., 1979)	Tris	3.03 g	25.0 mM
	Glycin	14.41 g	192.0 mM
	Methanol p.A.	200.00 ml	20.0% (v/v)
	Prepare immediately before use.		
Tris buffered saline (TBS)	Tris/HCl pH 7.6	2.42 g	20.0 mM
	NaCl	8.00 g	137.0 mM
TBS-T	For TBS-T, add 0.1% (v/v) Tween® 20 to TBS.		
Blocking buffer	Milk powder in 50 ml TBS-T	5.00 g	10.0% (w/v)
3-amino-9-ethylcarbazole solution	3-amino-9-ethylcarbazole	20.00 mg	
	Ethanol p.a.	1.00 ml	
	Potassic acetate solution pH 5.0	50.00 ml	20.0 mM
	Triton X-100 10%	100.00 µl	
	H_2O_2	10.00 µl	
	Dissolve 3-amino-9-ethylcarbazole in ethanol, and mix with potassic acetate solution. Filter through a folded filter. Add Triton X-100 and H_2O_2 immediately before use.		
PIV buffer pH 7.5	Tris/HCl	1.21 g	10.0 mM
	NaCl	58.44 g	1.0 M
EC lysis buffer pH 7.5	Tris/HCl	0.73 g	6.0 mM
	NaCl	58.44 g	1.0 M
	Na_2-EDTA	27.22 g	100.0 mM
	Brij 58	5.00 g	0.5% (w/v)
	Desoxycholate	2.00 g	0.2% (w/v)
	N-Lauroylsarcosine	5.00 g	0.5% (w/v)
	Prepare buffer just before use. Adjust pH with 10 N NaOH to 8.0. Add RNase after autoclaving to a final concentration of 20 µg/ml.		

Table VII: List of buffers and (stock) solutions - continued.

Buffer/solution	Chemical agent	Amount	Concentration
ESP buffer	Na_2-EDTA	186,12 g	500.0 mM
	N-Lauroylsarcosine	10.00 g	1.0% (w/v)
	Add Proteinase K before use to a final concentration of 1 mg/ml.		
TNE	Tris/HCl pH 8.0	12.11 g	100.0 mM
	NaCl	2.92 g	50.0 mM
	Na_2-EDTA	18. 61 g	50.0 mM
Buffer A	Tris/HCl pH 8.0	60.57 g	500.0 mM
	NaCl	5.84 g	100.0 mM
	Na_3 citrate	0.29 g	1.0 mM
Buffer B	Tris/HCl pH 8.0	60.57 g	500.0 mM
	NaCl	5.84 g	100.0 mM
	SDS	4.00 g	4.0% (w/v)
NaCl/CTAB (1.0 ml)	NaCl	0.29 g	5.0 M
	CTAB	0.10 g	10% (w/v)
	Heat up to 65°C to solve.		

9 Media

Media compositions are given for one liter, the solvent is H_2O. The pH was measured at room temperature and adjusted with NaOH or H_2SO_4.

Table VIII: List of media.

Medium	Chemical agent	Amount	Concentration
MGG	NaCl	18.00 g	308.0 mM
(Bellack et al., 2011)	$NaHCO_3$	5.50 g	65.5 mM
	$MgCl_2 \times 6\ H_2O$	4.30 g	21.2 mM
	$MgSO_4 \times 7\ H_2O$	3.40 g	13.8 mM
	KCl	0.35 g	4.7 mM
	NH_4Cl	0.25 g	4.7 mM
	$CaCl_2 \times 2\ H_2O$	0.14 g	1.0 mM
	K_2HPO_4	0.14 g	0.8 mM
	$(NH_4)_2Fe(SO_4)_2 \times 6\ H_2O$	2.00 mg	5.1 µM
	10-fold trace mineral solution	1.00 ml	-
	Resazurin, 0.1% (w/v)	1.00 ml	-
	$Na_2S \times 3\ H_2O$	0.25 g	-
MJ	NaCl	30.00 g	513.4 mM
(Bellack et al., 2011)	$NaHCO_3$	1.00 g	11.9 mM
	$MgCl_2 \times 6\ H_2O$	4.10 g	20.2 mM
	$MgSO_4 \times 7\ H_2O$	3.40 g	13.8 mM
	KCl	0.33 g	4.4 mM
	NH_4Cl	0.25 g	4.7 mM
	$CaCl_2 \times 2\ H_2O$	0.14 g	1.0 mM
	K_2HPO_4	0.14 g	0.8 mM
	$(NH_4)_2\,Fe(SO_4)_2 \times 6\ H_2O$	10.00 mg	26.0 µM
	$NiCl_2 \times 6\ H_2O$	0.50 mg	2.0 µM
	10-fold trace mineral solution	1.00 ml	-
	10-fold vitamin solution	1.00 ml	-
	Resazurin, 0.1% (w/v)	1.00 ml	-
	$Na_2S \times 3\ H_2O$	0.25 g	-

Table VIII: List of media - continued.

Medium	Chemical agent	Amount	Concentration
Methanococcus medium for fermentors	NaCl	25.14 g	430.0 mM
	$NaHCO_3$	0.84 g	10.0 mM
	$MgCl_2 \times 6\ H_2O$	7.72 g	38.0 mM
	KCl	0.27 g	3.6 mM
	NH_4Cl	1.18 g	22.1 mM
	$CaCl_2 \times 2\ H_2O$	0.37 g	2.5 mM
	K_2HPO_4	55.60 mg	0.3 mM
	KH_2PO_4	55.80 mg	4.1 mM
	$(NH_4)_2\,Fe(SO_4)_2 \times 6\ H_2O$	12.00 mg	30.6 µM
	$(NH_4)_2\,Ni(SO_4)_2 \times 6\ H_2O$	17.20 mg	43.5 µM
	$Na_2MoO_4 \times 2\ H_2O$	2.44 mg	10.1 µm
	$Na_2WO_4 \times 2\ H_2O$	3.28 mg	9.9 µM
	Na_2SeO_4	8.00 mg	42.3 µM
	Modified 10-fold trace mineral solution	1.00 ml	-
	$Na_2S \times 7\text{-}9\ H_2O$	0.40 g	-
SME (Stetter et al., 1983)	NaCl	27.7 g	474.0 mM
	$MgSO_4 \times 7\ H_2O$	7.00 g	28.4 mM
	$MgCl_2 \times 6\ H_2O$	5.50 g	27.1 mM
	$CaCl_2 \times 2\ H_2O$	0.75 g	5.1 mM
	KCl	0.65 g	8.7 mM
	NaBr	0.10 g	1.0 mM
	H_3BO_3	0.03 g	0.5 mM
	$SrCl_2 \times 6\ H_2O$	15.00 mg	56.3 µM
	KJ solution, 0.1%	0.10 ml	0.6 µM
½ SME	K_2HPO_4	0.50 g	2.9 mM
	NH_4Cl	0.50 g	9.4 mM
	10-fold trace mineral solution	1.00 ml	-
	Resazurin, 0.1% (w/v)	1.00 ml	-
	$Na_2S \times 3\ H_2O$	0.25 g	-
addition of	Peptone	1.00 g	-
	Yeast extract	1.00 g	-
	Starch	1.00 g	-
	Dissolve reagents (by default without starch) in 500.00 ml SME.		
Trace mineral solution 10-fold (Huber and Stetter, 2006)	$MgSO_4 \times 7\ H_2O$	30.00 g	121.7 mM
	NaCl	10.00 g	171.1 mM
	$MnSO_4 \times H_2O$	5.00 g	29.6 mM
	$(NH_4)_2Ni(SO_4)_2 \times 6\ H_2O$	2.80 g (20.00 g)	7.1 mM
	$CoSO_4 \times 7\ H_2O$	1.80 g (1.00 g)	6.4 mM
	$ZnSO_4 \times 7\ H_2O$	1.80 g (1.00 g)	6.3 mM
	$FeSO_4 \times 7\ H_2O$	1.00 g	3.6 mM
	$CaCl_2 \times 2\ H_2O$	1.00 g	6.8 mM
	$AlK\ (SO_4)_2 \times 12\ H_2O$	0.18 g (0.10 g)	0.4 mM
	$CuSO_4 \times 5\ H_2O$	0.10 g	0.4 mM
	H_3BO_3	0.10 g	1.6 mM
	$Na_2MoO_4 \times 2\ H_2O$	0.10 g	0.4 mM
	$Na_2WO_4 \times 2\ H_2O$	0.10 g (0.05 g)	0.3 mM
	Na_2SeO_4	0.10 g (0.05 g)	0.5 mM
	Titrate pH 1.0 with 1 M H_2SO_4 before solving chemicals. Filter sterilize and store in the dark at 4°C. Use amounts given in parantheses for the modified solution (for fermentors).		

Table VIII: List of media - continued.

Medium	Chemical agent	Amount	Concentration
Vitamin solution	Pyridoxine hydrochloride (vitamin B_6)	0.10 g	386.0 µM
10-fold	Thiamine hydrochloride (vitamin B_1)	50.00 mg	148.0 µM
(Balch et al., 1979)	Riboflavin (vitamin B_2)	50.00 mg	133.0 µM
	Nicotinic acid	50.00 mg	406.0 µM
	DL-Calcium pantothenate	50.00 mg	105.0 µM
	p-aminobenzoic acid (PABA)	50.00 mg	365.0 µM
	Lipoic acid	50.00 mg	242.0 µM
	Biotin	20.00 mg	81.9 µM
	Folic acid	20.00 mg	45.3 µM
	Cyanocobalmin (vitamin B_{12})	1.00 mg	3.7 µM
	Filter sterilize and keep in the dark at 4°C.		
LB	NaCl	10.00 g	171.1 mM
	Peptone	10.00 g	-
	Yeast Extract	5.00 g	-
	Agar (for plates)	15.00 g	-
antibiotics	Ampicillin stock	5.00 ml	100 µg/ml
	Chloramphenicol stock	1.00 ml	34 µg/ml
	Adjust pH 7.2 before autoclaving.		

10 Organisms

Table IX: Archaea and host bacteria.

Archaea	Strain	DSM-No.	Reference	Supplier[a]	Temp in °C[b]	Medium
Methanocaldococcus fervens	AG86	4213	Jeanthon et al., 1999	DSMZ	85	MJ
Methanocaldococcus indicus	SL43	15027	L'Haridon et al., 2003	DSMZ	85	MJ
Methanocaldococcus infernus	ME	11812	Jeanthon et al., 1998	DSMZ	85	MJ
Methanocaldococcus jannaschii	JAL-1	2661	Jones et al., 1983	DSMZ	85	MGG[h]/MJ
Methanocaldococcus vulcanius	M7	12094	Jeanthon et al., 1999	DSMZ	80	MJ
Methanocaldococcus sp.[c]	KIN24-T80	22612	Bellack, 2007	IHCC[g]	80	MGG/MJ
Methanotorris igneus	Kol5	5661	Burggraf et al., 1990	IHCC[g]	85	MGG/MJ
Pyrococcus furiosus	Vc1[d]	3638	Fiala and Stetter,1986	DSMZ	95	½ SME
	Vc1[e]	-	-	IHCC	95	½ SME
	Vc1[f]	-	-	L	95	½ SME

Host bacteria	Genotype	Temp in °C	Medium
Escherichia coli DH5α	F-, *deo*R, *end*A1, *gyr*A96, *hsd*R17, (rk-mk+), *rec*A1, *rel*A1, *sup*E44, Φ80*lac*ZΔM15, *thi*-1, Δ(*lac*ZYA-*arg*FV169)	37	LB
Escherichia coli Rosetta(DE3)pLysS	F^- *ompT hsdS*$_B$ (r_B^- m_B^-) *gal dcm* (DE3) pLysS RARE2^C(Cam^R)	37	LB

[a] DSMZ German Collection of Microorganisms and Cell Cultures; Braunschweig, Germany, IHCC in-house culture collection; Institute of Microbiology and Archaea Center, University of Regensburg, Germany, L continuous culture in the laboratory

[b] Organisms were incubated at their optimal growth temperature as given in the reference. Exception: Optimal growth temperature of *M. igneus* is 88°C and of *P. furiosus* 100°C.

[c] Described as new species *M. villosus* (Bellack et al., 2011)

[d] Named *P. furiosus* DSM 3638^T in this thesis

[e] Named *P. furiosus* Vc1 in this thesis

[f] Named *P. furiosus* LS in this thesis

[g] Originally isolated at our institute

[h] MGG medium has to be complemented with vitamin solution

4 Methods

1 Sterilization procedures

Media and heat-stable buffers were sterilized by autoclaving for 20 min at 121°C and 200 kPa. Glyerol and DMSO were autoclaved for 1 h at 100°C. For solid items, the procedure was prolonged to 40 min or reduced to 15 min for centrifugation tubes; materials were dried afterwards at 60°C for at least 12 h. Glass pipets were dry heat sterilized for 4 h at 160°C. Heat-sensitive liquids were filter sterilized.

2 Cultivation of anaerobes

2.1 Preparation of media

Anaerobic media were prepared according to the anaerobic technique described by Balch and Wolfe (1976). Chemicals were dissolved in water and gased with either N_2 (media without $NaHCO_3$) or N_2/CO_2 (media with $NaHCO_3$). After reduction by adding sodium sulfide, the pH was adjusted and media were portioned into 100 ml serum bottles (20 ml aliquots) with N_2/CO_2 for *Pyrococcus furiosus* (200 kPa; 80:20, v/v) or H_2/CO_2 for *Methanocaldococcaceae* (250 kPa; 80:20, v/v) as gas phase.

Media for 1-L bottles were prepared as described for serum bottles except using aliquots of 200 ml for *Methanocaldococcaceae* and 500 ml for *P. furiosus*, respectively, and a lower gas pressure (maximum of 200 kPa).

For large scale cultivation in fermentors, organisms were grown in media designed for the fermentation process. Media were autoclaved in the fermentor; organic compounds, minerals, vitamins, sodium sulfide, and acids/bases for pH adjustment were sterilized separately and added sterile afterwards. Fermentors were pressurized (200 kPa) before inoculation. Grown cultures were cooled down and harvested by centrifugation in a continuous centrifuge with a through-flow rate of 100 ml/min at 8,000–9,000 × g.

2.2 Cultivation

Unless stated otherwise, routine incubation was done in serum bottles, and cells were grown over night with agitaion at their optimal growth temperatures resulting in stationary cultures. Inoculation volumes were 1:100 for serum bottles, 1:200 (methanogens) or 1:500 (*P. furiosus*) for 1-L bottles, and 1:20,000 (*Methanocaldococcus villosus*) or 1:250,000 (*P. furiosus*) for fermentors. Cell densities of grown cultures were determined by direct cell counting using a Thoma counting chamber.

2.3 Growth experiments

To ascertain the pH dependence of the growth of *M. villosus*, medium was prepared as described above. After autoclaving, pH of the medium was adjusted with sterile diluted sulphuric acid or sodium hydroxide to pH 5.0–8.0 (pH steps of 0.5; pH indicator stripes) without usage of additional buffers.

For testing a requirement or stimulus of trace elements or organic compounds for growth of *M. villosus*, MGG medium was prepared as described above but without trace minerals (= MGG-M medium). The following sterilized substances were added after autoclaving individually or in combination: yeast extract (0.1 g/l), selenate (0.05 g/l), tungstate (0.05 g/l), 1-fold trace mineral solution (10 ml/l), 1-fold vitamin solution (10 ml/l). Additionally, medium was prepared with a trace mineral solution that did not include tungstate and selenate. To remove traces of the minerals, all equipment was rinsed extensively with $H_2O_{millipore}$ before use.

2.4 Adhesion studies

For adhesion studies, medium was prepared as described above but before aliquoting grids for electron microscopy placed in Teflon holders (~ 9 mm × 22 mm × 3.8 mm; with four holes) were added to the serum bottles. To prevent adaption of organisms to growth on surfaces, inoculation was done with cells from cultures without any solid support. Serum bottles with grids were incubated horizontally under shaking to different growth phases. After counting planktonic cells and, mostly, fixation with glutardialdehyde, grids were analyzed by either fluorescent labeling and microscopy or electron microscopy.

2.5 Long-term storage

For long-term storage, cells were anaerobically centrifuged (3,000 × g, 30 min; Megafuge) in rubber stopped glass bottles and resuspended in fresh culture medium containing 5% (v/v) DMSO. The cell suspension was filled into glass capillaries, which were heat sealed and stored over liquid nitrogen at our in-house culture collection. Cultures were checked for regrowth after at least five days of storage: A glass capillary was opened sterile, and cells were serially diluted into growth medium (undiluted, 1:20, 1:400).

Furthermore, *M. villosus* was deposited at the Japan Collection of Microorganisms (Riken BRC, Saitama, Japan) and at the German Collection of Microorganisms and Cell Cultures (DSMZ, Braunschweig, Germany), respectively.

3 Cultivation of *Escherichia coli*

3.1 Preparation of media and cultivation

Chemicals were dissolved in water and LB medium was filled either into test tubes and sealed with aluminium caps or into Erlenmeyer flasks to a maximum of 20% and sealed with cellulose stoppers. If necessary, antibiotics were added to the medium after autoclaving and cooling to 55°C. For preparation of solid media, agar was added to a concentration of 1.5% (w/v) before autoclaving.
For inoculation, cells were scraped from a glycerol stock, or a single colony was picked. By default, *E. coli* was incubated overnight at 37°C – plates in an incubator, test tubes in a Rollerdrum, and Erlenmeyer flasks in a water bath shaker.

3.2 Long-term storage

E. coli hosts or positive clones were stored as glycerol stocks. Thereto, glycerol was aliquoted à 500 µl in cryovials and autoclaved. Cells were harvested by centrifugation (5,000 × g, 15 min; Labofuge GL), resuspended in 500 µl sterile culture medium and pipeted into the cryovials containing glycerol. Vials were stored at -20°C.

4 Microscopic preparation techniques

Most of the preparation techniques for electron microscopy used herein were summarized by Rachel *et al.* (2010) or were given in Jogler et al. (2011). This section emphasizes the methods optimized for the organisms and scientific setups of this study.

4.1 Fluorescent staining

4.1.1 DAPI and Calcofluor staining

DAPI forms a fluorescent complex when bound to AT-rich DNA sequences and staining was used as a first approach to detect cells grown on grids for adhesion studies. For that, glutardialdehyde was added to a culture containing grids to a final concentration of 1% (v/v), and cells were fixed for 10–15 min. Non-adherent cells were removed by briefly washing the grid on a drop of PBS. Grids were placed onto a glass slide with 2 µl of DAPI solution and 3 µl of PBS, and were analyzed immediately by epifluorescence microscopy.
Calcofluor indicates the presence of β-glycosidic polysaccharides and staining was performed to firstly analyze EPS production of adherent cells. Preparation was the same as described for DAPI, except that the final concentration of glutardialdehyde was 0.25% (v/v) and staining was with 5 µl of Calcofluor solution.

4.1.2 Alexa Fluor® staining

A) Staining of adherent cells

The staining of microorganisms with fluorescence dyes was described previously by our group (Wirth et al., 2011) and was adapted for cells grown on a surface.

Portioned Alexa Fluor® dyes (~ 83 µg) were dissolved in 500 µl PBS and supplemented with 25 µl of 1 M $NaHCO_3$ to raise the pH to 8.0–8.5 for optimal coupling of the dye with free $–NH_2$ groups, particularly those of lysines (Haugland, 2005). Grids with adherent cells (non-fixed) were removed from serum bottles, washed in two drops of PBS and added to the vial containing the dye. Incubation was performed protected from light for 1 h at room temperature with gentle agitation (100 rpm; Thermomixer). Grids were washed three times in a drop of PBS to remove unbound dye and were stored shaded in PBS until examined by confocal microscopy.

B) Labeling of antibodies with Alexa Fluor® 488

Labeling of antibodies was performed with the Alexa Fluor® 488 Protein Labeling Kit according to the manufacturer's instructions.

Concentration of protein in the sample was calculated from NanoDrop measurment of the labeled protein at 280 and 494 nm using the formula:

$$\text{protein concentration (M)} = \frac{[A_{280} - (A_{494} \times 0.11)] \times \text{dilution factor}}{203{,}000}$$

Therewith, the degree of labeling was calculated:

$$\text{moles dye per mole protein} = \frac{A_{494} \times \text{dilution factor}}{71{,}000 \times \text{protein concentration (M)}}$$

The optimal degree of labeling for IgG's should be 4–9 moles of Alexa Fluor® 488 dye per mol of antibody. The labeled protein was stored at -20°C.

C) Labeling of cells with antibodies coupled with Alexa Fluor® dyes

Primary antibodies coupled with Alexa Fluor® dye were diluted 1:200 in PBS. Grids with non-fixed adherent cells were washed twice in a drop of PBS and added to the antibody dilution. The sample was incubated in the dark for 1 h at 37°C, and grids were washed afterwards three times in PBS.

For signal enhancement, the secondary antibody was coupled with AlexaFluor® dye. Grids were incubated in a 1:100 dilution of the primary antibody (in PBS) for 1 h at 37°C, washed three times in a drop of PBS and labeled with the secondary antibody (1:10 in PBS). Incubation was for 1 h at 37°C protected from light.

4.2 Uranyl acetate staining

1 ml freshly grown cells were fixed with glutardialdehyde [final concentration 1% (v/v)] for 10 min and centrifuged using a table-top centrifuge (3,000–14,000 × g, 10 min). The pellet was resuspended in 10–50 µl medium, the suspension was applied onto a glow-discharged carbon-coated copper grid, left for 30–60 s, and blotted with a filter paper. In case of grids incubated for adhesion studies, glutardialdehyde was directly added to serum bottles [final concentration 1% (v/v)] and cells were fixed for 15 min. Both, suspensions and grids for adhesion studies were washed briefly on a drop of water (or a suitable buffer if the fixation step was omitted) once or twice, depending on the salt concentration and/or organic compounds in the culture medium. The grid was placed with the sample side on a drop of uranyl acetate solution for 30–60 s, blotted with filter paper and air-dried.

4.3 Freeze etching

Cells were pelleted by centrifugation using a table-top centrifuge (3,000 × g, 10 min) and resuspended in 10 µl medium. 2 µl of the suspension was applied onto a cleaned gold specimen carrier (BAL-TEC, Witten, Germany). The sample was cryofixed immediately in liquid nitrogen at -196°C; the carrier was mounted on a precooled specimen transfer holder under liquid nitrogen and transferred into the precooled, ultra-high vacuum freeze etch unit (at least -170°C, $p < 10^{-6}$ mbar). Further preparation was performed by Andreas Klingl and is provided in his PhD thesis (Klingl, 2011); key parameters are described here.

The specimen transfer holder was warmed to -97°C. After 7 min (to ensure temperature adaption) the specimen was freeze-fractured with a cold knife (-180°C), and surface water was sublimated with a precooled copper block for 3.5–4 min. The specimen was shadowed immediately with 1 nm Pt/C (45°, unidirectional) and 10 nm C (90°). The holder was removed from the freeze-etch unit and gold carriers were immersed into freshly diluted 70% (v/v) sulfuric acid. After incubation overnight, replicas were washed twice for 30 min in H_2O_{bidest} and transferred onto hydrophilized 700 mesh hexagonal copper grids.

4.4 Metal shadowing

Metal shadowing of flagella together with Phalloidin-stabilized F-actin (sample: gift from Edward H. Egelman, Department of Biochemistry and Molecular Genetics, University of Virginia, VA, US) was performed by Reinhard Rachel (Center for Electron Microscopy/ Anatomy, University of Regensburg, Germany). After application onto carbon-coated grids, specimens were frozen in liquid N_2, freeze-dried at -80°C for 2 h, and shadowed with 1 nm Pt/C (45°) and 3 mm C (90°) by electron-gun evaporation.

4.5 Chemical fixation of cells for electron microscopy

Preparation of specimens was performed in the group of Gerhard Wanner (Ultrastructural research group, Botany Department, LMU Munich, Germany).

Harvested and concentrated cells of *M. villosus* were incubated for 2 d in an appropriate volume of fixative buffer (with 340 mM or 480 mM NaCl for cells grown either in MGG or MJ) supplemented with 2.5% (v/v) glutardialdehyde. After rinsing four times in fixative buffer (10 min, 15 min, 30 min, 1 h), specimens were postfixed for 2.5 h with 1% (w/v) osmium tetroxide in fixative buffer. Samples were then washed twice with fixative buffer (10 min, 60 h) and three times with distilled water (10 min, 20 min, 1 h). Cells were stained *en bloc* for 30 min with 1% (w/v) uranyl acetate in 20% acetone and dehydration was performed with a graded series of acetone solutions. Samples were then embedded in Spurr's low-viscosity resin and analyzed by electron microscopy.

For scanning electron microscopy (SEM), harvested cells were dropped onto a glass slide and covered with a cover slip. After rapidly freezing in liquid N_2, the cover slip was removed using a razor blade and the glass slide was immediately fixed with 2.5% (v/v) glutardialdehyde in 75 mM cacodylate pH 7.0. Specimens were then postfixed in 1% (w/v) osmium tetroxide in fixative buffer and dehydrated in graded acetone series. This was followed by transfer to liquid CO_2, critical-point drying, mounting onto stubs, and subsequent coating with 3 nm platinum using a magnetron sputter coater.

4.6 High-pressure freezing, freeze-substitution, and embedding

4.6.1 Preparation for transmission electron microscopy

1 ml of freshly grown cells was harvested using a table-top centrifuge (3,000 × g, 10 min), resuspended in 10 µl medium and directly applied onto a gold-plated flat specimen carrier (depth 200 µm, 1.2 mm in diameter; Leica, Wetzlar, Germany). Further preparation was done by Carolin Meyer and is briefly summarized below (Meyer, 2010).

The carrier was fixed in the appropriate holder and high-pressure frozen at about 210 MPa in liquid N_2 using an EM PACT2. Specimens were transferred under liquid nitrogen to the freeze-substitution facility EM AFS2 containing the precooled (-140°C) substitution solution and freeze-substituted. The standard procedure was: -90°C for 30 h, -60°C for 8 h, -30°C for 8 h, and 0°C for 3 h, and the temperature was raised between the steps for 5°C per hour. The ice-cooled samples were rinsed three times with pure ice-cold acetone and infiltrated consecutively with Epon:acetone (1:1) for 2 h, Epon:acetone (2:1) overnight at room temperature, and freshly prepared Epon for 2 h at 30°C and for 2 d at 60°C. After

polymerization, resin around the flat specimen carrier was cut with a razor blade and the carrier was removed by cooling in liquid N_2 and heating on a hot plate.

4.6.2 Preparation for scanning electron microscopy

For focused ion beam (FIB) scanning electron microscopy (SEM), high cell densities are recommended. On that account, 60 ml of logarithmic cells or 40 ml of stationary cells were harvested by centrifugation (5,000 × g, 10 min), concentrated using a tabletop centrifuge (6,000 × g, 10 min) and resuspended in 50 µl supernatant. Further preparation was done by Silvia Dobler (lab of Gerhard Wanner, LMU Munich), differences to 4.6.1 are given.
High-pressure freezing was done with a Leica HPM100. Freeze-substitution was: -90°C for 24 h, -60°C for 7 h, and -30°C for 7 h; temperature was raised between the steps with 15°C per hour. The samples were washed twice with pure acetone for 45 min and 30 min and embedded in Spurr:acetone (1:1) for 1 h, Spurr:acetone (2:1) for 45 min and pure Spurr for 1 h and 3 h.

4.7 Ultramicrotomy and contrasting of sections

Ultrathin sections were prepared with either a Reichert-Jung UltraCut E or an EM UC6 using a diamond knife with a knife-angle of 35° or 45°. For doing so, the resin block with embedded cells was clamped in an ultramicrotomy carrier and trimmed with a razor blade. The cutting edge was adjusted parallel to the diamond blade, and sectioning was controlled using a binocular. Ultrathin sections (50–70 nm thick) appearing silver-grey on the water surface were transferred onto copper grids (400 × 100 mesh) and air-dried. For contrasting, grids were applied onto a drop of uranyl acetate for 30 min, washed twice in H_2O_{bidest}, incubated with lead citrate solution for 1 min, and washed in H_2O_{bidest} three times.
For immuno-labeling, resin-embedded cells were ultrathin sectioned by Cornelia Niemann one day before or at the day of labeling and applied onto nickel grids. After labeling, contrasting was performed with uranyl acetate for 30 min.

4.8 Immuno-labeling

4.8.1 Immuno-labeling for electron microscopy

Immuno-labeling for electron microscopy was achieved with ultrathin sections and grids with adherent cells. All solutions were dropped step-by-step onto parafilm, on which the grids were placed with the sample facing downwards. Antibody dilutions were prepared freshly and centrifuged (13,000 × g, 3 min; table-top centrifuge) before use. Negative controls were prepared by incubation in 0.1% (w/v) PBS-BSA without primary antibody.

Table X: Immuno-labeling scheme of ultrathin sections and cells adherent to gold grids.

	Ultrathin sections		Gold grids with adherent cells	
	Buffer	Time	Buffer	Time
Saturation of aldehydes	PBS glycine	5 min	-	-
Washing	-	-	growth medium	3 × 2 min
Blocking	PBS-BSA 1%	5 min	PBG	5 min
Primary Antibodies	in PBS-BSA 0.1%	45–60 min	in PBG	25 min
Washing	PBS-BSA 0.1%	5 × 2 min	PBG	3 × 2 min
Secondary Antibodies	in PBS-BSA 0.1%	60 min	in PBG	45 min
Washing	PBS-BSA 0.1%	5 × 2 min	PBG	3 × 2 min
Washing	PBS	2 × 2 min	-	-
Cross-linking of epitops and antibodies	PBS-GA	5 min	PBG-GA	2 min
Washing	PBS	2 × 2 min	PBG	2 × 2 min
Washing	H_2O	3 × 2 min	H_2O	2 × 1 min

4.8.2 Detachment studies

Previous studies in our group have shown that *P. furiosus* and *Methanothermobacter thermoautothrophicus* detach from a surface if antibodies against their cell appendages were added (Näther et al., 2006; Thoma et al., 2008). A similar approach was performed with *M. villosus* grown on carbon-coated gold grids to test if its flagella are functional adhesins. For this purpose, grids were removed from overnight cultures and were checked for adherent cells by phase contrast light microscopy. Grids were then added to one of the following *M. villosus* whole-flagella antibody solutions: antibodies diluted 1:50, 1:100, 1:250, and 1:500 in aerobically prepared growth medium. Preparations were incubated at room temperature with agitation (600 rpm; Thermomixer) for 90 min. Grids were transferred to fresh aerobically prepared growth medium and shaken for another 5 min. Negative controls were performed without antibodies and with anti-Fla Pfu antibodies. Grids were analyzed either by DAPI staining or electron microscopy.

5 Microscopy

5.1 Phase contrast and epifluorescence microscopy

For phase contrast light microscopy, a Nikon Labophot-2 was used with 10 × ocular lenses and 40 × objective lenses (n = 0.65) or 100 × oil immersion objective lenses (n = 1.25). All of the following microscopes were equipped with a mercury light source (HBO 50 DC3). The methanogen-specific fluorescence was detected using a Nikon Microphot. DAPI and Alexa Fluor® staining was recorded with an Olympus BX50, digital images were taken with either a pco.pixelfly or a pco.1600 camera controlled by the CamWare® software. Analysis of Calcofluor staining together with the methanogen fluorescence was performed using an Olympus BX60.

Table XI: Filter sets

Dye	Mirror Unit	Excitation filter	Beam splitter	Emission filter
Calcofluor/DAPI	MNU2	360370	DM 400	Sperr 420
Cofactor F420	MWBV2	BP 400-440	DM 455	Sperr 475
Alexa Fluor® 488	F41-054	HQ 480 ± 20	Q 505 LT	HQ 520 ± 15
Alexa Fluor® 555	F41-003	HQ 546 ± 6	Q 560 LT	HQ 585 ± 20

5.2 The optical tweezer

Single cell isolation of *M. villosus* was achieved by utilizing the optical tweezer technique (Huber et al., 1995a). The inverted microscope Axiovert IM35 is equipped with an oil immersion objective (100/1.3) and a strongly focused ND-YAG laser (wavelength 1064 nm; output power 2.5 W; ADLAS, Lübeck, Germany).

The cell seperation unit was filled anaerobically with sterile medium and mid-logarithmic cells and fixed to the microscope stage. An optically trapped single cell was separated from other cells by movement of the microscopic stage and inoculated into fresh culture medium. Cultures were incubated for seven days or until growth was detected.

5.3 Confocal laser scanning microscopy

For confocal laser scanning microscopy (CLSM), the inverse Laser Scanning Microscope 510 Meta (Department of Cell Biology and Plant Biochemistry, University of Regensburg, Germany) was used. The microscope was controlled via the LSM 510 software package (Zeiss, Munich, Germany).

Grids with adherent cells were analyzed with a Plan-Apochromat 100 × oil DIC objective (n = 1.4). For Alexa Fluor® 488 stained specimens, the excitation was set to 488 nm (Ar-laser) and the detection of emission to >505 nm long pass, while for Alexa Fluor® 555 the excitation was 543 nm (HeNe-laser) and the detection 560–615 nm band pass. 3D models were constructed from z-sections performed with a 50% overlap of 0.5 nm thick stacks.

5.4. Synchrotron radiation-based Fourier transform infrared (SR-FTIR) spectromicroscopy imaging and data analysis

Measurement was performed by Hoi-Ying N. Holman at the synchrotron infrared beamline at the Advanced Light Source (Lawrence Berkeley National Laboratory, CA, US). Used in its transflective mode, measuring and comparison of the chemistry changes in the EPS production of adherent *M. villosus* cells was allowed. SR-FTIR spectromicroscopy in the mid-infrared region (~2.5-5.5 µm wavelength, or ~4000–650 cm^{-1} wavenumber) is a label-free biochemical imaging technique with nanometer accuracy (Holman et al., 2010).

Cells were grown on gold-coated aperture discs in two different media (MGG or MJ). Afterwards, growth medium was completely removed from the disc, and cells were dry-fixed onto the surface under a stream of nitrogen gas. Mid-infrared photons emitted from the synchrotron were focused by the Nicolet Nic-Plan IR microscope with a numerical aperture objective of 0.65 (Thermo Scientific Inc., MA, US). Before raster scanning, the entire field of view was typically divided into 2 µm × 2 µm squares. In a reflectance mode, the infrared beam transmitted through the *M. villosus* cells, reflected off the gold-coated surface, and then transmitted through the cells a second time before reaching the highly sensitive single-element mercury cadmium telluride (MCT) detector. Background transflectance spectra were acquired from neighboring cell-free areas. Each transflectance spectrum represents an average of eight scans at a spectral resolution of 4 cm^{-1}. The absorption peak position accuracy is 1/100 cm^{-1}.

All recorded SR-FTIR transflectance spectra were subjected to an array of data preprocessing and processing calculations using Thermo Electron's Omnic version 7.3. Processing includes the computational conversion of transflectance to absorbance, spectrum baseline removal, and univariate analysis. Through the Beer-Lambert Law, the calculated infrared absorbance at each wavenumber in the mid-infrared region could be related to the relative concentration of a particular chemical component.

5.5 Transmission electron microscopy

5.5.1 Transmission electron microscopy

Transmission electron microscopy (TEM) was performed using a transmission electron microscope CM12 equipped with a LaB_6 cathode operated with 120 keV. Digital documentation was done with a slow scan CCD camera TEM-0124 controlled with the software EM-Menu 4. Images were processed with Adobe Photoshop CS4.

Ultrathin sections from resin-embedded cells, which were intended to be analyzed in 3D using FIB-SEM, were recorded with an EM912 electron microscope (Zeiss, Munich, Germany) by Gerhard Wanner (Ultrastructural research group, Botany Department, LMU Munich, Germany).

5.5.2 Cryo-electron microscopy and image processing

Cryo-EM was applied for 3D-reconstruction of flagella and was performed in cooperation with Edward E. Egelman and Xiong Yu (Department of Biochemistry and Molecular Genetics, University of Virginia, VA, US). For high resolution studies of frozen-hydrated, unstained flagella, a 200 keV Field Emission Gun (FEG) Tecnai F20 cryo-electron

microscope was used. The sample was cooled to or below -170°C in a liquid-nitrogen cooled cryo-transfer holder (626; Gatan Inc., Pleasanton, CA, US). Micrographs were taken at a magnification of 50,000 × and negatives were scanned with a Nikon Coolscan 8000 as 16 bit images using a raster of 2.4 Å/pixel.

For a preliminary three-dimensional reconstruction, electron micrographs of negatively stained flagella, taken with a pixel size of 0.46 nm at the CM12, were provided as full resolution 16-bit TIFF files to Edward H. Egelman. Microscopy data were analyzed and 3D reconstructions determined using the iterative helical real space reconstructions (IHRSR) algorithm (Egelman, 2007). Averaged power spectra were generated from overlapping segments, which were prior aligned and masked to improve the signal-to-noise ratio.

5.6 (Focused ion beam) scanning electron microscopy

All scanning electron microscopic studies were done by Gerhard Wanner (Ultrastructural research group, Botany department, LMU Munich, Germany).

Specimens prepared for scanning electron microscopy (SEM) were examined either with a Hitachi S-4100 using Digiscan hardware and Digital micrograph (Gatan, Pleasanton, CA, US) for image recording, or with a Zeiss Auriga (Zeiss, Munich, Germany). The high tension was varied between 1–1.5 keV.

Focused ion beam (FIB)-SEM was performed using a Zeiss-Auriga workstation with a FIB consisting of Ga^+ ions accelerated by a voltage of 30 kV. Depending on the magnification, sections ranging in the thickness of 5–10 nm were produced with the FIB in the cut-and-view mode. Field emission (FE)SEM images were recorded at 1.5 keV using an in-lens energy selective backscattered (EsB) detector. As specimens were tilted to an angle of 54°, images had to be tilt corrected for undistorted surface view.

6 Isolation and characterization of flagella

6.1 Preparation of flagella

Preparation of flagella of *M. villosus* and *P. furiosus* DSM 3638^T were accomplished with the technical aid of Yvonne Bilek. The protocol was adapted from recent studies (Kalmokoff et al., 1988; Näther et al., 2006).

Organisms were grown to early stationary phase in a 50-L fermentor. After concentration of cell mass (3,500 × g, 30 min, 4°C; Sorvall RC 5C plus, rotor GS3) flagella were sheared (Ultraturrax T25; 1 min at 13,000 rpm and 10 s at 22,000 rpm). Cell debris was removed by centrifugation (34,500 × g, 4°C; Sorvall RC 5C plus, rotor SS34) for 20 min, prolonged

to 80 min if necessary. Flagella were pelleted from the supernatant by ultracentrifugation (60,000 × g, 90 min, 4°C; Beckman Optima LE-80K, rotor 70Ti), resuspended in 150 µl 0.1 M HEPES pH 7.0 and purified for 48 h (250,000 × g, 4°C; Beckman Optima LE-80K, rotor SW60-Ti) using a CsCl gradient (0.45 g/ml). Fractions were taken by puncturing the ultracentrifuge tubes with sterile syringes, dialyzed against aerobic ½ SME/5 mM HEPES pH 7.0 and analyzed by SDS-PAGE to identify the flagella-containing band. After addition of sodium azide to a final concentration of 0.001% (w/v), samples were stored at 4°C.

6.2 Stability of flagella

The influence of chaotropic agents on the stability and bending of flagella was tested in accordance to recent studies (Faguy et al., 1992; Näther, 2007). For that, 5 µl of flagella were stocked up with ½ SME/5 mM HEPES pH 7.0 to 50 µl and an equal volume of one of the following solutions was added: 3 M urea, 6 M urea, 3 M guanidine/HCl or 5 M guanidine/HCl. Samples were incubated for 1 h at 37°C or 80°C and centrifuged for 30 min at 13,000 × g. The supernatant and the pellet (resuspended in 5 µl ½ SME/5 mM HEPES pH 7.0) were prepared for SDS-PAGE or TEM.

7 Isolation of cell envelopes and membrane vesicles

Cell envelopes were isolated according to (Näther, 2007). In brief, 20 ml of exponential or stationary cells were harvested by centrifugation (8,000 × g, 15 min; Sorvall RC 5C plus, rotor SS34) and incubated overnight (*P. furiosus*) or for 15 min (*M. villosus*) in hypotonic solution (1:5) with 10 µl DNase (2.5 mg/ml). Cell lysis was proven by phase contrast light microscopy and cell envelopes were pelleted (13,000 × g, 30 min). The instable white pellet was washed off from darker unbroken cells by gently resuspending in 50 µl 10 mM HEPES pH 7.0. Cell envelopes were then analyzed by SDS-PAGE and TEM. In the subsequent steps, different parameters were modified to optimize the protocol. The influence of the rotational speed and time on the stability of cell envelopes was tested as and the composition of the hypotonic solution (addition of salts for stabilization or PMSF for inhibition of proteolysis).

For (partial) solubilization, cell envelopes were incubated with detergents (Triton X-114, taurodeoxycholate, Tween® 20, Tween® 80, and DDM) for 1 h at room temperature or 2 h at 8°C. Samples were then applied on top of either a sucrose [8.5−70% (w/v)] or CsCl (0.45 mg/ml) gradient (both in ½ SME/10 mM HEPES pH 7.0) and separated for 2.5 h by ultracentrifugation (250,000 × g, 4°C; Beckman Optima LE-80K, rotor SW60-Ti).

To isolate the granum-like body of *P. furiosus*, the protocol for preparation of polar caps of *Halobacterium salinarum* was adapted (Kupper et al., 1994). 500 ml of culture were harvested, resuspended in 100 ml of basal salt solution and lysed by addition of 12.5 µl DNase (10 mg/ml) and 0.01% (w/v) taurodeoxycholate. After incubation at room temperature for 90 min, cell envelopes were pelleted by centrifugation (5,800 × g, 30 min, 10°C; Sorvall RC 5C plus, rotor GS-A) and resuspended in 30 ml basal salt solution. 10 ml of solubilization buffer were added, and the sample was stirred on ice for 20 min. Cell debris was removed by centrifugation (6,000 × g, 10 min, 10°C; Sorvall RC 5C plus, rotor SS34). Purification of the supernatant containing the granum-like body using a Sepharose column was omitted since flagella of *P. furiosus* used to stack on the matrix (personal communication, Daniela Näther). For pelleting granum-like bodies, the supernatant was ultracentrifuged (60,000 × g, 2 h, 4°C; Beckman Optima LE-80K, rotor 70Ti).

For preparation of membrane vesicles, protocols designed for preparation of viruses were adapted (Häring, 2005). An exponential or stationary 20-ml culture was centrifuged (5,000 × g, 10 min; Labofuge GL). The supernatant was filtered (0.2-µm filter) and ultracentrifuged using UltraClear tubes at 250,000 × g for 1 h (4°C; Beckman Optima LE-80K, rotor SW60-Ti). The pellet was then resuspended in 50 µl TE and analyzed by TEM. After successful isolation, vesicles were prepared by precipitation with PEG6000 from three pooled 500-ml cultures as described for virus purification (Häring, 2005; Vestergaard et al., 2005).

8 Generation and purification of polyclonal antibodies

8.1 Generation of antibodies

The recombinant expression of the glutamate dehydrogenase is summarized briefly as this work was performed in a Bachelor thesis (Loose, 2009).

The glutamate dehydrogenase gene was amplified using primers Gdh_pET21a_EcoRI_F and Gdh_pET21a_SalI_R and cloned into vector pET21a using *E. coli* DH5α. Plasmids from positive clones were transformed into *E. coli* Rosetta(DE3)pLsyS, grown on LB plates containing ampicillin and chloramphenicol at 37°C. Overexpression of the target protein was induced by 1 mM IPTG when cells reached an OD_{600} of 0.6. After incubation for 3 h, cells were lysed by lysozyme and subsequent sonication (3×30 s, duty cycle 50%, output level 5). Cell debris was removed and the supernatant was subjected to a heat step. The resulting protein extract was separated by SDS-PAGE; the corresponding protein band at 47 kDa was cut out, and used for immunization of a rabbit (Davids Biotechnologie,

Regensburg, Germany). Western blotting using a preimmune serume or a test serume as primary antibody was described recently (Schießl, 2010).

8.2 Saturation and purification

To increase the specificity, anti-Gdh Pfu antibodies were saturated with a protein extract of *E. coli*. 2.4 L of *E. coli* Rosetta(DE3)pLysS were harvested by centrifugation (6,100 × g, 15 min; Sorvall RC 5C plus, rotor GS3) and resuspended in 20 ml PBS. After addition of 30 mg lysozyme, the suspension was stirred on ice for 90 min. Cells were completely disrupted by sonication (3×30 s + 3×1 min, duty cycle 50%, output level 5) and centrifuged (30,600 × g, 30 min; Sorvall RC 5C plus, rotor SS34). The protein extract obtained was mixed with the antibody containing serum in equal concentrations and stirred at 8°C for 1 h. The solution was centrifuged twice (30,600 × g, 30 min; Sorvall RC 5C plus, rotor SS34) to remove saturated antibodies and unbound protein.

Immunoglobulin G was purified from the serum by protein-G affinity column chromatography. Prior to use, the column was equilibrated with an 11-fold column volume of 20 mM NaP_i pH 7.0 and the serum was centrifuged for 10 min at 5,000 × g, 10min. The supernatant was loaded onto the column, washed with a 9-fold volume of 20 mM NaP_i pH 7.0 and eluted with a 7-fold volume of 0.1 M glycine/HCl pH 2.7 followed by a 2-fold volume of 0.1 M glycine/HCl pH 2.0. The eluate was collected in 1.7-ml fractions and directly neutralized by addition of 0.3 ml 1 M Tris/HCl pH 7.5. Finally, the column was washed with a 10-fold volume of 20 mM NaP_i pH 7.0 and stored in 20% (v/v) ethanol.

9 Protein-biochemical methods

9.1 SDS-polyacrylamide gel electrophoresis

Molecular weight separation of proteins was performed by vertical, discontinuous SDS-polyacrylamide gel electrophoresis (SDS-PAGE) according to Laemmli (1970). The gel system (gel size 9.5 cm × 7.5 cm × 0.1 cm) consisted of a lower separating gel [10.0–12.5% (v/v) acrylamide] and an upper stacking gel [4.5% (v/v) acrylamide]:

Table XII: SDS gels.

	separating gel		stacking gel
	10.0%	12.5%	4.5%
$H_2O_{millipore}$ (sterile)	2.5 ml	2.0 ml	1.2 ml
Acrylamide bis solution 30% (37.5:1)	2.0 ml	2.5 ml	0.3 ml
Lower Tris buffer	1.5 ml	1.5 ml	-
Upper Tris buffer	-	-	0.5 ml
APS, 10% (w/v)	30 µl	30 µl	15 µl
TEMED	5 µl	5 µl	3 µl

Unstained protein marker for Coomassie and silver staining, and prestained protein marker for periodic acid-Schiff (PAS) staining and Western Blot were used as molecular weight markers. Samples were mixed with an equal volume of loading dye and, by default, heated for 15 min in a 100°C water bath. If denaturation was performed at lower temperatures, a thermomixer was used. Gels were run at 10 mA per gel for 10 min, and further at 25 mA per gel for 1 h or until the bromphenol blue band reached the bottom of the gel.

9.2 Staining and drying

9.2.1 Staining

For detection of (glycosylated) proteins one of the following staining methods was applied on gels after SDS-PAGE. Documentation was done using a Nikon Coolpix 950, images were processed with Adobe Photoshop CS4.

Table XIII: Staining protocols.

Coomassie staining[a]		Silver staining[b]		PAS staining[c]	
Solution	Time	Solution	Time	Solution	Time
Coomassie staining	30 min	Silver Fixation	30 min	PAS fixation	30 min
Coomassie destaining	-	Silver washing I	10 min	PAS oxidation	2 h
		Silver washing II	10 min	PAS reduction	30 min
Change destaining solution until the background is completely destained		Silver blocking	1 min	Schiff's reagent	12 h
		$H_2O_{millipore}$	3 × 20 s	PAS destaining	-
		Silver staining	20 min		
		$H_2O_{millipore}$	2 × 20 s	Change destaining solution until the background is completely destained	
		Silver developing	Until desired intensity		
		Silver stopping	-		

[a] Detection limit for Coomassie staining is 300–1,000 ng per 0.5 cm of protein band.
[b] Silver staining modified from Blum et al., 1987. Detection limit is 10 ng per 0.5 cm of protein band.
[c] Periodic acid Schiff (PAS) staining for detection of glycoproteins modified from Segrest and Jackson,. 2010

9.2.2 Drying of gels

For long-term storage, cells were dried using the DryEase® gel drying system. Gel and cellophan foils were equilibrated in gel drying buffer for 20 min and the gel was mounted into the corresponding frame between two foils. Drying was overnight.

9.3 Western Blotting

After SDS-PAGE, proteins were blotted from the gel to a PVDF membrane by semi-dry transfer. For doing so, the membrane was soaked in methanol p.a. for 2 min and then in blotting buffer together with Whatman paper and the gel for 10−20 min. Three layers of Whatman paper, the membrane, the gel, and three more layers of Whatman paper were placed on the lower electrode (anode) of the transfer device, and air bubbles were removed carefully. The blot was run at a maximum of 16 V for 30 min.

PVDF membranes can be stained with Ponceau S to control if all proteins were transferred properly. Staining was for 1–3 min at room temperature; thereafter, the membrane was washed with water.

9.4 Detection of proteins

After blotting, the PVDF membrane was blocked with blocking solution overnight while shaking. The membrane was transferred to a tray containing the first antibody dilution [appropriate dilution in TBS-T with 3% (w/v) milk powder] and shaken for 3–5 h. After washing twice with TBS-T for 10 min each, the membrane was incubated with a secondary antibody coupled to horseradish peroxidase [1:2,000 in TBS-T with 3% (w/v) milk powder] for 1 h along with shaking. The membrane was washed in TBS-T three times for 10 min. The peroxidase reaction was visualized using 3-amino-9-ethylcarbazole solution, the staining of proteins bands was stopped by rinsing the membrane in water.

9.5 Protein identification

An in-gel digestion assay was used to identify proteins separated by SDS-PAGE. Gels were Coomassie stained, and protein bands of interest were excised. Slices were cut into pieces and destained by sequential washing in the following solutions for 30 min at a time: 50 mM NH_4HCO_3, 50 mM NH_4HCO_3 in 25% (v/v) acetonitrile, 25% (v/v) acetonitrile, and 50% (v/v) acetonitrile. After drying, proteins were digested at 37°C overnight by addition of 2 µg trypsin per 100 µl gel volume diluted in 50 mM NH_4HCO_3. The resulting peptides were extracted from the gel matrix by two-fold incubation with 100 mM NH_4HCO_3 in 50% (v/v) acetonitrile for 1.5 h. The supernatants were analyzed by Rainer Deutzmann and Eduard Hochmuth (both Central Protein analytical Facility of the Biology Department, University of Regensburg, Germany) using mass spectrometry (combined MS + MS/MS search) with a 4700 Proteomics Analyzer (ABI). Proteins were identified by searching the non-redundant NCBInr database release February 2008 using the Mascot search program (http://www.matrixscience.com/). Protein scores with a cutoff value >80 were called statistically significant [$P < 0.05$; score: $-10*\log(P)$; P is the probability that the observed match is a random event].

9.6 Bioinformatic analysis

For bioinformatic studies, annotated genome and protein sequences deposited in the NCBI database (http://www.ncbi.nlm.nih.gov/genomes/static/a.html) were analyzed with public applications/databases summarized in Table XIV.

Table XIV: Bioinformatic analysis tools.

Algorithm/ Database	Used for	URL	Reference
blastp	Sequence alignment	http://blast.ncbi.nlm.nih.gov/Blast.cgi	Altschul et al., 1990
ClustalW2	Multiple sequence alignment	http://www.ebi.ac.uk/Tools/msa/clustalw2/	Larkin et al., 2007
ProtParam	Molecular mass calculation	http://www.expasy.ch/tools/protparam.html	Gasteiger et al, 2005
NetNGlyc 1.0	N-glycosylation site prediction[a]	http://www.cbs.dtu.dk/services/NetNGlyc/	-
FlaFind	Prediction of archaeal class III SPs and peptidase cleavage sites	http://signalfind.org	Szabó et al., 2007b
Phobius	SP and transmembrane topology prediction	http://www.ebi.ac.uk/Tools/pfa/phobius/	Käll et al., 2007
TMHMM 2.0	Transmembrane region prediction	http://www.cbs.dtu.dk/services/TMHMM/	Krogh et al., 2001
PSORTb 3.0.2.	Prediction of protein subcellular localization	http://www.psort.org/psortb/	Yu et al., 2010

SP signal peptide
[a] SignalP 3.0 (http://www.cbs.dtu.dk/services/SignalP/) is automatically run on all sequences

10 Purification of nucleic acids

10.1 Isolation of genomic DNA

10.1.1 Method for *P. furiosus*

After harvesting 40 ml of freshly grown cells (27,000 × g, 30 min; Sorvall RC C5 plus, rotor SS34), the resulting pellet was resuspended in 800 µl TNE and supplemented with 100 µl 10% SDS (w/v), 100 µl 10% (w/v) N-Lauroylsarcosine, and 10 µl RNaseA (10 mg/ml). The mixture was incubated for 15 min at room temperature and further on for 1 h at 55°C after adding 50 µl ProteinaseK solution.

10.1.2 High-salt method (Bellack et al., 2011)

60 ml of freshly grown culture were harvested (27,000 × g, 30 min; Sorvall RC C5 plus, rotor SS34) and resuspended in 400 µl buffer A. For cell lysis, one volume of buffer B and 8 µl RNaseA (10 mg/ml) were added and the mixture was incubated for 30 min at room temperature. After addition of 50 µl ProteinaseK solution, the sample was further incubated for 1 h at 65°C. Proteins and carbohydrates were removed from the resulting cell lysate by thoroughly mixing with 130 µl 5M NaCl and 100 µl NaCl/CTAB for 10 min at 65°C.

10.1.3 Isolation of high quality gDNA

High quality gDNA e.g. for whole-genome sequencing was isolated using the Genomic-tip (100/G or 500/G) system according to the manufactors's instructions for Bacteria. Addition of lysozyme to the cell suspension could be omitted as the *Methanocaldococcaceae* possess a proteinaceous S-layer and lyse rapidly in detergents. DNA was precipitated with isopropanol and resuspended in TE.

10.2 Plasmid isolation

Plasmid DNA of *E. coli* was isolated with either the Miniprep Kit of Peqlab designed for up to 4 ml of culture or the QIAGEN Plasmid Maxi Kit.

10.3 Phenol/chloroform extraction

For DNA extraction, an equal volume of phenol:chloroform:isoamylalcohol (25:24:1) was added to the cell lysate and mixed. Samples were centrifuged (14,000 × g, 10 min, 4°C; Centrifuge 5402), the upper aqueous phase was transferred to a new tube, and extraction was repeated until there was no more interphase. Traces of phenol were removed from the sample by addition of one volume chloroform and centrifugation (as above). Alternatively, DNA was extracted from cell lysates by an equal volume of phenol, by phenol:chloroform:isoamylalcohol (25:24:1) and chloroform:isoamylalcohol (24:1).

10.4 Precipitation of DNA

DNA was precipitated from aqueous solution with either ethanol or isopropanol.
For precipitation with ethanol, 0.1 volumes of 3M sodium acetate pH 7.5 and 2.5 volumes of ice-cold pure ethanol were added to the sample which then was frozen to -20°C overnight (or at least 1 h). DNA was pelleted by centrifugation (14,000 × g, 30 min, 4°C; Centrifuge 5402), and the pellet was washed with ice-cold 70% (v/v) ethanol to eliminate salt. The pelleted DNA was air-dried for 15 min and resuspended (overnight for gDNA) in TE or water.
Alternatively, precipitation of DNA was accomplished by addition of 0.6 volumes isopropanol and incubation at -20°C overnight. Pelleting and washing was as described above; here the pellet adhered less tightly to the tube and the air-drying step had to be prolonged.

10.5 Purification of PCR products

PCR products were purified using the MinElute PCR Purification Kit from QIAGEN.

11 Enzymatic manipulation of DNA

11.1 Polymerase chain reaction

All PCR-related manipulations were carried out on ice in a laminar flow.

Table XV: Reaction mixtures for PCR.

PCR for	Reaction volume	Reagent	Amount
16S rRNA	20 µl	10 × PCR buffer (buffer Y, incl. $MgCl_2$)	2.0 µl
		dNTP mix (each 10 mM)	0.5 µl
		Forward primer 8aF (25 ng/µl)	1.0 µl
		Reverse primer 1406ur or 1512ur (25 ng/µl)	1.0 µl
		H_2O (LiChrosolve®)	14.375 µl
		Taq DNA Polymerase (5 U/µl)	0.125 µl
		Template	1.0 µl
Cloning	50 µl	5 × PCR buffer (Phusion® HF buffer, incl. $MgCl_2$)	2.0 µl
		dNTP mix (each 10 mM)	1.0 µl
		Forward primer	2.5 µl
		Reverse primer	2.5 µl
		H_2O (LiChrosolve®)	33.0 µl
		Phusion® DNA Polymerase (5 U/µl)	0.5 µl
		Template	0.5 µl

Table XVI: PCR amplification conditions

PCR for	PCR step	Temperatue [°C]	Time	Cycle number
16S rRNA	Initial denaturation	95	2 min	1
	Denaturation	96	30 s	10
	Annealing	60	30 s	
	Elongation	72	60 s	
	Denaturation	94	30 s	25
	Annealing	60	30 s	
	Elongation	72	60 s	
	Final elongation	72	10 min	1
	End	8	forever	
Colony PCR	Initial denaturation	95	3 min	1
	Denaturation	95	30 s	35
	Annealing	60	30 s	
	Elongation	72	60 s	
	Final elongation	72	10 min	1
	End	8	forever	
Cloning PCR	Initial denaturation	96	30 s	1
	Denaturation	96	10 s	35
	Annealing	gradient	30 s	
	Elongation	72	40 s	
	Final elongation	72	10 min	1
	End	8	forever	

11.2 Sequence specific restriction endonucleases

Restriction enzyme digestion of PCR products and vectors was performed with buffers and enzymes provided by New England Biolabs. The reaction was set up in a total volume of

30 µl containing 1–3 µg of DNA, 10–20 U of each restriction enzyme (in a double digest), and 3 µl 10 × restriction enzyme buffer. The mixture was incubated at 37°C for 2–4 h and afterwards purified using a PCR purification kit. Digested vectors were stored at -20°C until use.

11.3 DNA ligation

For DNA ligation, the quantity of restriction endonucleases digested DNA was measured by UV spectrometry. A 20 µl ligase reaction contained vector DNA and insert DNA in a molar ratio of 1:1 or 1:3, 2 µl 10 × ligase buffer (included 10 mM DTT and 1 mM ATP), and 1 µl of T4 DNA ligase. The ligation assay was incubated for 1–2 h at room temperature or overnight at 16°C and the resulting ligation product was either directly transformed in *E. coli* or afore purified by ethanol precipitation.

12 Quantitative, qualitative, and sequence analysis of DNA

12.1 UV spectrometry

The concentration of DNA samples was measured using NanoDrop UV spectrometry at a wavelength of 260 nm. Concomitantly, absorbance was measured at 230 and 280 nm to determine contaminations, e.g. with proteins. For pure DNA, the ratio of OD_{260}/OD_{230} has to be ≥ 2.0 and of OD_{260}/OD_{280} between 1.8 and 2.0.

12.2 Agarose gel electrophoresis

0.7–2.0% agarose gels in 1 × TAE with ethidium bromide (final concentration 1 µg/ml) were casted in a gel slide and electrophoresis was performed with 1 × TAE as running buffer. After a 20-min run with 60 mA and 75 V, gels were observed and documented using the BioDoc-it™ imaging system.

For determination of gDNA concentrations, samples and the following amounts of Lambda DNA were loaded to the gel: 10 ng, 20 ng, 40 ng, 60 ng, 80 ng, and 100 ng. The gDNA was diluted 1:50 before loading.

12.3 Pulsed field gel electrophoresis

Pulsed field gel electrophoresis (PFEG) was performed for determination of the genome size of *M. villosus* using gDNA of *M. jannaschii* as reference. The protocol was modified from Murray et al. (1990). Stationary cells of both organisms were harvested by centrifugation (27,000 × g, 10 min; Sorvall RC 5C plus, rotor SS34) and concentrated in PIV buffer to a final cell density of 4×10^8 cells per 100 µl. The cell suspension was

preheated to 50°C, mixed with an equal volume of agarose (80 mg InCert agarose molten in 5 ml water), and immediately pipetted into a plug mold (Bio-Rad, Munich, Germany). After hardening for 1–2 h at 4°C, the plugs were subjected to cell lysis in 10 ml EC lysis buffer at 37°C with agitation overnight. The solution was replaced with 10 ml of ESP buffer and incubation was with agitation for at least 24 h at 50°C. The plugs were washed three times with TE for at least 1 h and 200 µl of PMSF solution were added to the second wash step. 1.0% (w/v) 0.5 × TBE agarose gels were directly loaded with the plugs and DNA was separated on a CHEF-DRIII system. The run time was 24 h at 6 V/cm with a switching time of 1.17 s at the beginning and 4.26 min in the end, and at an included angle of 120°. Afterwards, the gel was stained with ethidium bromide (final concentration 1 µg/ml) and destained in distilled water.

To determine the fragment size of gDNA for whole-genome sequencing, gDNA was supplemented with an equal amount of loading dye and directly loaded to a 0.8% (w/v) 0.5 × TBE agarose gel. Here, the run time was 18 h at 6 V/cm with an initial switching time of 1 s and a final switching time of 15 s, and at an included angle of 120°.

12.4 Determination of the G+C content

Freshly grown cells of *M. villosus* were sent to the DSMZ for determination of the G+C content. As unexplicably, this attempt failed two times, estimation of the G+C content was done from shotgun sequencing of 96 clones. For that, gDNA was purified using the Genomic-tip 100/G system. Sequence analysis was performed by LGC Genomics (Berlin, Germany).

12.5 Whole-genome sequencing

During this thesis, Reinhard Wirth submitted a proposal for whole-genome sequencing of *M. villosus* as part of the Community Sequencing Program (CSP) of the Joint Genome Institute (JGI; Walnut Creek, CA, US) under supervison of Hans-Peter Klenk (Head of Department of Microbiology, DSMZ, Braunschweig, Germany). As the proposal was approved for CSP 2011, the required high quality DNA was isolated in consultation with Evelyne Brambilla (Department of Microbiology, DSMZ, Braunschweig, Germany). For this purpose, cells were grown in a 50-L fermentor and gDNA was isolated using the Genomic-tip 500/G system. Before shipping of gDNA to the DSMZ, its quality was checked by PFGE and identity of the organism was proven by 16S rRNA gene sequencing.

12.6 Sequencing of PCR products and sequence analysis

Sequencing of PCR products was done by GENEART or Entelechon (both Regensburg, Germany). Sequences were edited and analyzed using the following applications: BioEdit, blastn, and ARB (Ludwig et al., 2004).

13 Manipulation of *Escherichia coli*

13.1 Preparation of electrocompetent cells

E. coli was grown overnight in test tubes and inoculated into 250 ml fresh (selective) LB medium to an OD_{600} of 0.03. Incubation was done at 37°C to an OD_{600} of 0.4–0.6, and cells were harvested (6,100 × g, 15 min, 4°C; Sorvall RC 5C plus, rotor GS 3). On ice, cells were resuspended/centrifuged in steadily decreasing volumes of 10% (v/v) glycerol (250 ml, 100 ml, 50 ml, 20 ml, and finally 2 ml). Cells were aliquoted à 40 µl and stored at -70°C.

13.2 Transformation by electroporation

For electroporation, a UV-sterilized cuvette and LB medium were precooled on ice, and competent cells were thawed carefully on ice. 5 µl of plasmid DNA was pipeted to the cells and left on ice for 5 min. The approach was transferred into the cuvette which was dried off and cells were electroporated using the Gene Pulser II (2,000 V, 800 Ω, 25 µF). Cells were resuspended in 500 µl precooled LB medium, transferred to a 1.5-ml tube and left on ice for 5 min. Samples were incubated for 1 h at 37°C to induce antibiotic resistance coded on the plasmid, and then plated onto selective prewarmed LB plates in different dilutions (10 µl, 50 µl, 150 µl, and remainder). Plates were incubated overnight at 37°C.

5 Results

1 Morphological analyses and adhesion studies of *Pyrococcus furiosus*

During this thesis, three *Pyrococcus furiosus* strains were analyzed whose different origin is shown in Figure 1. In the course of time, it became obvious that the *P. furiosus* strain cultured continuously in the lab of Reinhard Wirth over years (named below *P. furiosus* **L**ab **S**train) changed abnormally. The effects were not only limited to its morphology, also the growth and adhesion behavior changed (Schopf, 2011). Hence, the strain deposited as *P. furiosus* Vc1 at the in-house culture collection of our institute was regenerated and included in the research of this study (= *P. furiosus* Vc1). Comparison of the two strains revealed apparent differences influencing the progress of this thesis. Since other groups at our institute also faced problems with their *P. furiosus* cultures, Southern blotting analyses were performed, which has proven deletions in strain Vc1 (personal communication, Winfried Hausner). Consequently, the original type strain was ordered from the German Collection of Microorganisms and Cell Cultures, DSMZ (= *P. furiosus* DSM 3638^T).

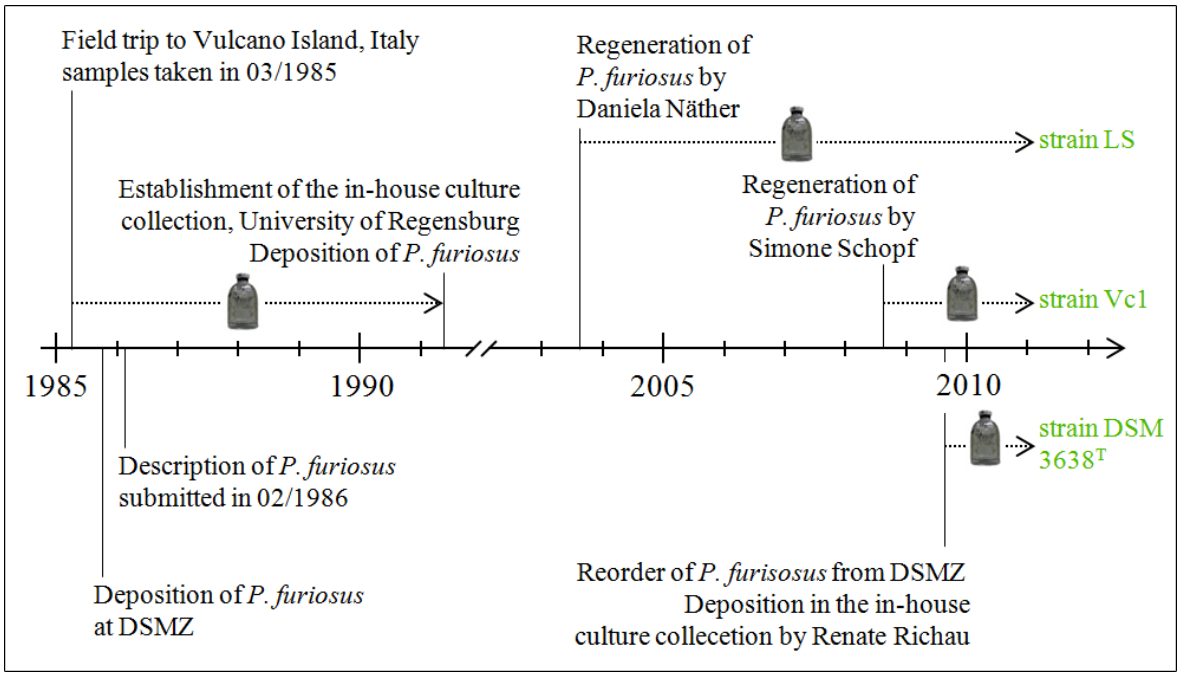

Figure 1: Origin of the different *P. furiosus* strains used within this thesis.

This chapter will summarize initial electron microscopic studies of *P. furiosus* LS, will give a comparison of this strain to *P. furiosus* Vc1 and *P. furiosus* DSM 3638^T, and will show how the results influenced the focus of this thesis.

1.1 Cell morphology and flagellation of the *P. furiosus* lab strain

As basis for the cell envelope preparations, *P. furiosus* LS was analyzed regarding its flagellation by electron microscopy. In case of incubation overnight at 95°C, like it was performed standardly in this thesis, cells were regular to irregular cocci having an average diameter of 0.8–1.0 µm. They possessed at least 15 monopolar flagella with 12 nm in diameter and a mean length of 2–3 µm. When not centrifuged for TEM preparation, cells were observed with curled flagella of up to 6 µm in length (Figure 2).

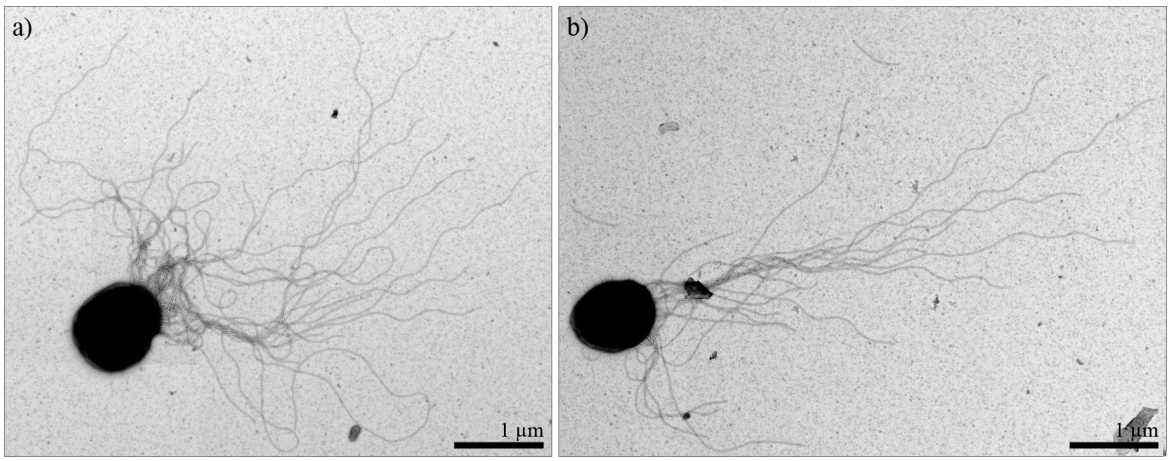

Figure 2: Coccoid cells of *P. furiosus* LS with multiple flagella. Transmission electron micrographs of *P. furiosus* LS cells that show regular cocci with curled flagella. Cells were fixed with glutardialdehyde but not centrifuged, and negative stained with uranyl acetate.

A former study demonstrated that the addition of starch to the growth medium stimulated the growth of *P. furiosus* LS cells but had no influence on their flagellation (Näther, 2007). During this thesis, further growth parameters were tested and their results are summarized in Table 1.

At first, the influence of the growth temperature was analyzed. Fiala and Stetter described *P. furiosus* to have a temperature range of 70–103°C (Fiala and Stetter, 1986). In this study, no growth was detected for *P. furiosus* LS at 70°C, so that the incubation temperature was raised to 72°C. Compared to data at 95°C, changing the growth temperature did not only affect the cell size but also the number of flagella. Cells incubated at 72°C were slightly bigger having an average diameter of 1.5 µm but revealed less flagella. With increasing temperature, cells possessed more flagella with a maximum of approximately 50 filaments at the optimal growth temperature of 100°C.

Furthermore, cells of different growth phases were analyzed. It was apparent that cells of the exponential growth phase exhibited less flagella than cells of the stationary phase, but no differences in length were detected. The number of flagella increased until cells were

stationary, and prolonged incubation time caused only cell lysis. Therefore, cells were incubated in further experiments at 95°C for 14 h (= overnight), if not stated otherwise.

Table 1: Influence of temperature and growth phase on the flagellation of *P. furiosus* LS. Cells were grown in ½ SME at different growth temperatures.

Growth temperature	Doubling time[a] in min	Incubation time in h	Final cell count in cells/ml	Average cell size[b]	Flagellation[b]
72°C	270 (at 70°C)	72	7.7×10^6	1.5 µm	no or 5–10 flagella
80°C	80	48	6.3×10^7	1.2 µm	on average 10 flagella
90°C	50	24	7.7×10^7	1.0 µm	10–20 flagella
95°C	70	12	1.5×10^8	0.9 µm	15–30 flagella
100°C	37	12	2.0×10^8	0.9 µm	at least 25 flagella
Growth phase		Incubation time in h	Final cell count in cells/ml	Light microscopy	Flagellation[b]
early exponential		3	2.5×10^7	dividing cells	no or 5–10 flagella
late exponential		6	7.5×10^7	dividing cells	10–15 flagella
early stationary		9	8.8×10^7	cells singly and in pairs	15–20 flagella
stationary		12	1.7×10^8	cells singly and in pairs	15–30 flagella
stationary		24	8.0×10^7	10% of cells lysed	20–30 flagella

[a] as determined by Fiala and Stetter, 1986
[b] analysis of 20 cells

Throughout this thesis, phase contrast light microscopic analyses showed that the cells of *P. furiosus* LS were very irregular, and often appeared in chains of 3–5 cells. Electron micrographs of negatively stained cells confirmed this result, but despite the morphological changes, no differences in flagellation were detected. To analyze the cell morphology in more detail, ultrathin sections of high-pressure frozen and resin-embedded cells were prepared. As can be seen from Figure 3, the shape of the cells was very diverse within one culture including regular cocci, oval- to rod-shaped cells, and lobed cells. Additionally, structures made of 2−5 cells not separated after cell division were observed.

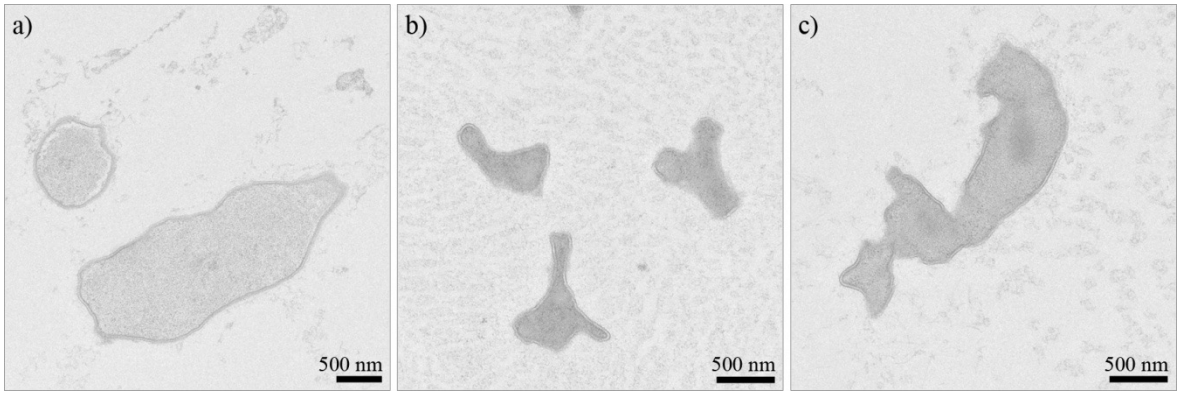

Figure 3: Morphological diversity of *P. furiosus* LS. Ultrathin sections of *P. furiosus* LS cells that were high-pressure frozen, freeze-substituted, and embedded in resin. Contrasting was performed with uranyl acetate and lead citrate.

1.2 Comparison of different *P. furiosus* strains

Due to the diversification of the cell morphology of *P. furiosus* LS, two additional *P. furiosus* strains were included in this thesis. A comparative study was set up focusing on the growth rate, the cell morphology, the flagellation, and the adhesion behavior to carbon-coated gold grids of the different strains (summarized in Table A1).

1.2.1 Source and growth conditions

When this thesis was started in June 2007, ***P. furiosus* LS** has been continuously cultured in the lab for four years. Since incubation was by default at 95°C without addition of starch to the medium, growth was slower compared to the data described in the literature (Fiala and Stetter, 1986); incubation overnight resulted in stationary cells. Over time, it was obvious that the growth rate and final cell densities of the strain decreased. In November 2010, growth in ½ SME had to be prolonged to 24 h to reach stationary phase. Final cell densities were two- to four-fold lower as described in Table 1; in some cases only 3.0×10^7 cells/ml were reached. Inoculation into media containing starch increased the growth rate and the final cell counts.

The ***P. furiosus* Vc1** strain used herein was provided as active culture originally derived from our in-house culture collection. It was regenerated in late 2008 and subsequently cultured in the lab (Schopf, 2011). The growth of this strain was similar to that of strain LS at the beginning of this thesis. Within the two years of continuous culturing in the lab no changes in growth were detected as proven in direct comparison to a freshly regenerated culture in November 2010.

***P. furiosus* DMS 3638^T** was ordered from the DSMZ by our institute in 2009, and long-term stored in our in-house culture collection. For regeneration, growth medium was prepared with starch, in which the observed growth rate was much higher (50% of cells of the 1:400 dilution were lysed after incubation overnight). Therefore, when cells were inoculated into starch medium, incubation was reduced to 6 h. For continuous culturing, cells were transferred into ½ SME without starch, wherein growth was slower but still faster than that of *P. furiosus* Vc1.

1.2.2 Cell morphology and flagellation

To compare the three different *P. furiosus* strains morphologically, cells were grown in ½ SME either with or without starch and were subjected to microscopic analysis. For strain LS, the incubation time in both media had to be prolonged to obtain the same cell density as for the other two strains.

Using phase contrast light microscopy, no differences were detected between *P. furiosus* Vc1 and DSM 3638^T. Cells of both strains were regular cocci with an average diameter of 0.9–1 µm and were clearly distinguishable from the irregular *P. furiosus* LS cells.

Electron microscopic analysis of stationary cells (Figure 4) revealed *P. furiosus* DSM 3638^T to possess about 15–30 polarly inserted flagella as described above for *P. furiosus* LS, whereas strain Vc1 had no or a maximum of 10 flagella. For all three strains, the diameter of flagella was 12 nm, and an additional kind of filament with a diameter of 6.5 nm was detected. If all three *P. furiosus* strains were grown in medium with starch, the cell diameter increased to an average of 1.2 µm. In consistence with earlier results (Näther, 2007), the addition of starch had a no influence on the number or length of flagella.

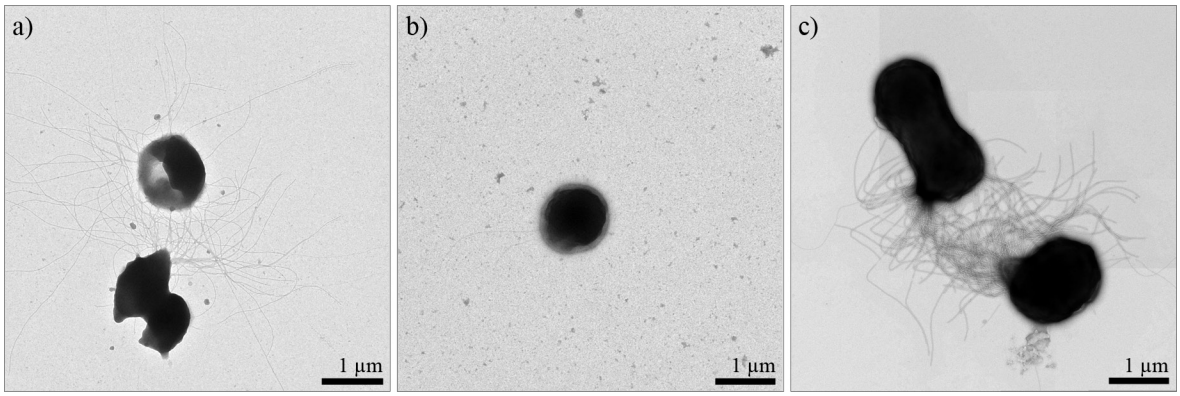

Figure 4: Comparison of different *P. furiosus* strains. Cells of a) *P. furiosus* LS, b) *P. furiosus* Vc1, and c) *P. furiosus* DSM 3638^T were grown to stationary phase in ½ SME medium with starch. Samples were prepared and analyzed in 2010.

When examining cells fixed with glutardialdehyde, cell-cell contacts were visible, except for *P. furiosus* Vc1, also by light microscopy. Without the fixation step, the flagella of *P. furiosus* DSM 3638^T turned out to be more labile to centrifugal forces than those of *P. furiosus* LS: Many cells of the type strain were observed without flagella, and others had a maximum of 20 flagella (data not shown).

Consistent with these findings, freeze-etched cells of *P. furiosus* DSM 3638^T were often non-flagellated. The diameter of detected flagella, however, was confirmed to be 12 nm from line scan analysis. Enlarging the region of flagella insertion, it seems that the membrane differs in this region in its ultrastructure compared to other cell parts (Figure 5a). In contrast, the cells did not show any detail of their surface relief, and only in some rare cases the S-layer was visible (Figure 5b).

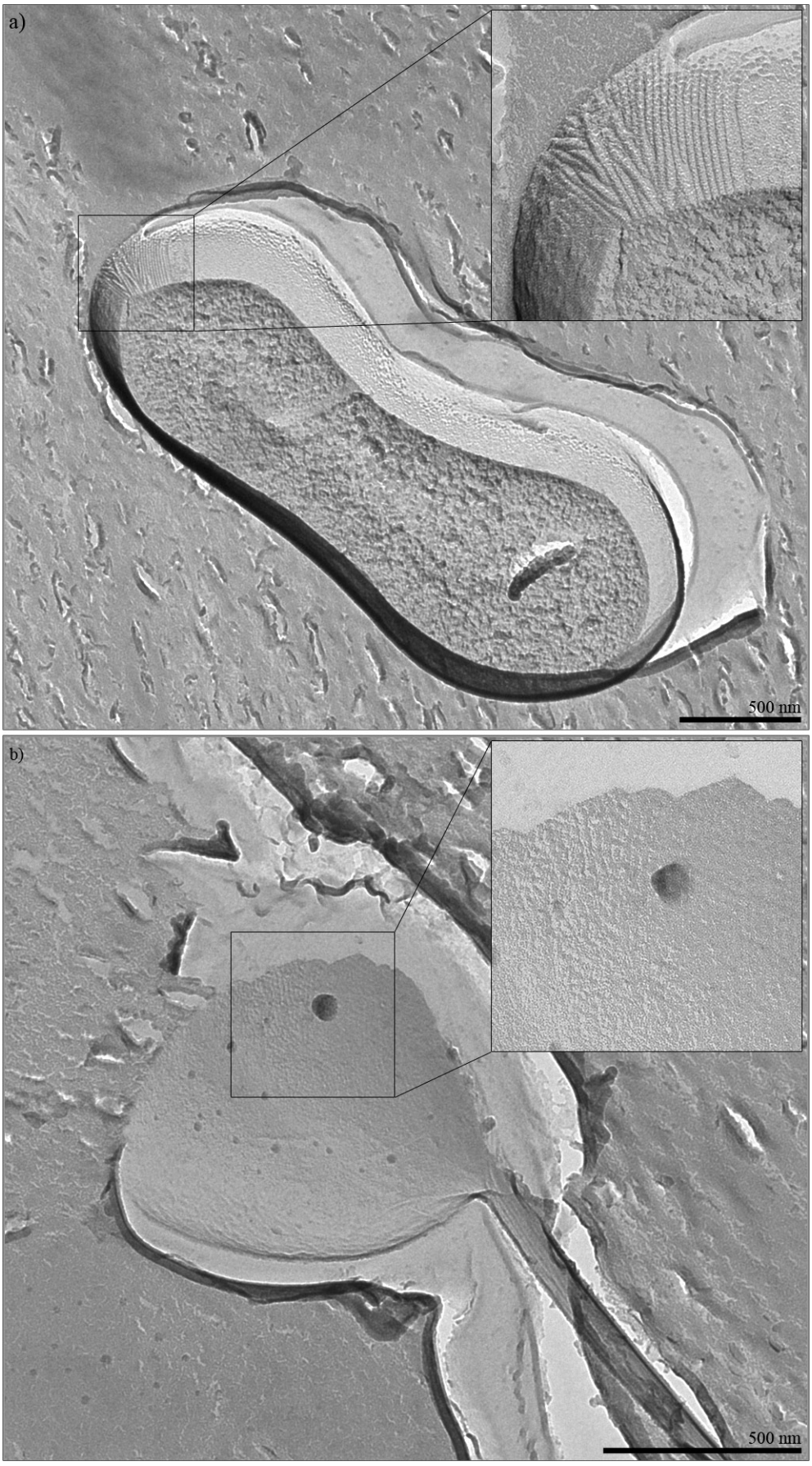

Figure 5: Freeze etching of *P. furiosus* DSM 3638^T. Transmission electron micrographs of freeze-etched stationary cells. a) Dividing cell; the enlargement shows emerging flagella and the distinctly more complex ultrastructure of the cell membrane in this part of the cell. b) Fractured cell exposing its S-layer.

1.2.3 Adhesion

Since flagella of *P. furiosus* are also functional adhesins (Näther et al., 2006), the question was raised whether the differences in flagellation between the three strains described above were reflected in their adhesion behavior. Therefore, cells were grown on carbon-coated gold grids and analyzed by DAPI staining and TEM.

Examining the grids in first instance with DAPI staining, evident differences were detected between the three strains. After incubation overnight, strong adherence was observed for *P. furiosus* LS: Cells covered the gold grid and the carbon film and formed microcolonies of up to 100 cells. For *P. furiosus* Vc1 apparently less cells were attached to the surface, whereas in the case of *P. furiosus* DSM 3638^T rarely any cells were seen on the surface (data not shown). For a detailed analysis, each strain was incubated to different growth phases determined by cell counts of planktonic cells (final cell densities as given in Table 1). Figure 5 compares the data of the three *P. furiosus* strains obtained by TEM.

Adhesion studies performed at the beginning of this thesis showed that the adherence of ***P. furiosus* LS** depends on time. After incubation for 3 h, some single cells were detected on the surface possessing at least 10 flagella. With increasing time, cells attached densely to the carbon film as thin layered cells or even as microcolonies of 10−100 cells. In these biofilm-like structures, flagella were often seen to form bundles or cell-cell contacts. The cell density on the grid increased further when cells were grown overnight. However, in conjunction with the morphological diversification and the poor growth observed in the course of this thesis, *P. furiosus* LS attached decreasingly to the supplied surface. Addition of starch increased the cell density of adherent cells but obscured the analysis of the grids because it was precipitated thereon.

In early exponential growth phase, only single cells of ***P. furiosus* Vc1** attached to the grid, which exhibited no or up to five flagella. Prolonging the incubation to late exponential phase, considerably more cells were found on the surface also forming small microcolonies of 5–20 cells. Most of the cells possessed multiple cell appendages, which formed short bundles around 100 nm in length or interconnected cells with one another. It was obvious that the adherent *P. furiosus* Vc1 cells had, on average, 15 cell appendages, and therefore significantly more than planktonic cells of the same growth phase. For some adherent cells, ~50% of the cell appendages were flagella, the other half consisted of 6.5-nm filaments. Contrary, thin filaments represented only up to 5% of cell appendages in the other two strains. After incubation overnight, fewer cells were attached to the carbon film, which were mostly very irregular or already lysed.

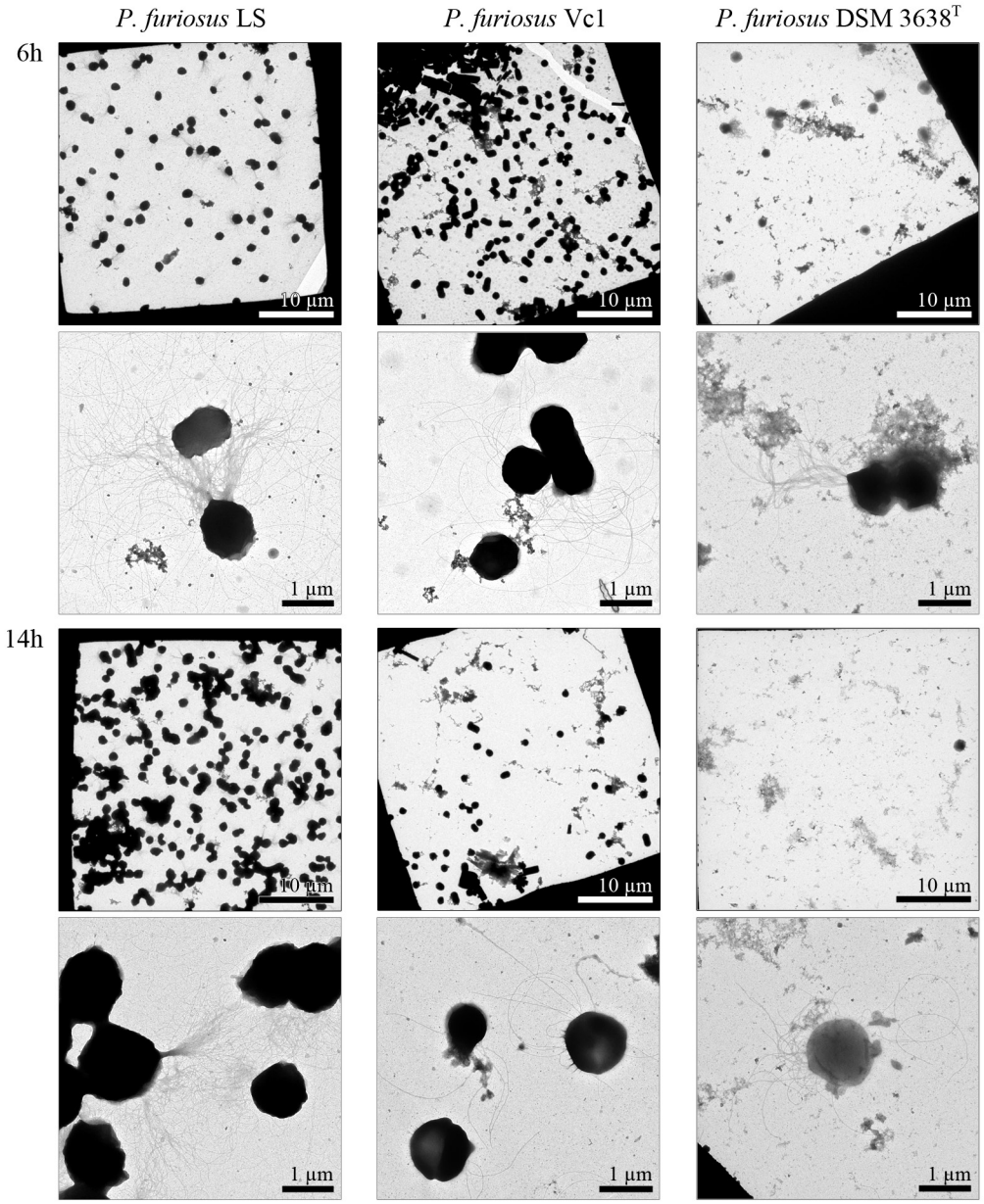

Figure 6: Adhesion behavior of different *P. furiosus* strains to carbon-coated gold grids. Transmission electron micrographs of *P. furiosus* LS (in 2007; left), *P. furiosus* Vc1 (in 2009; middle), and *P. furiosus* DSM 3638^T (in 2010; right) grown to late exponential and stationary phase on gold grids.

Analyzing ***P. furiosus* DSM 3638^T**, the result of the preliminary test was confirmed: In early exponential phase, very few single, flagellated cells were observed on the grid, the number of which increased by a factor of five until early stationary phase. DAPI staining revealed that early exponential cells grew preferably on the bars of the grid than on the carbon film. TEM analysis of the grids provided evidence that 50% of the cells were non-flagellated and/or lysed. The cells were attached in pairs with at least one of the cells possessing multiple flagella. This indicates that cells can divide on the grid, but were

unable to initially attach to the surface. Apparently, in stationary phase, no cells were detected on the grid.

Comparing the results of the abovementioned studies, it seems clear that the number of flagella of planktonic cells does not correlate with the adhesion behavior. *P. furiosus* Vc1 was identified to possess no/the fewest flagella of all three strains but adhered much better than the wild type strain *P. furiosus* DSM 3638^{T}. Having as many flagella as the wild type, the continuous lab culture *P. furiosus* LS showed the best adhesion to the grids which, however, decreased over a period of three years. Interestingly, adherent cells of all three strains possessed more flagella and formed more cell-cell contacts than their planktonic counterparts.

The comparison showed that *P. furiosus* LS and *P. furiosus* Vc1 are completely different to the wild type strain with regard to flagellation and adhesion behavior. Therefore, it can be concluded that results obtained for these strains cannot be generalized. Considering the changes in *P. furiosus* LS, the verification of previous results failed increasingly with progress of this thesis, whereby it renders impossible to directly compare earlier to later data of this study.

2 Cell envelopes and flagella-associated proteins of *P. furiosus*

Previous studies have indicated that flagella of *P. furiosus* are anchored in close proximity to a granum-like body (Fiala and Stetter, 1986; Näther, 2007). In the latter investigation, the analysis of cell envelopes showed that the pattern of the membrane changed in the region of flagella insertion. Several attempts to obtain detailed 3D structures of the anchor by electron tomography failed because of unsatisfactory resolution.

One aim of this thesis was to identify flagella-associated proteins involved in the assembly, rotation or adhesion of *P. furiosus* flagella. The method for this investigation was lysis of cells and analysis of resulting cell envelopes using TEM and SDS-PAGE. After correlating both methods, proteins of interest were subjected to in-gel digestion and the resulting extracts were analyzed using MALDI-TOF. Further steps included cloning/expression of identified proteins and their localization in the cell by immune-labeling.

2.1 Cell envelope analyses

2.1.1 Preparation of cell envelopes of *P. furiosus* LS

This thesis continued the analyses of Daniela Näther (2007), and hence the method used by her for preparation of cell envelopes was applied and modified.

In a first attempt, exponential and stationary *P. furiosus* LS cells were lysed in hypotonic solution (1:5) at 8°C overnight according to her protocol, except that only 20 ml of grown culture were used instead of 1 L. Compared to her data that described a bright pellet containing the cell envelopes after centrifugation layering the dark unbroken cells, no lysis was detected. As a consequence, the experiment was repeated diluting the hypotonic solution 1:10. Analyzing the resulting preparation using TEM, no cell envelopes were seen, but small membrane patches ranging from 100 × 200 nm to 200 × 500 nm associated with some flagella (Figure 7a). Therefore, the step to pellet the cell envelopes performed for 45 min at 13,800 × g was modified, since it was demonstrated above that centrifugal forces affected the stability of flagella. Decreasing the centrifuge to low speed (3,000 × g), cell envelopes were well-preserved with up to 30 flagella (Figure 7b). Moreover, the centrifugation time was reduced to 10 min, as this was sufficient to pellet most of the cell envelopes. But compared to long-time centrifugation, the carbon film of the grid was often covered with proteinaceous contaminants. Only minor differences were found between exponential and stationary cell envelopes, except in the protein concentration and in flagellation as already described above (see Table 1).

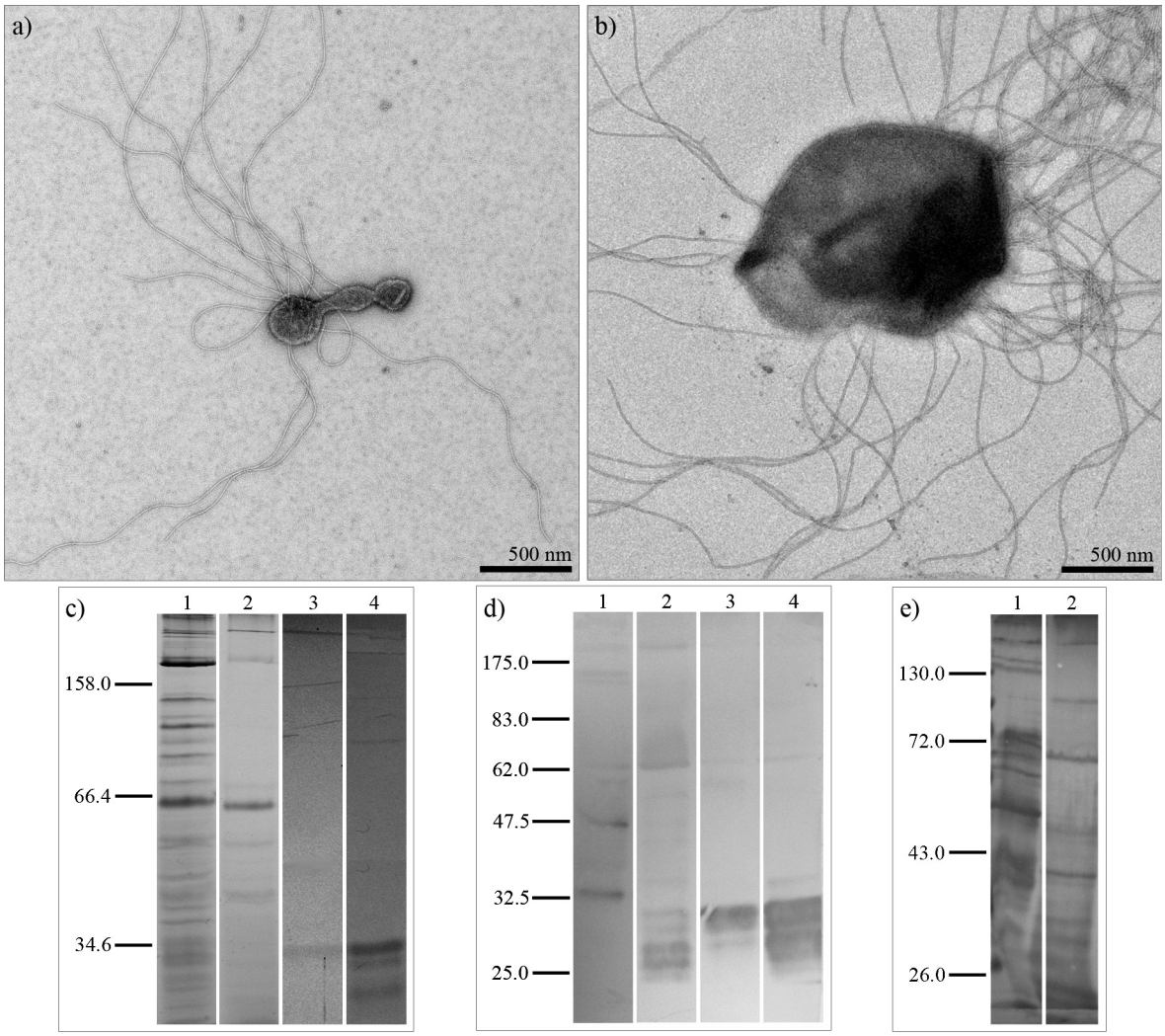

Figure 7: Cell envelope analyses of stationary *P. furiosus* LS cells. Transmission electron micrographs of negatively stained cell envelope preparations centrifuged a) at 13,800 × g resulting in small fractures, and b) at 3,000 × g resulting in cell envelopes with multiple flagella. Electrophoretic analysis of cell envelopes and flagella (10% gels; molecular masses of size markers given in kDa): c) Coomassie staining. d) and e) Western blotting of denaturated cell envelopes. d) Primary antibodies against whole flagella of *P. furiosus* (diluted 1:10,000). e) Primary antibodies against *P. furiosus* surface proteins (diluted 1:5,000).

In parallel, cell envelope preparations were analyzed using SDS-PAGE (Figure 7c-e) and compared to whole cell extracts of *P. furiosus* LS and the soluble protein fraction present in the supernatant. Flagella of planktonic and adherent *P. furiosus* LS cells (Barth, 2008) were used as reference. Planktonic flagella possessed a major flagellin at 30 kDa whereas adherent flagella showed two additional flagellins with lower molecular mass (Table 2). In cell envelope preparations different proteins were detected by Coomassie staining, but flagellins could not be identified (Figure 7c). Therefore, Western blotting was performed to match protein bands of the cell envelope preparation to flagella (anti-Fla Pfu; Figure 7d) or surface proteins (anti-OF Pfu; Figure 7e). Polyclonal antibodies were generated by immunization of rabbits with either sheared and purified flagella (Näther et al., 2006) or sheared whole cells (Schopf, 2011) of *P. furiosus* LS. It can be concluded from the data

presented in Table 2 that the anti-Fla Pfu antibodies labeled additional bands not visible in Coomassie staining for both flagellar preparations. Interestingly, protein bands detected at about 25−30 kDa in cell envelope preparations (denaturated at 100°C) were more similar to flagella of adherent cells. Using the anti-OF Pfu antibodies, flagella were also visualized in the cell envelope preparations denaturated at 100°C. This result is consistent with a recent study showing that these antibodies, coupled with fluorescent dyes, labeled intact flagella of *P. furiosus* (Schopf, 2011). Comparing the data of Western blotting analyses, not only the flagellins reacted with both antibodies suggesting that these are flagella-associated proteins.

Table 2: Verified proteins band of Western blotting analyses of cell envelopes. Cell envelopes were denaturated at different temperatures (40°C or 100°C) and proteins were detected by Western blotting using either anti-Fla Pfu or anti-OF Pfu as primary antibodies. For comparison, flagella were denaturated at 100°C and flagellins were visualized using anti-Fla Pfu. **Bold** cell envelope proteins were detected with both antibodies.

Sample	Denaturation temperature in °C	Mr in kDa (experimentally) of identified protein bands Coomassie staining	Anti-Fla Pfu
Planktonic flagella	100	30	27, 29, 30 (65, 200)[a]
Adherent flagella	100	26, 29, 30 (65, 200)[a]	25, 26, 27, 29, 30 (35, 65, 200)[a]
Sample	Denaturation temperature in °C	Mr in kDa (experimentally) of identified protein bands Anti-Fla Pfu	Anti-OF Pfu
Cell envelopes	40	35, 48, **60**, **65**, **150**, **200**	43, 50, **60**, **65**, 70, **150**, **200**
	100	**25−30**, **65**, **200**	**25−30**, 40, 48, **65**, 100, **200**

[a] minor bands are given in parentheses

The adapted cell lysis protocol was proven to be reproducible and further modified to identify flagella-associated proteins. Given that *P. furiosus* is a strictly anaerobic organism (Fiala and Stetter, 1986), cell envelopes were prepared anaerobically to prevent the dissociation or degradation of oxygen-sensitive complexes. Cells were centrifuged either anaerobically or aerobically and cell lysis was carried out in an anaerobic chamber. Comparing these preparations using TEM and SDS-PAGE to the aerobically prepared cell envelopes, no differences were detected (data not shown). These findings suggest that none of the proteins is oxygen-sensitive, and the preparation was performed further on aerobically.

2.1.2 Ultrastructural details of *P. furiosus* LS cell envelope analyses

Examining the cell envelopes of *P. furiosus* LS by TEM, a variety of ultrastructural details were detected that are illustrated in Figure 8.

A proteinaceous layer up to 600 nm in size was detected, which was either spherical (Figure 8a) or a circular segment (Figure 8b). Analyzing the layers at higher magnification

showed that they consisted of parallel lines with changing direction. The power spectrum revealed different reflections that did not harmonize with the predicted p6 symmetry for the S-layer of *Thermococcales* (König et al., 2007). An association of the layer with flagella as shown in Figure 8b and c is speculative, since it could be a preparation artefact. Equally, the function of an aggregated protein cord mostly associated with the layer and flagella (Figure 8b and c) remains unclear.

Another structure observed was a proteinaceous tube also detected in flagella preparations (Schopf, 2011). The tubes had a diameter of 45−65 nm and their length ranged between 100−400 nm. They always formed aggregates (Figure 8d) with a size of up to 800 nm in diameter and 1.5 µm in length, and therewith exceeding the dimensions of a single cell. Some tubes were identified to have circular inclusions with a diameter of 30−35 nm (Figure 8e). Analysis of the power spectrum revealed the tubes to possess double reflexes with a periodicity of 7.5 nm, suggesting that they consist of a double layer and that they are most likely hollow, cylindrical structures. Since the tubes were never or only occasionally associated with flagella, a functional association seems unlikely.

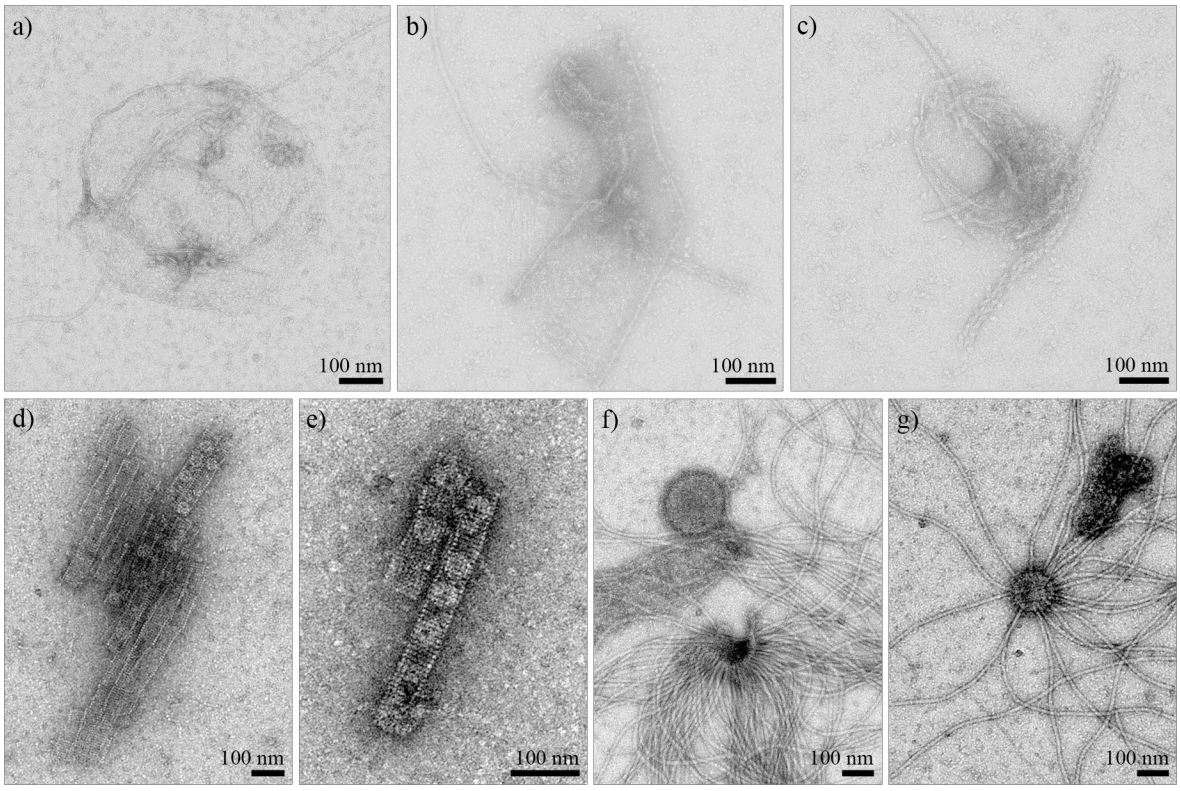

Figure 8: Ultrastructural details of the cell envelope analysis of *P. furiosus* LS. Transmission electron micrographs of negatively stained samples. a) Spherical proteinaceous layer, b) and c) Circular segment of the proteinaceous layer associated with a flagellum and proteins aggregated to a cord. d) Aggregate of tubes with a diameter of 480 nm and a length of 1.1 µm. e) Tubes at higher magnification with circular inclusions, 30−35 nm in diameter. f) and g) granum-like body with associated flagella.

The only ultrastructure that could be correlated with the anchoring of flagella is illustrated in Figure 8f and g. A circular membrane patch with a diameter of 100−150 nm was identified where multiple flagella emerged.

A similar membrane with emerging flagella was described as polar cap in *Halobacterium salinarum* (Kupper et al., 1994). Cell envelopes of *P. furiosus* LS were prepared according to that work, but unfortunately, this attempt failed. Therefore, 'polar caps' were prepared from cell envelopes by (partial) solubilization of membrane proteins using detergents, which were shown to preserve the ultrastructure of flagella (Näther, 2007). For comparison, flagella were also isolated by shearing of whole cells. Sheared flagella were 0.5−2.5 µm in length and did not show any associated proteins. None of the detergents was able to solubilize the envelopes to isolate the membrane patches. Some detached flagella seemed to possess a knob-like or round structure without a hook at one end, but the negative staining was too flat to definitely assign them to the anchor of flagella (Figure 9).

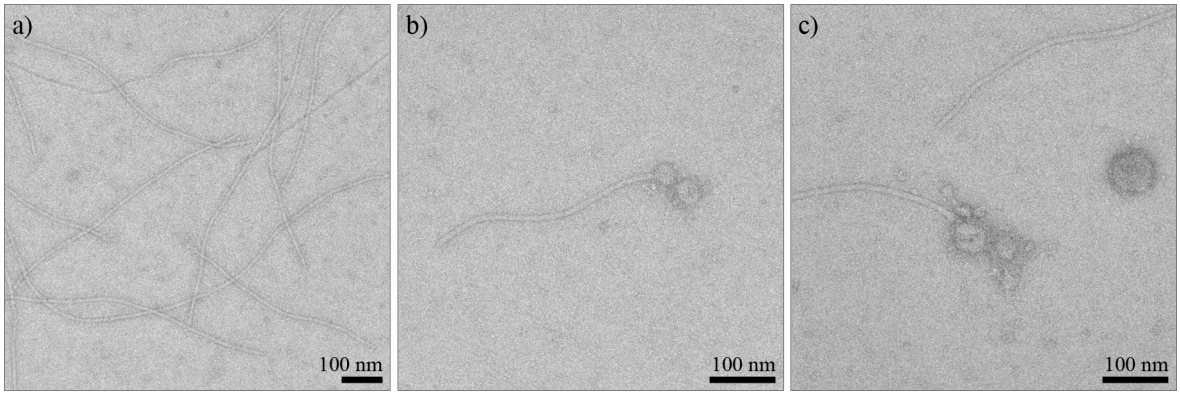

Figure 9: Flagella of *P. furiosus* LS. a) Sheared flagella in comparison to b) and c) detached flagella from cell envelope preparations. Some possible anchoring structures but no hook was detected.

Besides the ultrastructures described above, another feature was not only observed in cell envelope preparations but also in suspension of planktonic cells. As it can be seen from Figure 10a, a virus-like vesicle (800 nm in length) buds from the cell. In some cases, a single cell possessed multiple of such extensions (Figure 10b). The vesicles contained a bright core of 25 nm in diameter, which was most probably cytoplasm. A darker inner and a brighter outer layer covered the core, giving the vesicle an overall diameter of 70−80 nm. To isolate vesicles, the supernatant of exponential and stationary cultures was filtered and remaining particles were pelleted by ultracentrifugation, but electron microscopic analyses showed no or only few particles. In contrast, virus-like vesicles were detected in unfiltered controls of stationary supernatants and are illustrated in Figure 10c-h. The vesicles were heterogeneous in size, and were filamentous or short rods, which seemed to protrude from a spherical bulge. Other vesicles were spherical with a diameter of 80−200 nm or looked

like a string of pearls in which pearls made of cytoplasm were surrounded by a membrane. Enrichment of vesicles via PEG precipitation followed by CsCl gradient ultracentrifugation for further analyses like DAPI staining was not successful.

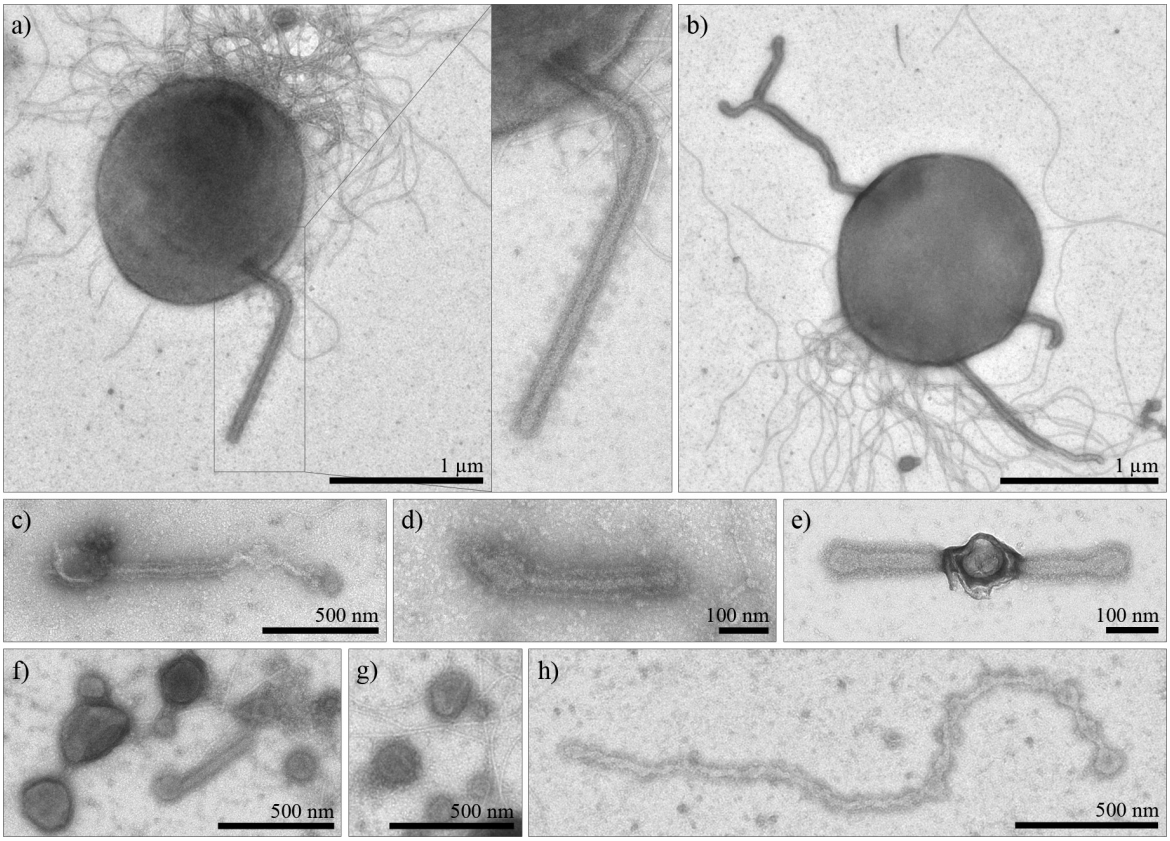

Figure 10: Virus-like vesicles of *P. furiosus* LS. Transmission electron micrographs of a) and b) negatively stained cells with protruding vesicles and c)-g) isolated vesicles. c), d) and e) Filamentous vesicles. f) and g) Spherical vesicles. h) String-of-pearl vesicle 1.5 µm in length.

2.1.3 Cell envelopes of adherent *P. furiosus* LS cells

The electron microscopic analysis of cell envelope preparations was limited because of inhomogeneous or insufficient dispersion of sample material on the grid. To overcome this problem, *P. furiosus* LS was grown on carbon-coated gold grids, which were used directly for cell lysis experiments. In a first attempt, grids were incubated in hypotonic solution (with/without shaking) overnight to analyze whether cells were detached by this procedure. Examining the grids by TEM showed that most of the cells were lysed but still attached to the surface. Based on these data, different methods for isolation of flagella (Kalmokoff et al., 1988; Schopf, 2011) were applied, in which centrifugation steps were replaced by extensive washing of grids in TBS. Afterwards grids were negatively stained with uranyl acetate and analyzed with regard to anchoring structures of flagella. Using Triton X-114 and DDM, the extraction of flagella seemed to be successful, but cell debris could not be removed from the grid and obscured further analyses (data not shown).

2.1.4 Cell envelope analysis of *P. furiosus* Vc1

In the group of Reinhard Wirth, multiple experiments were performed to isolate archaeal cell appendages from the supernatant of fermentor cultures (e.g. Müller et al., 2009). When harvesting a fermentor of *P. furiosus* Vc1, the dead volume of the centrifuge contained cell envelopes in high density, which were further analyzed in this thesis.

Interestingly, the protein pattern of cell envelopes separated via SDS-PAGE differed considerably to earlier preparations (Figure 11a and 7c). When denaturated at 40°C, prominent bands were detected in *P. furiosus* Vc1 at 35 kDa and 60 kDa not present in cell envelope preparations of *P. furiosus* LS. Beside these differences, both preparations revealed some similarities. For instance, the dominant protein band at 65 kDa was visible after application of both denaturing temperatures and those at 200 kDa only in the 40°C sample. In Western blotting analysis using the anti-OF Pfu antibodies similar bands were detected as described above for *P. furiosus* LS (Figure 11b and 7e) with exception of the flagellar proteins. Investigating the cell envelopes with TEM (Figure 11c and d), it was obvious that they possessed no flagella confirming the data obtained by Western blotting. At that time, the result was very surprising because *P. furiosus* Vc1 was believed to be the type strain and the loss of flagella was referred to centrifugation.

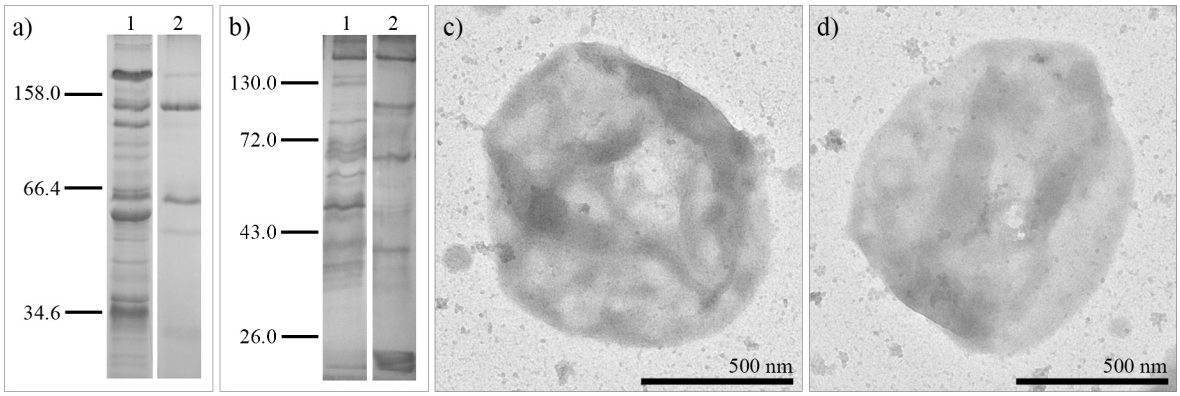

Figure 11: Cell envelopes of *P. furiosus* Vc1. a) SDS-PAGE (10% gel) and b) Western blotting (10% gel) using anti-OF Pfu antibodies (diluted 1:5,000). Cell envelopes were denaturated at either 40°C (Lane 1) or 100°C (Lane 2); molecular masses of size marker given in kDa. c) and d) Transmission electron micrographs of negatively stained cell envelopes showing that *P. furiosus* Vc1 did not possess any flagella.

2.2 Identification of proteins

By comparing the different cell envelope preparations of *P. furiosus* LS and *P. furiosus* Vc1 with the results of Western blotting experiments, potential flagella-associated proteins were detected. To this aim, the corresponding protein bands were in-gel digested and subjected to MALDI-TOF MS + MS/MS analysis (Central Protein analytical Facility of the Biology Department, University of Regensburg).

It can be seen from the data in Table 3 that the identification of interesting proteins took several attempts since most of them failed or gave no clear results, for unknown reasons. As a consequence, a double digest using trypsin and chymotrypsin was performed, and/or the denaturating temperature was reduced to 40°C. Both methods increased the number of identified proteins but also led to contradictory results. Analysis of the 200 kDa protein band gave three positive hits in four trials: The glutamate dehydrogenase (PF1602) had the highest Mascot score and a putative ATPase, vanadate sensitive, (PF1399) was hit with lower but still significant score, whereas the identification as oligopeptide transport system permease protein (PF0191) had to be neglected because of its low Mascot score.

Table 3: Protein bands subjected to MALDI

Strain	Denaturation temperature in °C	Mr in kDa (experimentally)	In-gel digestion using	Mascot score	Signifi-cance[a]	Protein ID
P. furiosus LS	40	55.0	trypsin	-	no	-
		200.0	trypsin	626	yes	PF1602
	100	55.0	trypsin	-	no	-
		65.0	trypsin	315	yes	PF0190
		200.0	trypsin	65	no	(PF0191)
P. furiosus Vc1	40	200.0	trypsin/chymotrypsin	131	yes	PF1399
	100	55.0	trypsin	-	no	-
			trypsin/chymotrypsin	-	no	-
		97.0	trypsin	-	no	-
		116.0	trypsin	99	yes	PF1935
		150.0	trypsin	-	no	-
		200.0	trypsin	-	no	-

[a] statistically significant result: protein score >80

Altogether, only four proteins were identified that were analyzed afterward with different public applications (Table 4). Three of the proteins are putative membrane or extracellular proteins, namely the putative ATPase (PF1399), the amylopullulanase (PF1935), and a hypothetical protein (PF0190), whereas the glutamate dehydrogenase is a cytoplasmic enzyme. Using PSORTb, the ATPase was predicted to be localized in the cell wall, a component that is, per definition, represented in the S-layer of *P. furiosus*. The putative localization was confirmed by prediction of a signal peptide (not present in the glutamate dehydrogenase) and of a transmembrane domain (only in the two membrane proteins).

It is apparent from the data in Table 4 that, except for the amylopullulanase, the molecular mass determined by SDS-PAGE differed substantially from the predicted value. Higher experimental masses can be explained by polymerization or glycosylation of proteins. Potential N-glycosylation motifs were predicted in all four proteins, but the glutamate dehydrogenase is unlikely to be exposed to the N-glycosylation machinery due to the lack of a signal peptide.

Table 4: *P. furiosus* proteins: biophysical and biochemical data.

Protein ID	Annotated function[a]	Local-ization[b]	Number of amino acids	Mr in kDa (predicted)	Mr in kDa (experimentally)	SP/TMH (Phobius)	SP/TMH (TMHMM)
PF0190	Hypothetical protein/CipA[c]	M/M	829	94.8	65.0	+/1	1/1
PF1399	Putative ATPase vanadate sensitive	M/W	605	65.7	200.0	+/1	1/0
PF1602	Glutamate dehydrogenase	Cyt/Cyt	420	47.1	200.0	-/1	-/0
PF1935	Amylopullulanase	M, E/?[d]	985	113.3	116.0	+/0	1/0

SP signal peptide, TMH transmembrane helix
[a] Function as annotated in the NCBI database
[b] Putative subcellular localization: X/Y with X based on the annotated function, and Y predicted (PSORTb) *Cyt* cytoplasmic, *E* extracellular, *M* cytoplasmic membrane, *W* cell wall.
[c] Described by Weinberg et al., 2005 as cold induced protein CipA, a membrane glycoprotein
[d] Identical localization scores for E, M, and W

The identification of the cytoplasmic glutamate dehydrogenase in the membrane fraction was surprising. However, an independent study succeeded to identify the enzyme in flagella preparations of *P. furiosus* by Edman degradation (Schopf, 2011). Therefore, it can be speculated whether the glutamate dehydrogenase of *P. furiosus* could be related to flagellar function or to adhesion. To answer this question, antibodies were generated to perform immuno-localization studies.

2.3 Localization of the glutamate dehydrogenase in *P. furiosus*

2.3.1 Generation, purification, and specificity of antibodies

Recombinantly expression of the glutamate dehydrogenase gene of *P. furiosus* in *E. coli* Rosetta(DE3)pLysS was achieved recently (Loose, 2009). DNA sequencing of the plasmid insert confirmed its identity, but showed that the C-terminal His-tag was not preserved due to a stop codon. Optimization experiments indicated that the highest protein yield (without the formation of inclusion bodies) was obtained when induction of the protein was performed with 1.0 mM IPTG and subsequent incubation at 37°C for 3 h.

The recombinant glutamate dehydrogenase was used for immunization of a rabbit; its preimmune serum did not react with a protein extract of *P. furiosus* Vc1. The antiserum was collected after a final titer of 1:10,000 was reached as detection limit by Western blotting against a protein extract of induced *E. coli* containing the plasmid for heterologous expression of the glutamate dehydrogenase. Since the antiserum weakly cross-reacted with other proteins present in a protein extract of *P. furiosus* Vc1, it was saturated and purified. As a result of this purification, the antibodies reacted specifically, only the titer had to be decreased to 1:1,000 (data not shown).

2.3.2 Immuno-labeling of cells

To localize the glutamate dehydrogenase in *P. furiosus*, its saturated and affinity-purified antibodies were used for different immune-labeling experiments. Because it was assumed that the function of the enzyme is related with adhesion, planktonic and adherent cells of all three *P. furiosus* strains were tested.

Initially, labeling with antibodies coupled to succinimidyl esters of fluorescent dyes was tried: On the one hand, the primary antibody was directly coupled to the dye; on the other hand signal enhancement with a secondary antibody was performed. Using direct labeling, neither the planktonic nor the adherent cells of any of the three strains could be labeled, even if the titer was raised to 1:20. Analyzing cells grown on carbon-coated gold grids to early stationary phase using signal enhancement with a secondary antibody, only weak labeling of the cells was detected. Additionally, the carbon film and debris on the grid were labeled. In a negative control without primary antibody, the same labeling was observed, allowing the conclusion that the secondary antibody did bind unspecifically at the high concentrations to be used (data not shown). Repeating the experiment with late exponential cells, weak labeling of the cells was confirmed for *P. furiosus* LS and *P. furiosus* Vc1. In the case of *P. furiosus* DSM 3638^T, adherent cells were clearly labeled showing the signal to be clustered on the cells surface (Figure 12 and supporting material). Labeling of planktonic cells gave ambiguous results: Some cells were homogeneously labeled, in others clusters only one half of the cell was fully stained (data not shown). These preliminary findings suggest that the glutamate dehydrogenase can be located on the surface of *P. furiosus*.

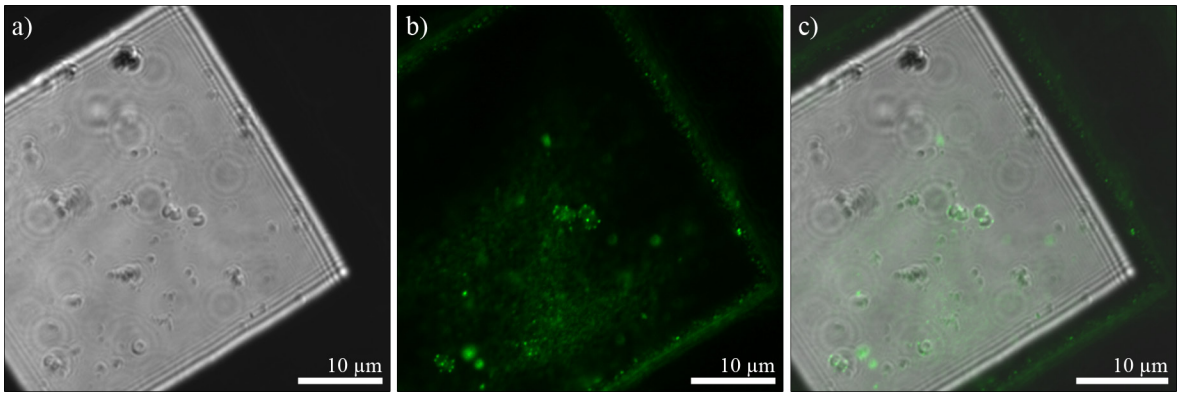

Figure 12: Localization of the glutamate dehydrogenase in *P. furiosus* DSM 3638^T. CLSM micrographs of adherent cells of *P. furiosus* DSM 3638^T that show the inhomogeneous distribution of the glutamate dehydrogenase on the cell surface. Dilution of the primary antibodies 1:100, secondary antibody coupled to Alexa Fluor® 488. a) Differential interference contrast (DIC) image. b) Localization of the glutamate dehydrogenase labeled with the saturated and purified antibodies raised against the 47 kDa protein recombinantly expressed in *E. coli*. c) Merge of Figure 12a and 12b.

To confirm this suggestion, immuno-localization studies for TEM were carried out on late exponential *P. furiosus* DSM 3638^T cells grown on grids (Figure 13a) and on ultrathin sections of *P. furiosus* LS (Figure 13b). The anti-Gdh Pfu antibodies were diluted 1:100 and 1:1,000, and the secondary antibody was coupled to 6-nm gold. Unfortunately, only weak labeling of the cytoplasm, of flagella, and of the background, but not of the cell envelopes was detected.

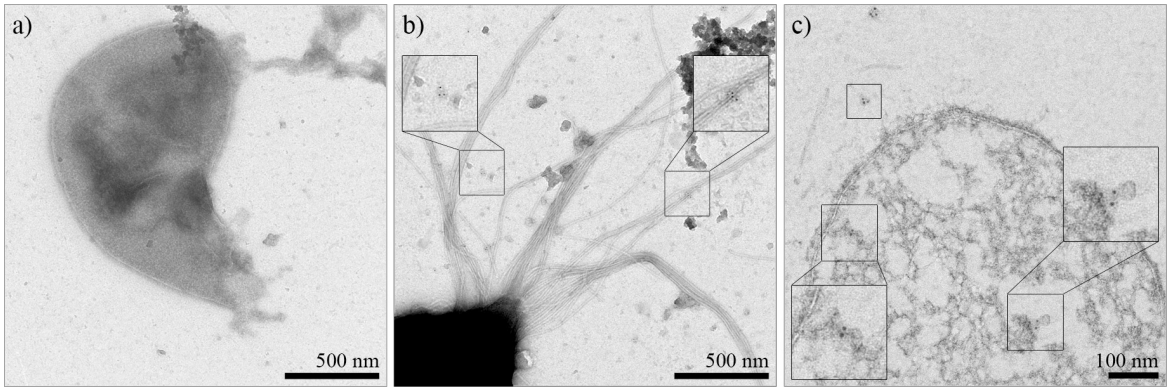

Figure 13: Localization of the glutamate dehydrogenase in *P. furiosus*. Transmission electron micrographs of a) adherent *P. furiosus* DSM 3638^T cells and b) ultrathin sectioned *P. furiosus* LS cells labeled with anti-Gdh Pfu antibodies. Boxes indicate labeling of the cytoplasm, of flagella, and in the background, maybe corresponding to transversely sectioned flagella. Dilution of the primary antibody 1:100, secondary antibody coupled to 6-nm gold. Contrasting was done with uranyl acetate.

Based on those experiments, the data of epifluorescence microscopy showing that the glutamate dehydrogenase is located on the surface of *P. furiosus* could not be confirmed. However, more research is required to clarify the contradictory results of this study. Assuming that the enzyme is related to adhesion, adherent cells should be embedded, sectioned and subjected to immune-labeling. In addition, TEM investigations are known to need antibodies with high sensitivity; therefore, another immunization attempt might be advantageous.

3 Description of *Methanocaldococcus villosus* sp. nov. KIN24-T80

As part of this thesis, the isolate *Methanocaldococcus* sp. KIN24-T80 was described as a novel strain. A maximum-likelihood tree was generated by Christine Moissl-Eichinger that confirmed the deep branching of the organism within the genus *Methanocaldococcus*. Since a physiological distinction of *Methanocaldococcus* sp. KIN24-T80 from the other *Methanocaldococci* failed, a description as novel genus was omitted. The new strain was named *Methanocaldococcus villosus* (vil.lo'sus, Latin meaning hairy, rough, shaggy, villous) referring to its multiple flagella that form bundles or a dense network and its extraordinary surface structure detected in SEM preparations.
This section will give the experiments performed to complete the characterization of *M. villosus* and some side projects related with this organism.

3.1 Culture purity and deposition

For a description of *Methanocaldococcus* sp. KIN24-T80, the optical tweezer was applied to isolate a single cell from cultures purified by serial dilution only. Two different strains frozen directly after isolation in 2005 were regenerated from our in-house culture collection (position 22/12/2 and 26/12/2). Optical trapping of cells showed that they did not easily focus in the laser beam, and altogether, only three of eight single cells grew into a culture.
Using the high-salt method, DNA was isolated from these cultures and a continuous one, and the 16S rRNA gene was amplified (primers 8af and 1406ur). Analysis of the sequences showed 100% identity of all four sequences with the sequence of strain KIN24-T80 determined during my diploma thesis (Bellack, 2007). Subsequently, isolate 22/12/2 L1 was chosen for deposition in DSMZ and JCM as *Methanocaldococcus villosus* type strain KIN24-T80; the accession numbers are DSM 22612 and JCM 16315. Moreover, the 16S rRNA gene sequence of *M. villosus* was submitted to GenBank and recorded as FJ766848.

3.2 Growth conditions and oxygen sensitivity

M. villosus had been characterized during my diploma thesis (Bellack, 2007) with exception of pH dependence of growth and the stimulatory effects of organic compounds or trace elements. These growth experiments were performed in duplicate herein.
The influence of the pH on growth was determined in MGG medium without additional buffering; the pH was measured using pH-indicator stripes. Growth was observed between pH 5.5 and 7.0, with an optimum pH of 6.5; there was no growth at or below pH 5.0 or at and above pH 7.5.

Experiments performed during my diploma thesis had shown that *M. villosus* was able to grow without selenium and tungsten (Bellack, 2007), a criteria used to differentiate between the genus *Methanocaldococcus* (both elements required) and *Methanotorris* (not required; Whitman et al., 2001). Repeating these analyses in this study using a trace mineral solution without selenate and tungstate, the results could not be confirmed. Hence, the experimental set up was changed: Medium was prepared without trace mineral solution (= MGG-M medium) and various supplements were added individually or in combination. Initially, the cells were inoculated consecutively in MGG-M medium to remove traces of minerals. The third subculturing provided evidence that *M. villosus* could indeed grow in MGG-M medium but growth was slower and resulted in two- to four-fold lower final cell densities compared to MGG medium. Interestingly, also *Methanocaldococcus jannaschii* grew in MGG-M medium, although cells required the addition of vitamins (= MGG+V medium) for optimal growth. Instead, growth of *Methanotorris igneus* was not affected by modification of the medium (Figure 14).

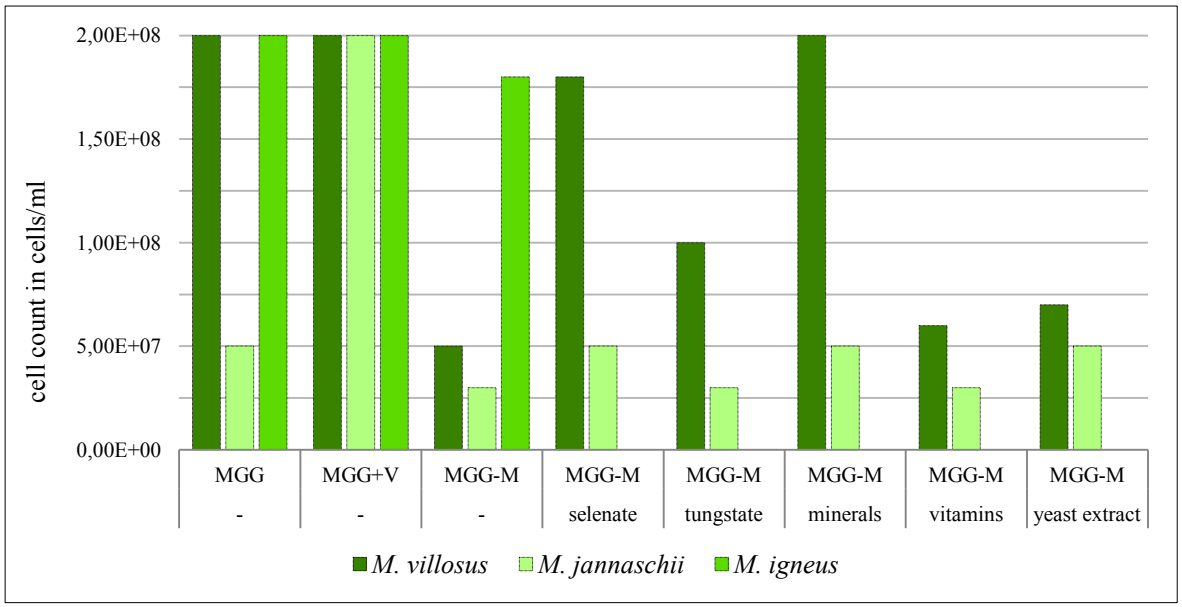

Figure 14: Influences of minerals and organics on the growth of *M. villosus*. Growth of *M. villosus* in MGG-M medium with different supplements was compared to growth of *M. jannaschii* and *M. igneus*. Cells were incubated overnight, cell densities were determined by cell counting.

For *M. villosus*, normal growth was restored when either trace minerals or selenate was added to the medium. Tungstate and yeast extract were much weaker stimulants, whereas vitamins did not affect the growth. Combinations of different supplements did not show any additive effects. In the case of *M. jannaschii*, selenate, minerals, and yeast extract were slightly stimulatory for growth. Supplemented along with vitamin solution, these effects

increased. Prolonging the incubation to 24 h, final cell densities were higher as shown in Figure 14 obscuring the effects of the supplements.

For further experiments it was of interest to determine the oxygen sensitivity of *M. villosus* at non-growth conditions. 1 ml of exponential (3×10^7 cells) or stationary (1.5×10^8 cells) cells was spotted on a cover slip and incubated at room temperature under protection from desiccation. Cells were then inoculated into fresh medium (1:20, 1:2,000, 1:200,000) and incubated for seven days or until growth was detected. Incubation for 1 h under aerobic conditions did not affect regrowth of the cells. After exposure for 12 h, only the 1:20 dilution of both, exponential and stationary cells could be inoculated successfully and no growth was detected after 24 h. The results of this simple study indicate that *M. villosus* is not sensitive to oxygen at non-growth conditions. Based on these results, cells were prepared under aerobic conditions e.g. for fluorescence staining.

3.3 Electron microscopic studies

First electron microscopic studies of *M. villosus* revealed the cells to be heavily flagellated (Bellack, 2007). Consequently, different preparation techniques e.g. freeze-etching and ultrathin sectioning were performed to analyze its flagella. Moreover, cell envelope preparations as described above for *P. furiosus* were also performed with *M. villosus*. On the one hand, the comparison of both organisms would usefully extend the current knowledge about (eury-)archaeal flagellation; on the other hand, the S-layer of *M. villosus* was analyze to describe the organism as a new species.

Lysis experiments of *M. villosus* done during my diploma thesis had shown a sensitivity of cells to hypotonic solution (Bellack, 2007). Therefore, cell envelopes were prepared in hypotonic solution at room temperature for only 15 min, and harvested by centrifugation. Analyzing the samples by TEM, well-preserved cell envelopes with multiple flagella were detected. In some preparations, cell envelopes were associated with the S-layer (Figure 15a). Diffraction analysis showed two main periodicities, one at $(11.6\ \text{nm})^{-1}$, with the second order at $(5.7\ \text{nm})^{-1}$, and the third at $(3.8\ \text{nm})^{-1}$, and another one at $(6.5\ \text{nm})^{-1}$, with the second order at $(4.3\ \text{nm})^{-1}$. From these reflexes (Figure 15c), subunits were determined to be arranged on a lattice with six-fold or pseudo-six-fold (e.g. three-fold) symmetry. The spectrum was Fourier filtered and a lattice constant of 13 nm was measured. These findings are consistent with data for S-layer of the *Methanococcales* (König et al., 2007).

In addition, cell envelopes gave some insights in the anchoring of flagella (Figure 15 e-h). Most of them ended in a knob-like structure, which was also detected in detached flagella

in the same preparation. Albeit the flagellum in Figure 15f possesses a hook region, this was hardly observed in other isolated flagella.

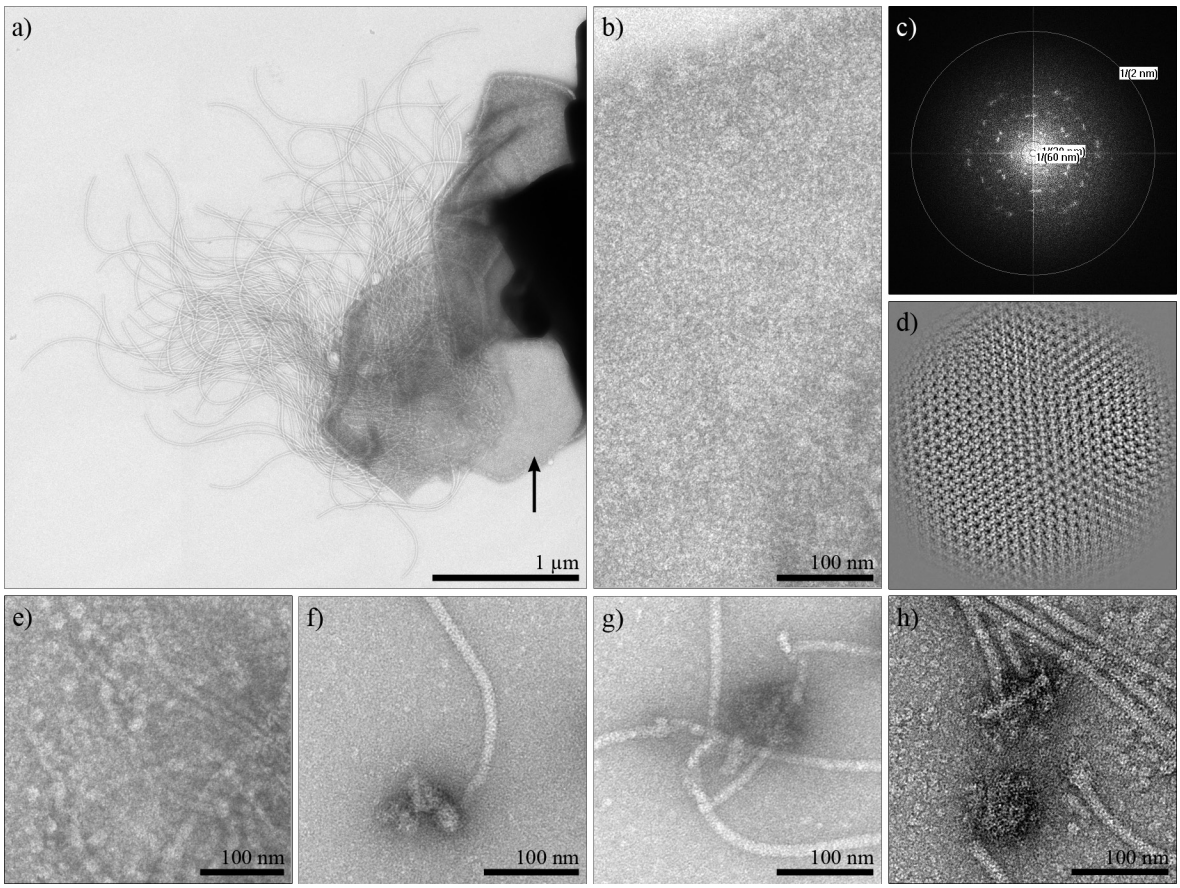

Figure 15: Cell envelope preparations of *M. villosus*. Transmission electron micrographs of negatively stained cell envelope preparations. a) Cell envelope of *M. villosus* associated with multiple flagella. The arrow points to the S-layer. b) S-layer at higher magnification together with c) the corresponding Fourier spectrum revealing the p6 symmetry and d) the Fourier-filtered analysis. e) Flagella inserted in the membrane. f), g) and h) Isolated flagella with knob-like or lined ending, which are suggested to be anchoring structures.

Further studies were set up to gain structural insights into flagellation and flagellar bundles of *M. villosus* with aid of freeze-etching. In contrast to *P. furiosus* DSM 3638^T, nearly all cells possessed multiple flagella suggesting that the *M. villosus* flagella are more stable to centrifugal forces. As shown in Figure 16a, some of the flagella formed bundles, which connected two cells with each other. The findings confirmed earlier data that the bundle is made only by one of the cells and that it disassembled when reaching the other cell (Bellack, 2007). Interestingly, in some cells the cytoplasmic membrane was structured in a distinct way in the area where flagella emerged, and clearly differed to other parts of the cell envelope (Figure 16b). Additionally, a few of the *M. villosus* cells exhibit an S-layer (Figure 16c), but, unfortunately, the surface relief was too flat to make any statements about its lattice constant.

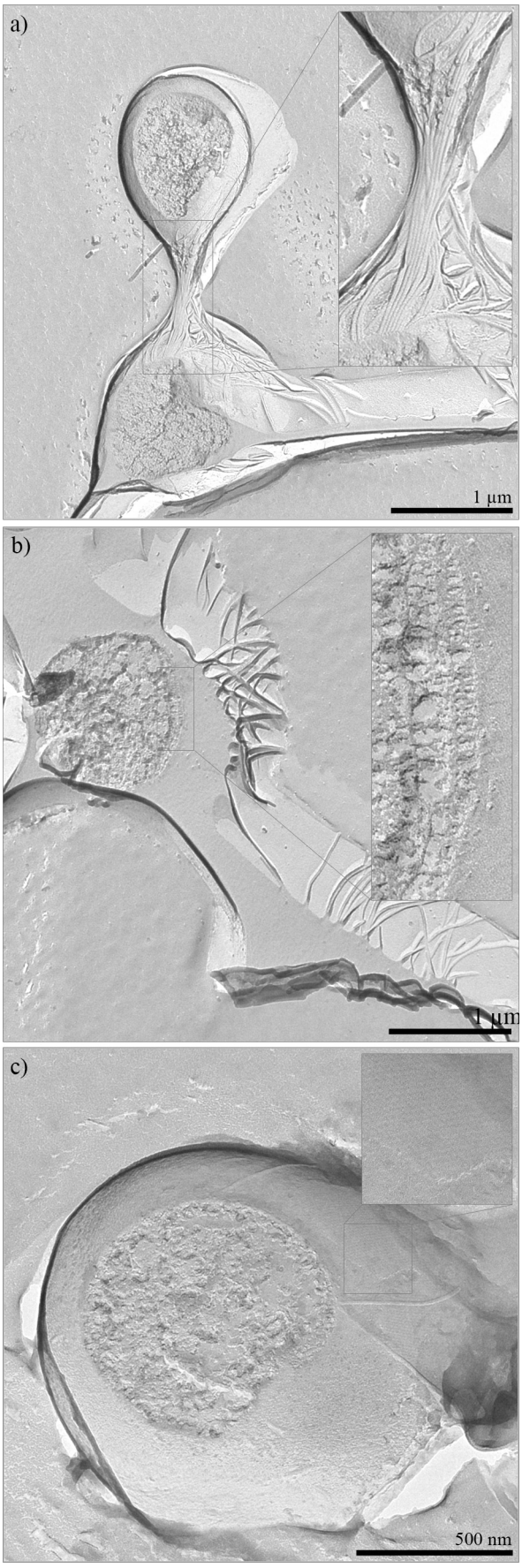

Figure 16: Freeze-etching of *M. villosus* cells. a) Cell-cell contact made by a bundle of flagella. b) Cell with emerging flagella showing a well-structured cytoplasm in proximity to the membrane. c) Cell of *M. villosus* with a fraction through the S-layer.

Upon preparation of *M. villosus* for FIB-SEM analysis, cells were also critical-point-dried and spotted on stabs. The examination of specimens by SEM revealed the extraordinary striated surface pattern of *M. villosus* on about 50% of the cells, while the others were seen to be coated with an unknown, amorphous substance (Figure 17).

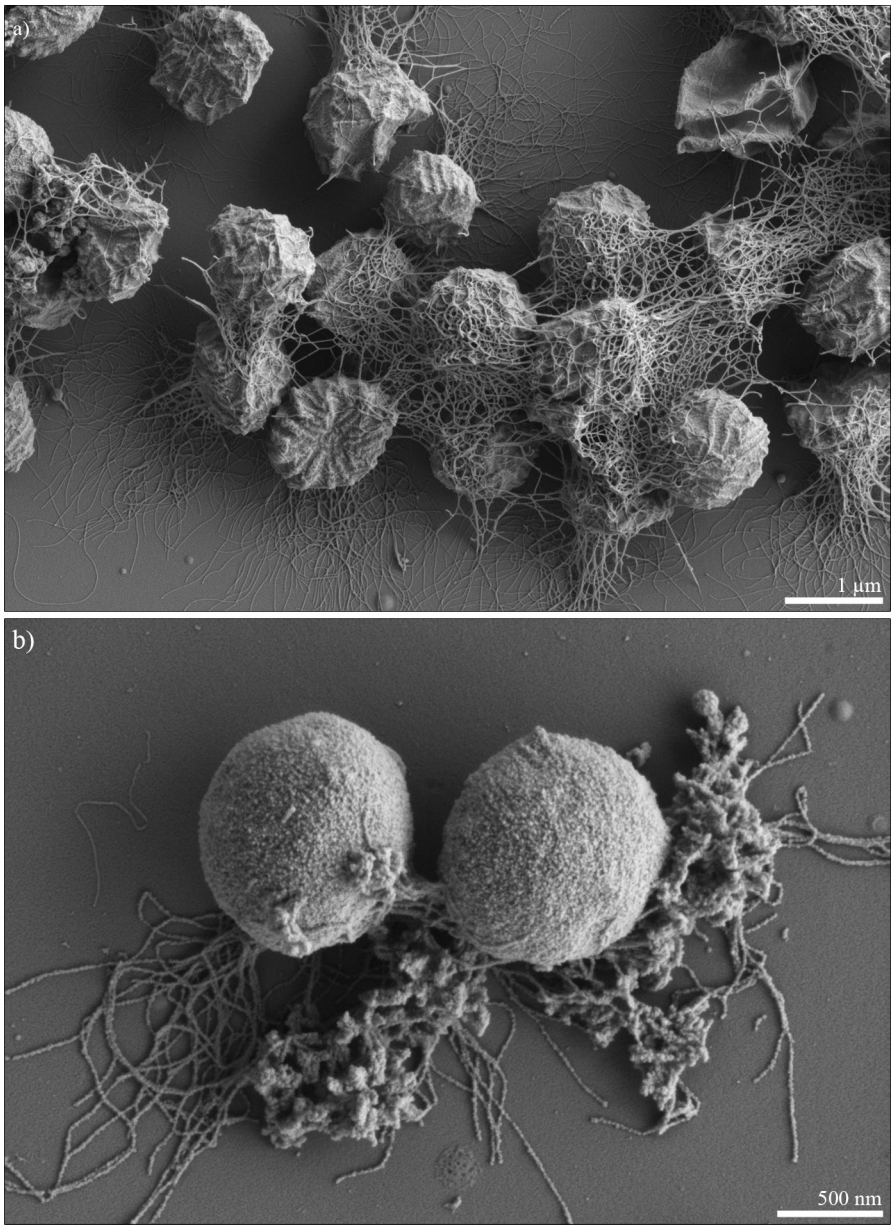

Figure 17: Scanning electron micrographs of *M. villosus*. a) Cells of *M. villosus* exhibiting a unique irregular striated surface pattern and multiple strongly interconnected flagella. b) Other cells and also flagella were densely coated with an unknown substance.

3.4 Genome size and G+C content

The genome size of *M. villosus* and the reference strain *M. jannaschii* was determined by pulsed field gel electrophoresis (PFGE). Concentrated cells were embedded in agarose, the plugs were subjected to cell lysis, and DNA was separated on a CHEF-DRIII system. In the case of *M. jannaschii*, the genome size was calculated to be 1.5 Mb, which was

somewhat smaller than the reported size of 1.66 Mb (Bult et al., 1996). Two additional bands with less than 100 kb were detected representing the two plasmids of *M. jannaschii* (18 kb and 58 kb in size, Bult et al., 1996). For *M. villosus* the genome size was in a range of 1.8–2.0 Mb and no additional bands could be identified; the presence of extra-chromosomal DNA like plasmids was therefore excluded.

The base composition of gDNA was intended to be determined by DSMZ (Braunschweig, Germany); for this purpose, cells grown in a 16-L fermentor were shipped. Unfortunately, the determination of the G+C content failed twice, also if purified gDNA was sent. This phenomenon had appeared only once before at DSMZ with a halophilic organism; in the case of *M. villosus*, it was speculated that precipitants of the medium inhibited the endonucleases used for DNA fragmentation (personal communication, Peter Schumann). To overcome this problem, the G+C content was estimated from shotgun sequencing of 96 clones and sequence analysis (LGC Genomics, Berlin, Germany). The assembled contigs represented 4.5% of the *M. villosus* genome and had a G+C content of 30%, which was very similar to the reported G+C content of *M. jannaschii* (Jones et al., 1983; Bult et al., 1996).

3.5 Preparation for whole-genome sequencing

Independent from the description of *M. villosus* as novel species, the organism was approved for whole-genome sequencing as part of the Community Sequencing Program (CSP) of the Joint Genome Institute (JGI, Walnut Creek, CA, US). The project requires 70–100 µg of high quality gDNA that was isolated from cells grown in a 50-L fermentor. The quantity of gDNA was estimated from agarose gel electrophoresis using a Lambda standard to be 100 µg. Length of gDNA was determined in both samples by PFGE to be higher than 50 kb, which meets the requirements of JGI (40 kb). The 16S rRNA gene was amplified using primers 8af and 1406ur, sequenced, and the identity of *M. villosus* was confirmed. At the end of this thesis, the JGI grouped the project in the production phase with the status of checkpoint sequencing.

4 Adhesion studies

In my diploma thesis, I have been able to show that *M. villosus* can adhere to various surfaces and that flagella mediate contact to the surfaces and to one another (Bellack, 2007). Part of this thesis was to study the surface adherence in more detail with regards to the function of flagella and biofilm formation. The adhesion data collected for *M. villosus* were compared to those of other *Methanocaldococci* and to *Methanotorris igneus*.

4.1 Adhesion behavior of *M. villosus*

4.1.1 Adherence over time

According to the growth rate determined for *M. villosus* during my diploma thesis, surfaces were analyzed in exponential (5 h), late-exponential/early-stationary (9 h) and stationary (14 h, 24 h, 48 h) growth phase. After incubation, the cell density of planktonic cells was determined, adherent cells were fixed on the grid with glutardialdehyde and analyzed by either DAPI staining or TEM (Figure 18).

In exponential growth phase, cells attached rarely to the grids. DAPI staining revealed that more cells were bound to the bars of the gold grid than to the carbon film. Examining the grids by TEM showed that all cells possessed many flagella that either loosely surrounded the cells or formed bundles disassembling not far from the cellular body. After 9 h, cells smoothly covered the surface with a distance of 3–5 µm between the cells. All cell-free areas were piled with flagella, which were much denser if cells were in close proximity (ca. 2 µm distance). Here, flagella of two or more cells formed a network and hence, cell-cell contacts. Additionally, some small microcolonies consisting of 5–20 cells were observed, whose number increased with prolonged incubation time of 14 h. These microcolonies were built of 10–100 cells and formed three-dimensional structures as shown also by confocal sectioning and SEM. Cells grown either in microcolonies or thin-layered on the surface were incorporated in a dense network of flagella, in which the cell appendages formed more bundles and cell-cell connections compared to earlier growth phases. After an incubation time of 24 h, the cell density on the surface further increased, although the cell count in the liquid medium had not changed compared to 14 h incubation. Cells had a maximum distance of one cell diameter between each other and were fully surrounded by flagella. In this stadium, it was nearly impossible to make any statements about the number of cell-cell contacts. It was also apparent that some cells on the grid already lysed, which was followed by nearly complete lysis after 48 h with cell envelopes remaining on the surface.

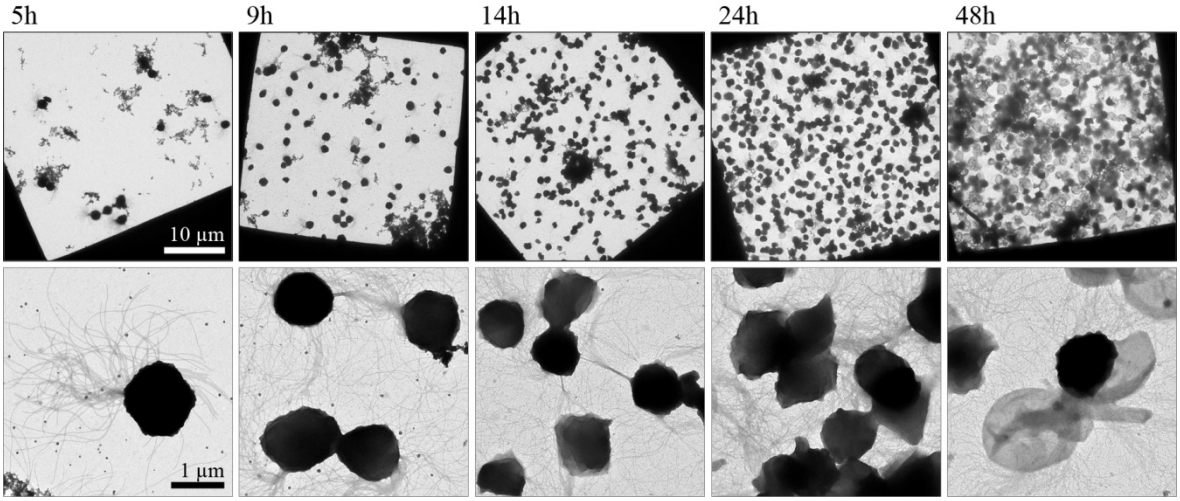

Figure 18: The adhesion behavior of *M. villosus* over time. The overview in the upper row shows that the cell density on the gold grids increases over time. From the lower row it is apparent that the more cells are attached to the surface the denser is the flagellar network and the more cell-cell contacts are formed. After 48 h, no detachment but cell lysis is visible. For better comparison, all images within one row were taken at the same magnification.

4.1.2 Biofilm formation

When analyzing scanning electron micrographs of cells grown on glassy carbon (Bellack, 2007), it was obvious that cells incorporated particles of unknown identity into their flagella network. This raised the question, if these particles form or are a part of a matrix of extracellular polymeric substances (EPS).

In a first attempt, cells grown on aperture discs were stained with Calcofluor, which indicates the presence of β-glycosidic polysaccharides. Cells were identified on the grid using the methanogen specific autofluorescence at 420 nm. In exponential growth phase, single cells adhered to the grid but no Calcofluor-signal was detectable. Analyzing overnight cultures, positive staining was recorded for microcolonies and cells that covered densely the surface (data not shown). To further analyze the chemical composition of adherent cells, SR-FTIR spectromicroscopy was performed. Cells were grown on aperture discs, which were then sent to Hoi-Ying N. Holman (Advanced Light Source, Lawrence Berkeley National Laboratory, CA, US). As can be seen from Figure 19a, the absorption spectra of cell-bearing samples showed clear infrared spectroscopic signatures of proteins, lipids, and carbohydrates compared with cell-free controls. Analysis of each spectral absorption band resulted in the construction of two-dimensional images visualizing the relative abundance of EPS components within the *M. villosus* cells (Figure 19b). Signals between 1200 and 950 cm^{-1} are attributed predominantly to the vibrations of C–O–P and C–O–C stretching of diverse extracellular carbohydrates/polysaccharide groups (Naumann, 2000). Analysis of these signals showed that *M. villosus* cells grown on a surface produced

exopolymers depending on the growth phase and therewith on the status of cellular aggregation. In single cells, very little EPS signals were detected, whereas significant FTIR signals were observed inside microcolonies. Cells forming a biofilm showed stronger polysaccharide and exopolysaccharide absorption and, additionally, an absorption peak at 1610 cm^{-1}, which indicates the presence of carboxylic groups and thus EPS proteins.

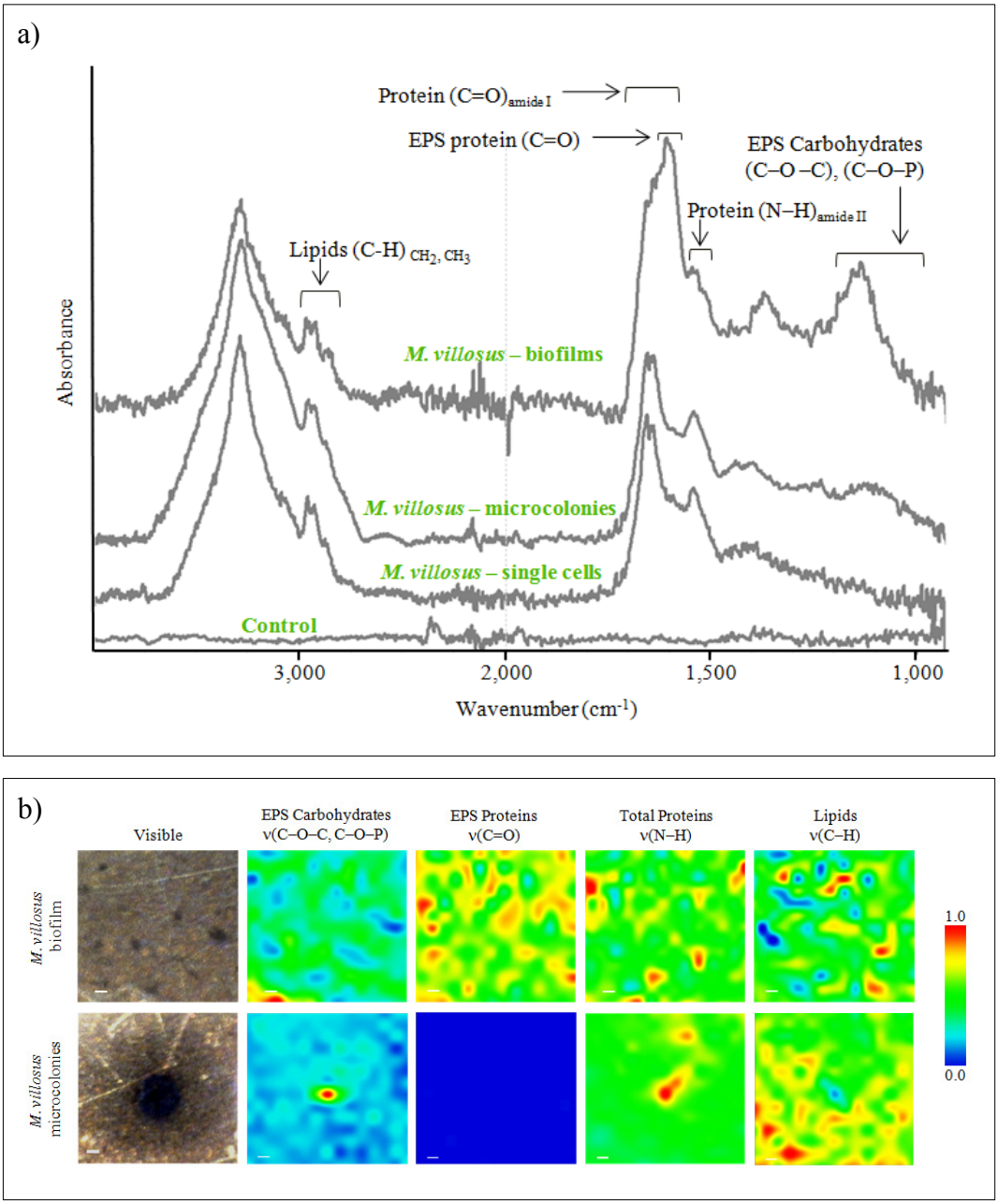

Figure 19: SR-FTIR analysis of adherent *M. villosus* cells. a) SR-FTIR spectra showing the biochemical composition in *M. villosus* grown in biofilms (top spectrum), in microcolonies (middle spectrum), and in single cells (bottom spectrum). Each spectrum was normalized by the N-H vibration of proteins (amide A at ~3300 cm^{-1}). Control: SR-FTIR spectra recorded in adjacent cell-free areas. b) SR-FTIR spectrum and images showing the relative distribution of *M. villosus,* EPS carbohydrates, EPS proteins, overall proteins, and lipids in a typical *M.villosus* biofilm (top) and microcolony (bottom). Distribution heat map of the EPS carbohydrates vibration modes at ~1130 cm^{-1}, of the normalized EPS protein vibration modes at ~1610 cm^{-1}, of the overall protein amide I vibration modes at ~1648 cm^{-1}, and of the long-chain groups of lipids at ~2880 cm^{-1}.

4.1.3 Differences of adherent versus planktonic cells

To further investigate the role of flagella for adhesion, cells in serum bottles without grids were incubated in parallel to those of adhesion studies to assure exclusive planktonic growth. Cell counting showed that planktonic cells reached same cell densities in both cases. If planktonic cells had already reached stationary phase, the cell density increased further on the grids. Moreover, after 48 h of incubation, nearly all cells on the grid were lysed, and also ca. 50% of planktonic cells of the same serum bottle. In contrast, no cell lysis was detected without solid support even when cells were incubated for 72 h (data not shown).

During preparation of cells grown in liquid media, high centrifugal forces and extensive pipetting were avoided to conserve flagellar filaments. Anyhow, planktonic cells possessed less flagella than cells adhering to a surface as can be seen from Figure 20 for late exponential cells. Only about 5% of the cells formed cell-cell contacts that consisted of only one bundle of flagella. Contrary, up to 50% of adherent cells possessed at least one flagellar bundle or cells were connected by loose flagella. Interestingly, flagella of cells grown on a surface surrounded the whole cell which was never observed for planktonic cells. Moreover, flagella of the latter cells always emerged polarly, whereas the region of flagella insertion was broader in adherent cells sometimes culminating in peritrichous flagellation (Figure 21d).

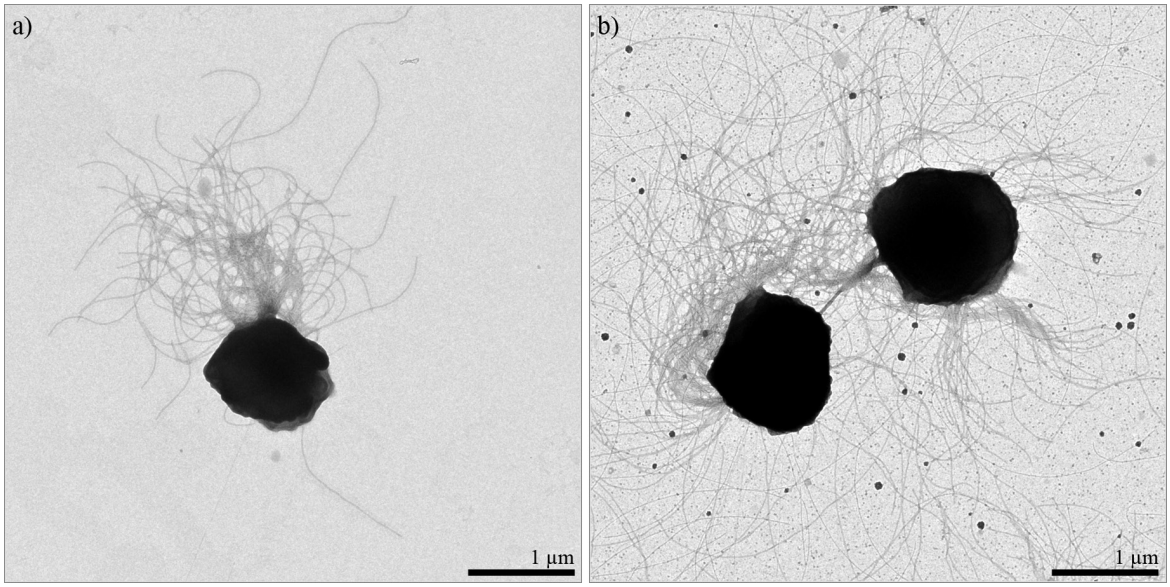

Figure 20: Comparison of planktonic and adherent *M. villosus* cells. Cells of *M. villosus* were grown to late exponential growth phase. a) Planktonic cells are polarly flagellated. b) Adherent cells on carbon-coated gold grids possess more flagella, which surround the whole cell.

4.1.4 Cell division studies

Because the adhesion studies indicate that cells adhering to surfaces are able to perform cell division, grids were examined in order to identify different stages of cell division. Additionally, scanning electron micrographs of planktonic *M. villosus* cells and of cells grown on glassy carbon prepared during my diploma thesis (Bellack, 2007) were analyzed.

When examining surfaces incubated to exponential growth phase, 10−20% of adherent cells were in the process of cell division. In early division stages, cells resemble polarly flagellated short rods with no or a broad waist. From scanning electron micrographs it can be seen that the irregular striated surface pattern surrounded the cell evenly and the septum was yet not identified (Figure 21a). With further progress, the septum was visible as a notch at the mid-plan of the cocci dividing the flagellated mother cell and the non-flagellated daughter cell (Figure 21b and c). When the cell division was nearly completed, the daughter cell starts to assemble flagella (Figure 21d). Analysis of planktonic cells showed that the flagella of both, the mother and the daughter cell were inserted on the distal pole of the cell division septum indicating that the new cell material is incorporated at the septum.

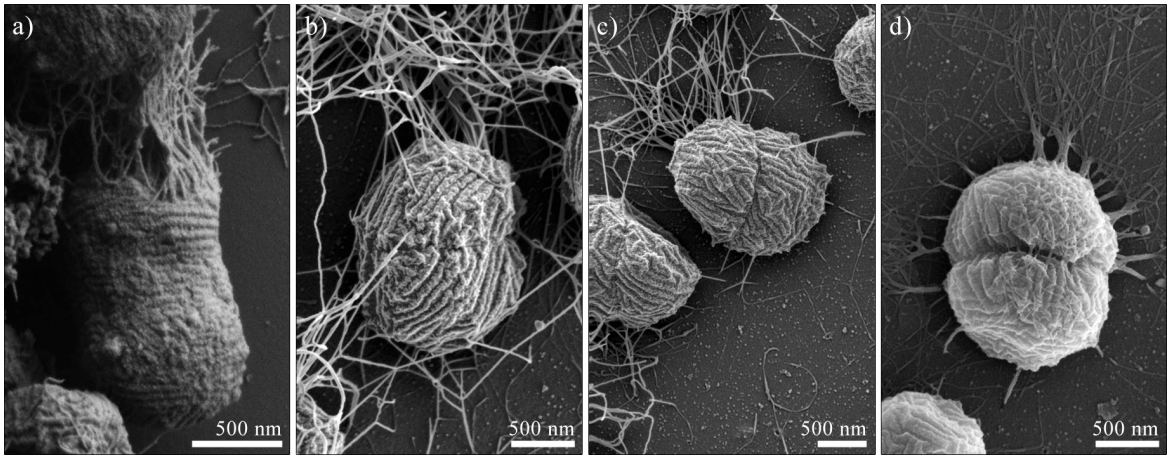

Figure 21: Cell division studies of *M. villosus*. Scanning electron micrographs of different cell division stages of a) planktonic and b-d) adherent *M. villosus* cells.

4.1.5 Detachment studies

Recent publications in our group have revealed that flagella of *P. furiosus* and fimbriae of *Methanothermobacter thermoautotrophicus* are functional adhesins since organism were detached from surfaces by antibodies directed against their cell appendages (Näther et al., 2006; Thoma et al., 2008). This raised the question if flagella of *M. villosus* have a similar function since the abovementioned adhesion studies described their important role in attachment and biofilm formation. Prior to the experiments, it was confirmed that all grids

were covered with similar cell densities. DAPI staining of the negative controls (without or with anti-Fla Pfu antibodies) showed that slightly fewer cells adhered to the grid than before treatment. Compared to the controls, none of the anti-Fla KIN antibody dilutions used herein resulted in detachment of cells. Transmission electron micrographs confirmed the results and showed that all cells possessed multiple flagella (data not shown).

4.2 Adhesion studies of the *Methanocaldococcaceae*

4.2.1 The genus *Methanocaldococcus*

Initial adhesion studies of *M. jannaschii* and *M. indicus* indicated that both organisms are able to grow on surfaces (Bellack, 2007). Here, also the other validly described species of the genus *Methanocaldococcus* (*M. fervens*, *M. infernus*, and *M. vulcanius*) were analyzed.

First analysis of carbon-coated gold grids incubated overnight using DAPI staining revealed the gold grid and also the carbon film to be covered with cells for each of the five species. Cells of all organisms grew either as a thin layer or in microcolonies. Further investigation by TEM showed that their adherence resembled the one described above for *M. villosus*: Cells were embedded in a dense network of flagella which also formed the previously mentioned tufts and cell-cell contacts. Comparison of adherent cells with planktonic ones revealed that the latter possessed less flagella for all five strains. As mentioned above for *M. villosus*, planktonic cells also formed less flagellar bundles and less cell-cell contacts (data not shown). These findings suggest that flagella of the members of the *Methanocaldococci* play an important role in adhesion and biofilm formation.
Beside the results described above, detached flagella were detected when analyzing grids of adherent *M. jannaschii* cells, which were 15 µm in length (Figure 22).

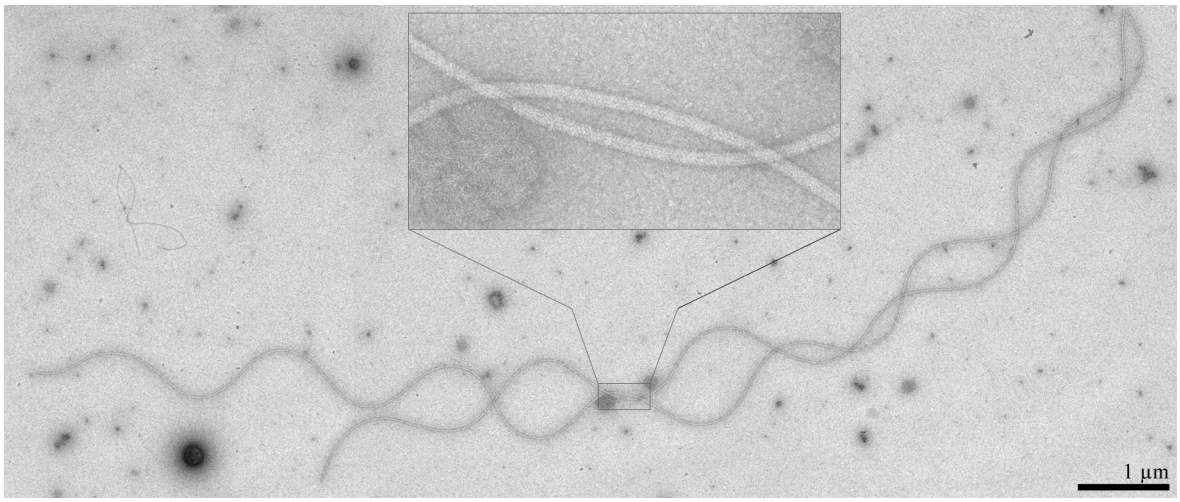

Figure 22: Curled flagella of *M. jannaschii*. Transmission electron micrograph of *M. jannaschii* flagella with a diameter of 12 nm and a length of 15 µm detected on gold grids with adherent cells. Negative staining.

4.2.2 *Methanotorris igneus*

The aforementioned results raised the question whether the cell appendages of *M. igneus* are also involved in attachment, even though they were described to be thinner and less numerous than those of *M. jannaschii* (Burggraf et al., 1990).

Again, carbon-coated gold grids were chosen and incubation was performed as described for *M. villosus* except that sampling was done also after three hours due to the rapid growth of *M. igneus*. Analysis of the grids revealed *M. igneus* to be able to attach to the surface via its cell appendages (Figure 23). In contrast to planktonic cells, the highest cell density on the carbon film was observed after five hours revealing a cell distance of 1−3 µm. Each cell possessed at least five cell appendages with 6.5−8 nm in diameter also forming tufts and cell-cell connections, as was described above for the *Methanocaldococci*. Increasing the incubation to 9 h and 14 h, respectively, showed that some cells detached from the solid support but most of the cell appendages remained on the grid. Examining these appendages with higher magnification revealed no hook but an anchor-like structure consisting of two rings and a possible rotation system (Figure 24). After incubation for 24 h, only single, mostly lysed cells were found attached on the carbon film, and a lot of background debris was seen. Nevertheless, various cell appendages were detected, of which few showed anchor-like structures again.

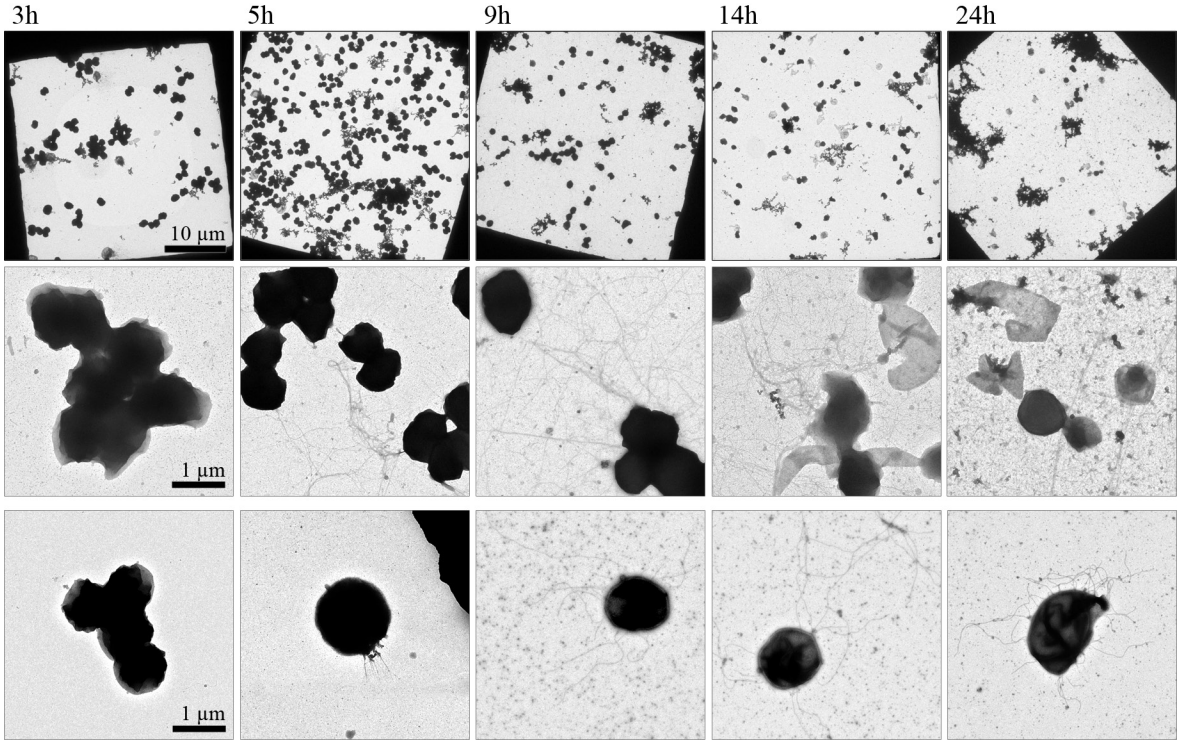

Figure 23: Comparison of adherent and planktonic *M. igneus* cells. The top row shows an overview of adherent cells on carbon-coated gold grids revealing that cell appendages play a crucial role in adhesion (middle row). The bottom row shows planktonic cells. Images within a row taken at the same magnification.

In parallel, cells grown in liquid media were examined and compared to adherent cells (Figure 23). In exponential growth phase, hardly any cell appendages were observed. After an incubation of 9 h or 14 h, most planktonic cells possessed on average five filaments with 6.5−7.5 nm in diameter, which is consistent with earlier data (Burggraf et al., 1990). Interestingly, cells also formed cell-cell contacts comprising the filaments of both cells. From the data obtained it can be concluded that the cells lysed rapidly when entering the stationary phase.

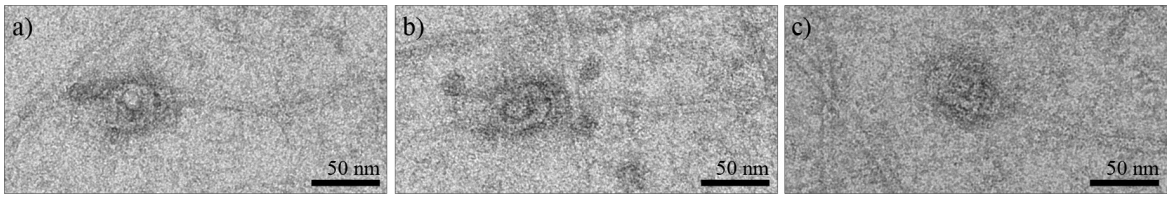

Figure 24: Potential anchors of *M. igneus* cell appendages. Transmission electron micrographs of cells grown for 9 h on carbon-coated gold grids. Cells were already detached but cell appendages with putative anchoring structures remained on the carbon film.

Examining both, planktonic and adherent cells, virus-like vesicles similar to those detected in *P. furiosus* LS cell envelope preparations were found. In contrast to these earlier results, in *M. igneus* vesicles were mostly of the string-of-pearl type or spherical. Filamentous vesicles up to 1 µm in length only rarely possessed a bulge as it was common in *P. furiosus* LS (Figure 25).

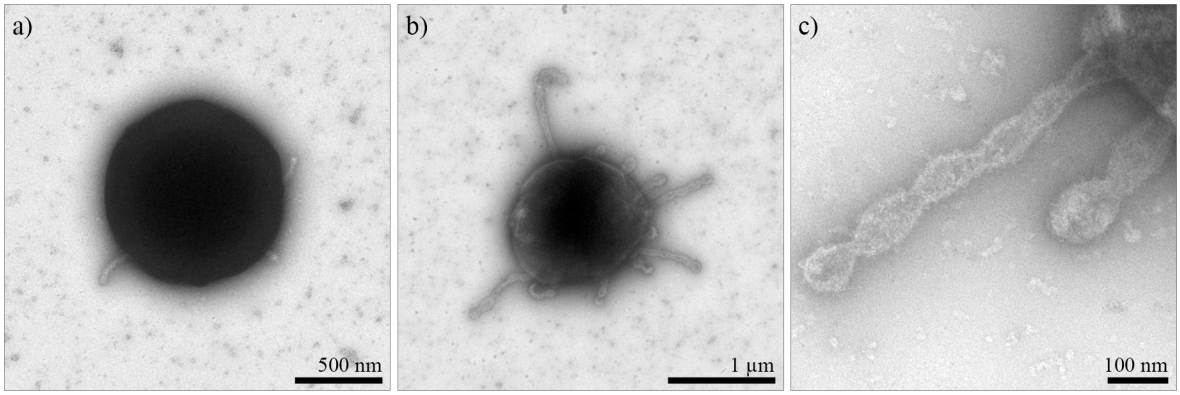

Figure 25: Virus-like vesicles of *M. igneus*. Transmission electron micrographs of negatively stained planktonic cells of *M. villosus* showing the protrusion of vesicles

5 The ultrastructure of flagella

Besides functional analyses, this study focused on the ultrastructural characterization of flagella. Therefore, flagella of *P. furiosus* DSM 3638^T and *M. villosus* were prepared by shearing and a three-dimensional reconstruction was targeted in cooperation with Edward H. Egelman (Department of Biochemistry and Molecular Genetics, University of Virginia, US). Additionally, flagella of adherent and planktonic cells were subjected to different immuno-labeling experiments and a bioinformatic analysis of methanogenic flagella was performed.

5.1 Flagella preparation

For isolation of flagella, *M. villosus* and *P. furiosus* DSM 3638^T were grown in a 50-L fermentor. After purification of sheared flagella using CsCl gradient ultracentrifugation, four bands were detected for both organisms, whereof the second (*M. villosus*) or the forth (*P. furiosus*) contained flagella, as identified by SDS-PAGE (Figure 26a). For *M. villosus*, earlier data were confirmed that flagella consist of (at least) four flagellins with apparent molecular masses of 27 kDa, 29 kDa, 33 kDa, and 35 kDa (Bellack, 2007). Compared to a flagella preparation stored for five years at 8°C, different relative quantities of the flagellins were observed. Flagella had to be diluted 1:50 for TEM analysis, which revealed a pure preparation of 11-nm filaments mixed with ~2% of a thinner type of filament, 6 nm in diameter (Figure 26b). Examining the older flagella, no ultrastructural differences were seen. In contrast to aforementioned results, two prominent protein bands possessing an apparent molecular mass of 26 kDa and 29 kDa were detected in electrophoretic analyses of *P. furiosus* DSM 3638^T flagella. When diluted 1:20 for TEM analysis, 12-nm flagella and 1−2% of 6.5-nm filaments were detected (Figure 26c).

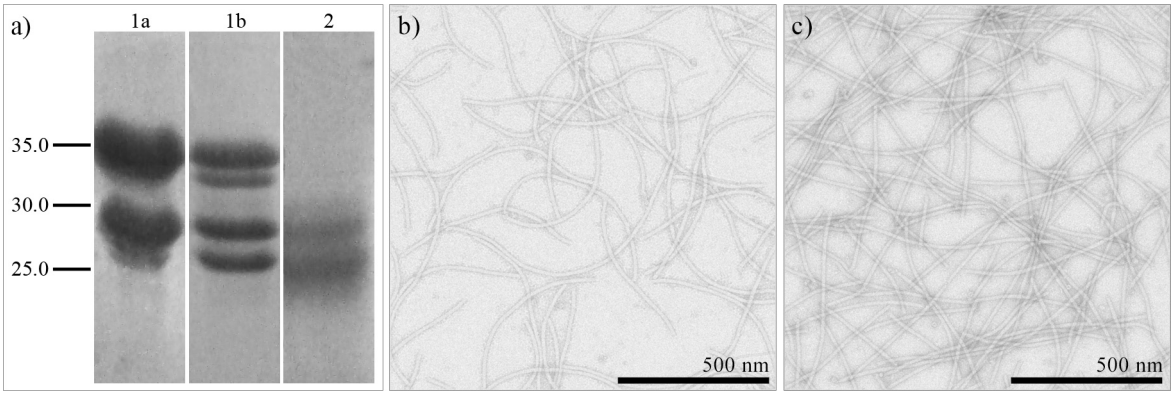

Figure 26: Flagella preparations of *M. villosus* and *P. furiosus* DSM 3638^T. a) Electrophoretic analysis of the flagella. Lane 1: *M. villosus* (a prepared in 2010, b prepared in 2005), lane 2: *P. furiosus* DSM 3638^T. 12.5% gel. Molecular masses of size marker given in kDa. Transmission electron micrographs of negatively stained purified flagella of b) *M. villosus* (diluted 1:50) and c) *P. furiosus* DSM 3638^T (diluted 1:20).

To analyze the stability *M. villosus* flagella, they were incubated with chaotropic agents at 37°C or 80°C. In TEM preparations, no differences were detected to untreated flagella.
In addition, flagella were analyzed by Western blotting using the antibodies against whole flagella (diluted 1:10,000). For *M. villosus*, results were consistent with earlier findings that beside the flagellins also three proteins at 55−65 kDa were labeled (Bellack, 2007). Labeling of *P. furiosus* DSM 3638^T flagella detected the two prominent flagellin bands and weak signals at 35 kDa and 65 kDa (compare to Table 2). Moreover, antibodies generated against recombinantly expressed parts of the three *P. furiosus* flagellins were used in a 1:100 dilution. A strong signal was detected with the anti-FlaB2-CT Pfu antibodies at 30 kDa and 35 kDa, whereas the anti-FlaB1-MT Pfu antibodies labeled the 30 kDa protein band and additional proteins at 23 kDa and 25 kDa. No reaction was observed with the anti-FlaB0-MT Pfu and anti-FlaB2-MT Pfu antibodies (data not shown).
For further analysis of flagella, 200 µl of each sample were sent to Edward H. Egelman for cryo-electron microscopy. Unfortunately, flagella of *M. villosus* and *P. furiosus* fell apart during preparation. Therefore, micrographs of negatively stained flagella were collected for processing, although this method is not suitable for obtaining micrographs aiming for high resolution reconstructions.

5.2 The flagella of *M villosus*

For ultrastructural analysis of *M. villosus* flagella, samples were diluted 1:500 before application onto carbon-coated copper grids. Specimens were searched for well-structured and contrasted flagella (Figure 27a) that show multiple reflexes in the Fourier spectrum (Figure 27b). Montages of 9−25 single images were taken (Figure 27c) and provided as full resolution 16-bit TIFF files (pixel size 0.46 nm; original final magnification of 52,500 ×) to Edward. H. Egelman for processing. Initially, a power spectrum was generated from relatively straight filaments showing a mixture of symmetries (Figure 27d). The strongest layer line at $(5.6\ nm)^{-1}$ arose from a three-start helix and the meridional layer line at $(3.4\ nm)^{-1}$ indicated that the rise per subunit is 3.4 nm. These findings suggest a point group symmetry, such as a three-fold axis, so that the axial rise per asymmetric unit corresponds to a ring of three subunits. Interestingly, a third layer line most likely from a one-start helix was detected, which is incompatible with any point group symmetry. The most likely explanation for these findings is that native flagella are composed of flagellin subunits arranged in a filament with a mixture of at least two different symmetries, which were superimposed in the power spectrum (personal communication, Edward H. Egelman).

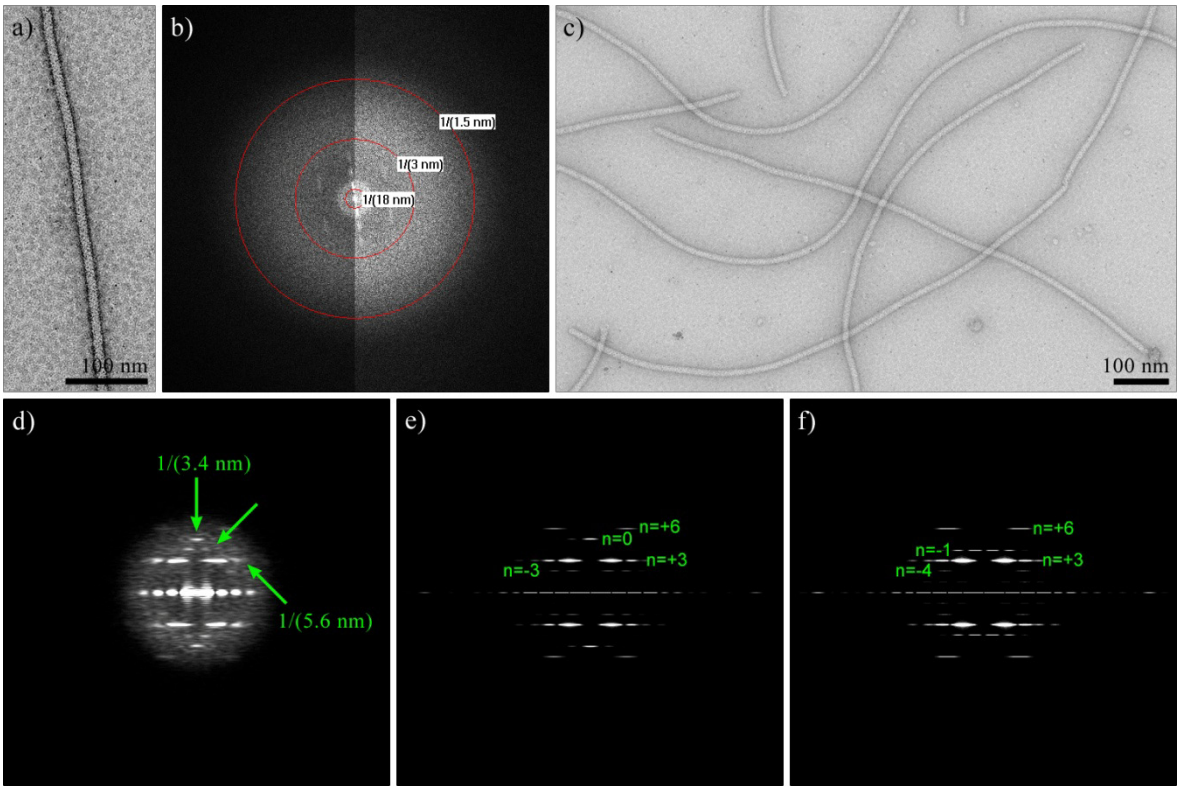

Figure 27: Ultrastructure of *M. villosus* flagella. a) Well-structured flagellum with the corresponding b) Fourier spectrum revealing multiple reflexes. c) Montage for processing. d) Generated power spectrum from relatively long straight filaments showing a mixture of symmetries. Bessel order of e) the C3 symmetry and f) the one-start helix. – left-handed, + right-handed, handedness can be inverted.

As flagella were not unbended by chaotropic agents, much more micrographs of negatively stained flagella were generated and sent for analysis. Here again, the two structural states could not be separated apart suggesting that both states are randomly mixed. Two different poor reconstructions were generated with the IHRSR algorithm, and the layer lines of the corresponding power spectrum were indexed with the Bessel order by Edward H. Egelman (- left-handed, + right-handed; Figure 27e and f). In case of the C3 symmetry, the meridional layer line was confirmed and, additionally, two right-handed helices (a three-start and a six-start helix) and a left-handed three-start helix were assigned. In the second power spectrum, layer lines were labeled with two right-handed helices (again a three-start and a six-start helix) and two left-handed helices (a one-start and a four-start helix).

To identify the hand of the dominant helix, flagella were metal-shadowed unidirectionally with Pt/C (angle: 45°). As reference, phalloidin stabilized F-actin was used, from which flagella could be easily distinguished by their much thicker diameter (Figure 28a and c). For F-actin, two layer lines were detected representing the right-handed 70-nm pitch two-start helices and the left-handed 5.9-nm pitch one-start helix (Figure 28b). In case of *M. villosus* flagella, the layer line at $(5.6\ \text{nm})^{-1}$ arises from a left-handed three-start helix (Figure 28d).

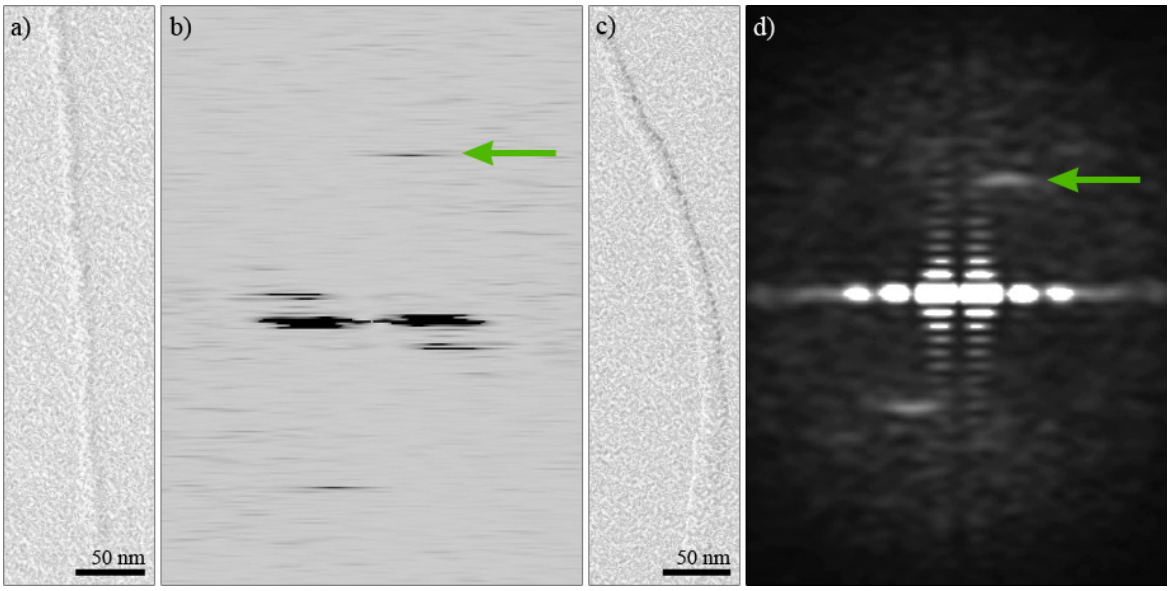

Figure 28: Ultrastructural analysis of flagella. a) Pt/C-shadowed (45°) F-actin filament. b) Arrow marking the left-handed 5.9 nm pitch one-start helix of the actin filament. The other reflex arises from the right-handed 70.0 nm pitch two-start helix. c) Pt/C-shadowed (45°) flagella of *M. villosus*. d) The arrow indicates the layer line at $(5.5\ nm)^{-1}$ arising from a three-started left-handed helix.

5.3 Database analyses of flagella of the genus *Methanocaldococcus*

Until November 2011, the genomes of five *Methanocaldococci* are publicly available. The annotated flagellins were analyzed using different bioinformatic tools, and compared to the results of flagellar analyses achieved during my diploma thesis (Bellack, 2007). The collected data are summarized in Table 6 and A2.

All genomes were predicted to encode multiple genes for archaeal flagellins, namely three in the case of *M. jannaschii* and five in *Methanocaldococcus* sp. FS406-22, *M. fervens*, *M. infernus*, and *M. vulcanius*. These predictions differ in some details from the results elaborated in my diploma thesis. Compared to the genome data, only two major flagellins were identified in SDS-PAGE for *M. jannaschii* and three for *M. vulcanius*. The results obtained for *M. jannaschii* are consistent with a study showing that its flagella were composed of two flagellins, but with a higher apparent molecular mass (27 and 32 kDa; Kalmokoff et al., 1992), compared to 26 and 28 kDa determined in my studies. Given that apparent molecular masses of flagellins from isolated flagella were larger than calculated masses from the gene sequence, post-translational modifications, e.g. glycosylation, are likely to occur throughout processing of these proteins. Positive glycoprotein staining was achieved for all flagellins except for one of the *M. infernus* proteins (confirmed by genome data analysis) and none of the *M. jannaschii* flagellins. The latter flagellins were described in different reviews to be not glycosylated (Jarrell et al., 1996; Thomas et al., 2001), although glycoprotein staining was not performed in the original study (Kalmokoff et al.,

1992). By contrast, possible N-glycosylation sites (Asn-Xaa-Ser/Thr sequons) with at least one potentially glycosylated Asn-residue were predicted for the three flagellins.

Table 5: Characteristics of the flagellins of the *Methanocaldococcaceae*. Electrophoretic analysis of denaturated flagella of validly described members of the genus *Methanocaldococcus* (upper part, see Bellack, 2007) compared to available genome data of *Methanocaldococci* and *M. igneus* (lower part, see Table A2).

Organism	Number of flagellins[a]	Mr of flagellins in kDa (experimentally)	Glycosylation (experimentally)[b]
M. fervens	5	27, 28, 33, 39, 47	all
M. indicus	4	25, 28, 31, 33	all
M. infernus	5	23, 24, 27, 29, 30	23, 27, 29, 30
M. jannaschii	2	26, 28	none
M. villosus	4	27, 29, 33, 35	all
M. vulcanius	3	31, 32, 34	all

Organism	Number of flagellins[c]	Mr of flagellins in kDa (predicted)[d]	Glycosylation (predicted)[e]	Genome accession number[c]
M. fervens	5	15.5, 16.3, 22.2, 22.8, 23.9	all	CP001696
M. infernus	5	15.3, 16.3, 22.3, 22.6, 23.3	15.3, 16.3, 22.3, 22.6	CP002009
M. jannaschii	3	22.6, 22,7, 23.1	all	L77117
M. vulcanius	5	15.7, 15.8, 22.4, 22.8, 22.8	all	CP001787
M. sp. FS406-22	5	15.6, 15.6, 22.4, 22.5, 23.3	all	CP001901
M. igneus	0	-	-	CP002737.1

[a] Determined by SDS-PAGE
[b] Determined by periodic acid-Schiff (PAS) staining
[c] Entrez genomes, NCBI database
[d] Prediction of the molecular mass of proteins (with signal peptide) using ProtParam
[e] Prediction of N-glycosylation sites with NetNGlyc 1.0 Server

A closer look at the amino acid sequences of the annotated flagellins revealed some similarities: The flagellar operons of the five analyzed organisms encode three larger flagellins with molecular masses between 22.2−23.9 kDa that contain the typical flagellin signal peptide and the consensus sequence of mature flagellins (Bardy et al., 2003). Except for *M. jannaschii*, two smaller flagellins were annotated ranging between 15.3−16.3 kDa, which lack the extremely conserved 40−50 N-terminal amino acids of archaeal flagellins. Interestingly, the flagellins do not possess highest homologies within one genome, but to corresponding flagellins of related species (Figure A1) suggesting that the flagellins/ flagellar operons had evolved from a common ancestor. The differences in their apparent molecular masses in SDS-PAGE most probably stem from differing numbers of N-glycosylation sites and/or variously linked glycans.

5.4 Immuno-labeling of flagella

Former studies had proven that antibodies directed against flagella of *M. villosus* bind to its denaturated flagella proteins in Western Blotting (Bellack, 2007). In the present study it was investigated if antibodies can be utilized to label native flagella on either whole cells or in ultrathin sections. Additionally, similar experiments were performed with *P. furiosus*.

5.4.1 Fluorescent staining

Since *M. villosus* was not detached from surfaces by anti-Fla KIN antibodies, it was tested if antibodies could be used for staining of flagella of adherent cells. A recent study showed that, in the case of planktonic *P. furiosus* cells, staining of flagella was not successful if the primary antibody was directly labeled with Alexa Fluor® dyes (Näther, 2007). Hence, in this study, signal enhancement with a secondary antibody coupled with succinimidyl esters of Alexa Fluor® 488 was done. The primary anti-Fla KIN antibody was diluted 1:100 and 1:1,000, and for visualization of cells, they were stained with Alexa Fluor® 555 after incubation with the secondary antibody. A first examination of labeled cells using epifluorescence microscopy showed that the 1:100 dilution was required for optimal detection of flagella. In addition, it was apparent that not only flagella but also the cells were labeled with the secondary antibodies (data not shown). As a result, labeling of adherent cells for CLSM analysis was only achieved with the 1:100 antibody dilution and the staining of the cellular bodies with Alexa Fluor® 555 was omitted. The results of the CLSM studies are illustrated in Figure 29 a-c demonstrating that cells of *M. villosus* can be visualized together with their flagella. The data obtained were completely consistent with those of the adhesion studies: Cells were embedded in a dense network of flagella that also formed bundles which were represented herein by much brighter signals. The recording of z-stacks was identified as a powerful method to analyze the three-dimensional growth of cells without the need of electron microscopy (supporting material).

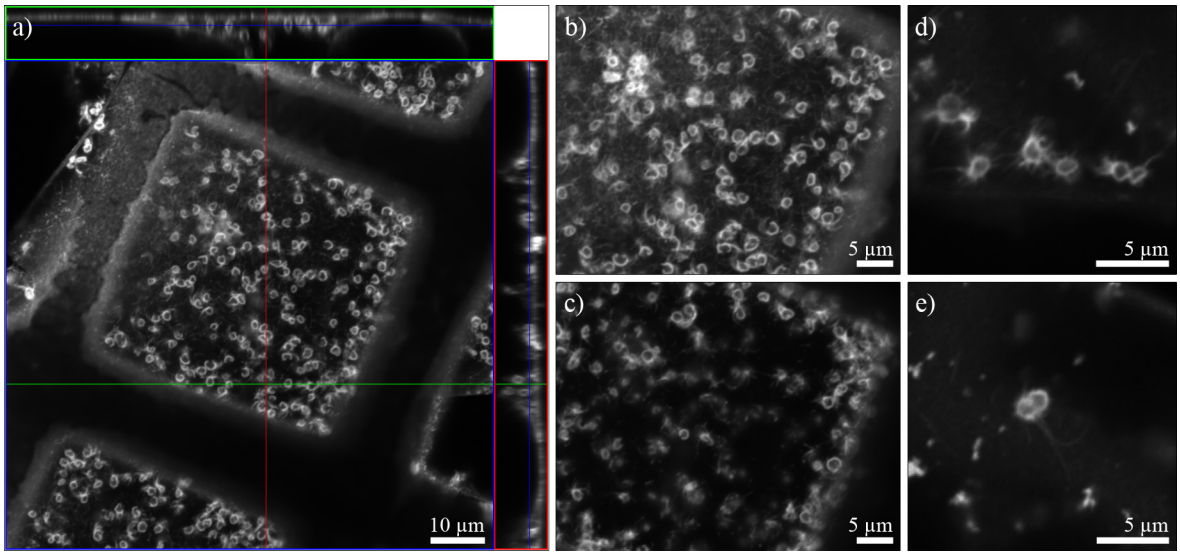

Figure 29: Fluorescent staining of flagella of adherent *M. villosus* and *P. furiosus* DSM 3638^T cells. Cells grown on carbon-coated gold grids were labeled with antibodies against their whole-flagella, signal enhancement was achieved by a secondary antibody coupled to Alexa Fluor® 488. a) z-Stack of adherent *M. villosus* showing the 3D growth of the cells. Thickness of z-stacks was 0.5 µm. b) and c) represent slices of the stack in a) with a distance of 1.5 µm. d) and e) Cells of *P. furiosus* DSM 3638^T with multiple flagella bundles also forming cell-cell contacts.

Besides the analyses of *M. villosus*, labeling was also achieved with *P. furiosus* DSM 3638^T grown on carbon-coated gold grids. As described above, cells were detached from the solid support by antibodies directed against their whole-flagella. Anyhow, the few remaining cells detected after the labeling procedure were clearly stained with the anti-Fla Pfu antibodies, and staining with Alexa Fluor® 555 was not necessary. In consistence with the data obtained for *M. villosus*, labeled flagella were observed to surround the cells and to form cell-cell contacts (Figure 29d and e).

5.4.2 Labeling for TEM

In a first attempt, whole cells of *M. villosus* grown on carbon-coated gold grids were labeled with anti-Fla KIN antibodies diluted 1:100, 1:1,000, and 1:10,000; the secondary antibody was coupled with 6-nm gold. Again, no detachment could be detected. Instead, both, the 1:100 and the 1:1,000 dilution labeled the flagella, but no signal was detected for the 1:10,000 dilution. The highest antibody concentration agglutinated flagella wherefore an analysis of the binding-site was impossible. Using the 1:1,000 dilution, agglutination was not observed. As can be seen from Figure 30a, the anti-Fla KIN antibodies labeled the flagella and not the cell body. Interestingly, the labeling was not distributed evenly all-over the flagellum (Figure 30b) but was also detected on the 6-nm filaments (Figure 30c).
In addition to adherent cells, also ultrathin sections of *M. villosus* were labeled with the anti-Fla KIN antibodies. Here again, labeling was achieved with the 1:100, the 1:1,000, and the 1:10,000 dilution. The antibodies reacted strongly with the membrane of the cells (Figure 30d), but since the cell envelope profile was not well-conserved, a precise localization failed. As can be seen from the enlargement, also clusters in the cytoplasm and cell-cell contacts were labeled (Figure 30e). Unfortunately, sectioned flagella were rarely detected in these preparations but were always labeled with antibodies (Figure 30f). Examining the negative control without primary antibody, a very weak cross-reactivity was detected (Figure 30g) that was clearly different from specific labeling.

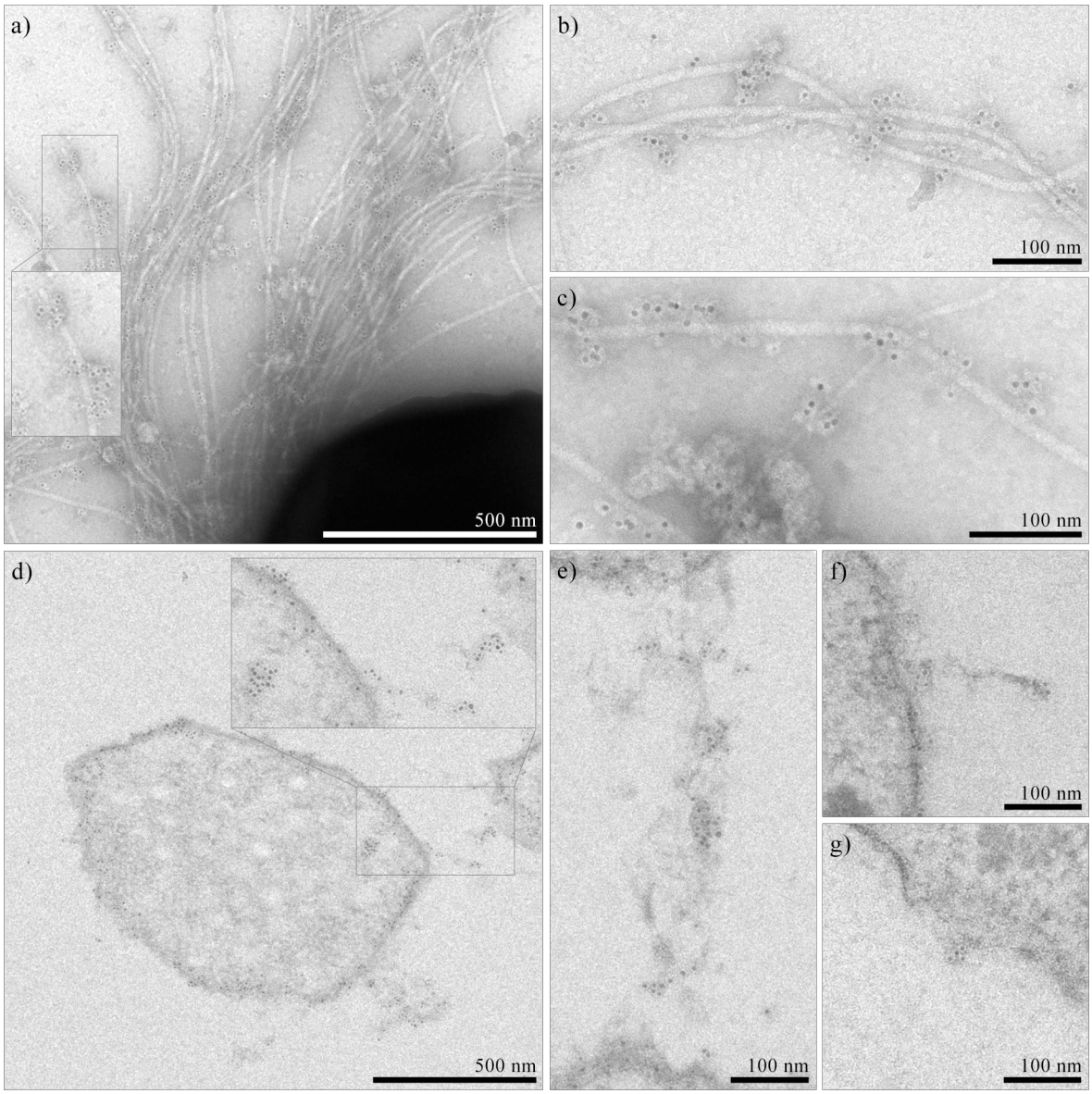

Figure 30: Immuno-labeling of flagella of *M. villosus* cells. Cells were a)-c) grown on carbon-coated gold grids or d)-g) resin-embedded/ultrathin sectioned and labeled with anti-Fla KIN antibodies, visualized by a secondary antibody coupled to 6 nm gold. a)-f) Primary antibodies were diluted 1:1,000. g) Negative control.

Besides the analysis of *M. villosus*, ultrathin sections of *P. furiosus* LS were subjected to immuno-labeling using anti-FlaB1-MT Pfu and anti-FlaB2-CT Pfu antibodies for which positive reaction with denaturated flagella was demonstrated above. Primary antibodies were diluted 1:50 and 1:250, and binding was visualized using a secondary antibody coupled to 6-nm gold. Labeling was detected in the 1:50 dilution and weakly in the 1:250 dilution of anti-FlaB1-MT Pfu, whereas both dilutions were sufficient for the anti-FlaB2-CT Pfu antibodies (Figure 31). For both antibodies, no reaction was visible when flagella where sectioned longitudinally. In contrast, strong labeling was observed around cells and sectioned flagella but not in the surrounding background. Similar to *M. villosus*, clusters in the cytoplasm were labeled; however, no signals were detected in the cell envelope.

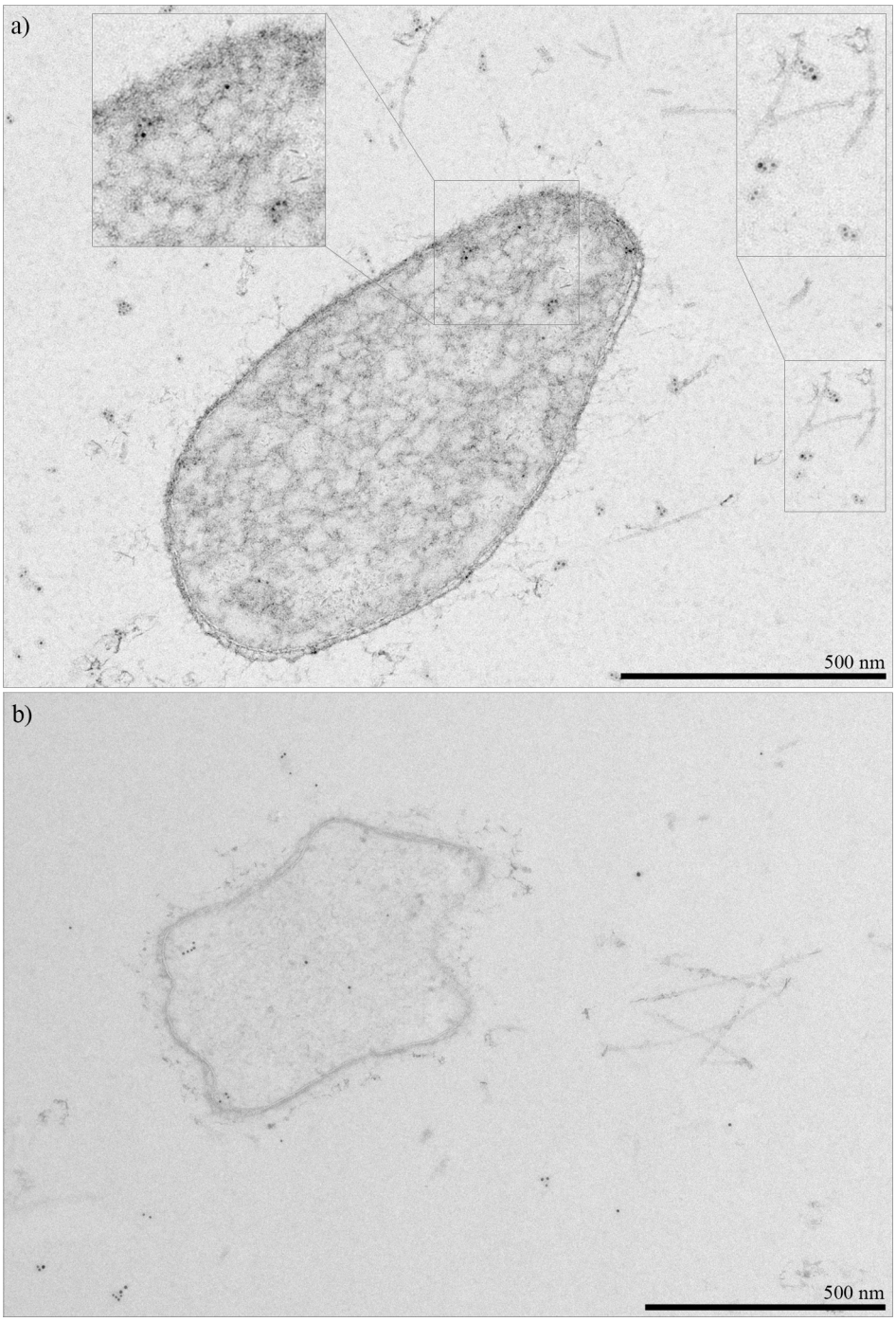

Figure 31: Immuno-labeling of flagella of *P. furiosus* LS cells. Cells were high-pressure frozen, resin-embedded, ultrathin sectioned and labeled with a) anti-FlaB1-MT Pfu antibodies or b) anti-FlaB2-CT Pfu antibodies, visualization was done by a secondary antibody coupled to 6 nm gold. Primary antibodies were diluted a) 1:50 or b) 1:250.

6 Ultrastructural characterization of *P. furiosus* and *M. villosus*

During this thesis, ultrathin sections of *P. furiosus* LS and *M. villosus* were prepared for immuno-labeling studies and for analyses of the cell wall profile. Analyzing the specimens by electron microscopy, interesting insights in the cellular organization and the anchoring of flagella were gained.

6.1 The ultrastructure of *P. furiosus* cells

The analysis of *P. furiosus* LS ultrathin sections, which were prepared by high-pressure freezing, freeze-substitution and resin-embedding, revealed that most of the cells were structurally in good condition. The cells exhibited a tightly packed, almost homogeneous cytoplasm, which was densely contrasted compared to the resin surrounding the cells. In most cases, the cell wall was preserved perfectly (Figure 32a and b). It consisted of a 4−5 nm wide cytoplasmic membrane, a 20−25 nm wide periplasm, a layer with a width of 6 nm which is most probably the S-layer, and extracellular polymeric glycoprotein material (up to 50 nm in width). The periplasm was not contrasted homogeneously, suggesting the (local) presence of secreted, extracellular proteins or the visualization of protein spacers from the S-layer. Interestingly, an additional membrane was detected in some cells, which was located 25 nm below the cytoplasmic membrane (Figure 32b).

As can be seen from Figure 32c, the highly ordered and an unordered cell envelope profile alternated within a single cell. Occasionally, the cytoplasm of the cells contained some parallel filaments localized variably within the cell. The whole complex was up to 500 nm in length and single filaments had a pitch of 40 nm (Figure 32c). The function of the cytoplasmic filaments remained unclear, but based on their size, it seems possible that these are truncated tubes of the type found earlier in cell envelope preparations.

In some cells, flagella were truncated (Figure 32d and e) that spanned the periplasm. An anchoring structure could not be clearly resolved since the cytoplasmic membrane lacks any structural detail in the region where flagella emerged. These findings are consistent with previously generated data of *P. furiosus* LS demonstrating the periplasm to be spanned by some unknown complexes and flagella (Schopf, 2011).

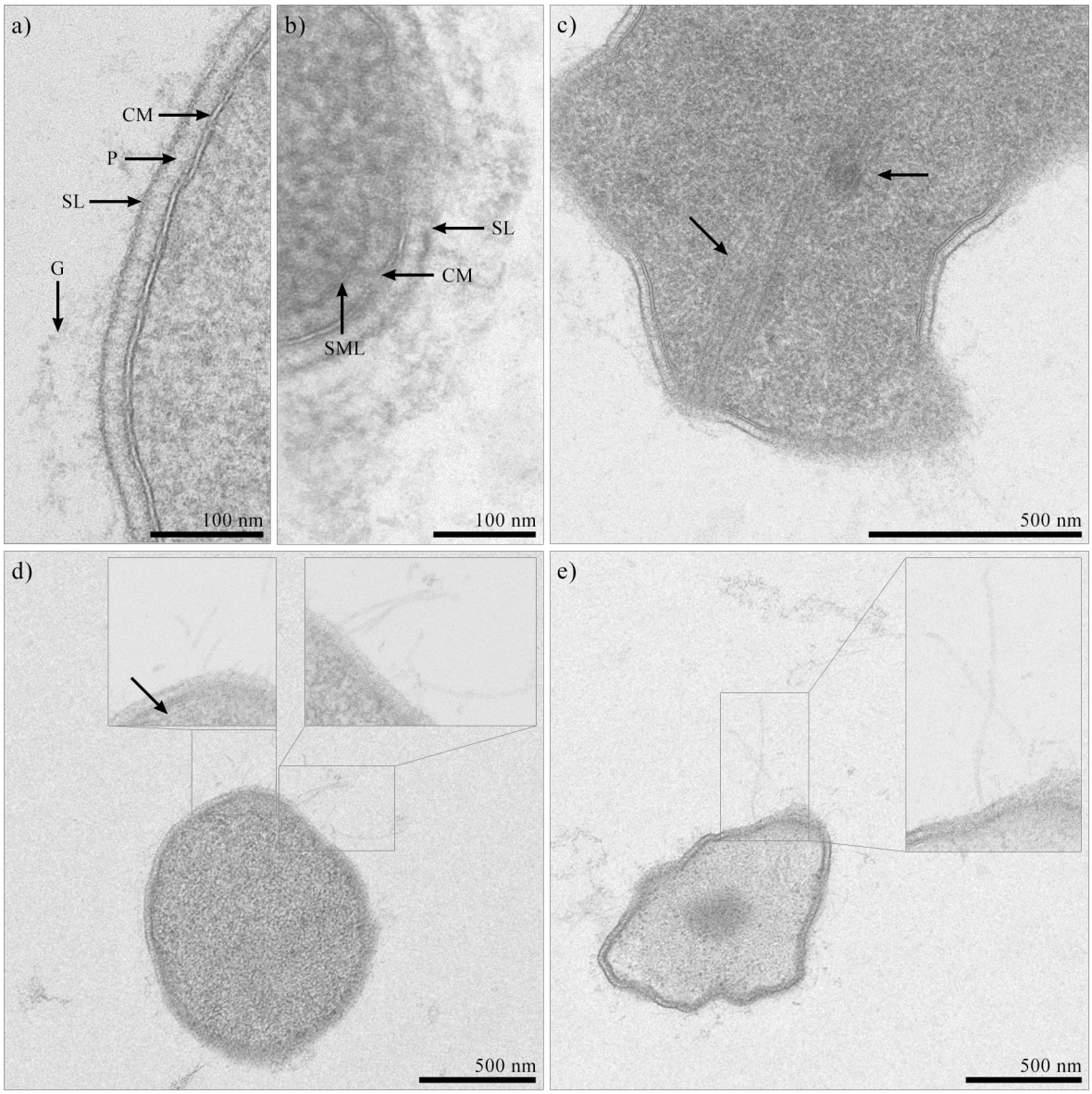

Figure 32: Ultrastructure of *P. furiosus* LS. Ultrathin sections of *P. furiosus* LS cells that were high-pressure frozen, freeze-substituted, resin-embedded, and contrasted with uranyl acetate and lead citrate. a) and b) Cell wall profile; arrows point to the cytoplasmic membrane (CM), the periplasm (P), the S-layer (SL), the long side chains of glycoproteins extending ~50 nm from the face of the S-layer (G), and the submembraneous layer (SML). c) Arrows pointing to cytoplasmic filaments with a pitch of 40 nm and a length of 500 nm. d) and e) Cells with truncated flagella enlarged in boxes. The arrow in d) marks a structure possibly being the submembraneous layer.

6.2 The cell architecture of *M. villosus*

In contrast to *P. furiosus* LS, *M. villosus* was prepared using two slightly different freeze-substitution protocols in which the substitution solution contained either ethanol and no osmium tetroxide (EGFU) or acetone with osmium tetroxide (AOUH). Obviously, in the sample freeze-substituted in AOUH some cells were coated with dark precipitates (Figure 33a) that were also observed in SEM preparations. These precipitates might be the result from a reaction of osmium tetroxide with components of the growth medium. However,

M. villosus was shown with both methods to exhibit a densely packed cytoplasm in which multiple globules with a diameter of 80−120 nm were detected (Figure 33b and d). A characterization of the globules failed, but based on their appearance they might be composed of elemental sulfur (personal communication, Gerhard Wanner). With each of the two protocols, a well-preserved cell envelope profile was obtained consisting of a cytoplasmic membrane with a width of 3−4 nm, a 9−12 nm wide periplasm, and an S-layer with a width of 3.5−5 nm, from which glycoproteins ~30 nm in length protruded (Figure 33c). Some of the cells additionally possessed a submembraneous layer 15−20 nm below the cytoplasmic membrane where probably flagella emerged from (Figure 33e). Despite these similarities, it was obvious that in AOUH freeze-substituted specimens the background noise was lower allowing an easier detection of flagella.

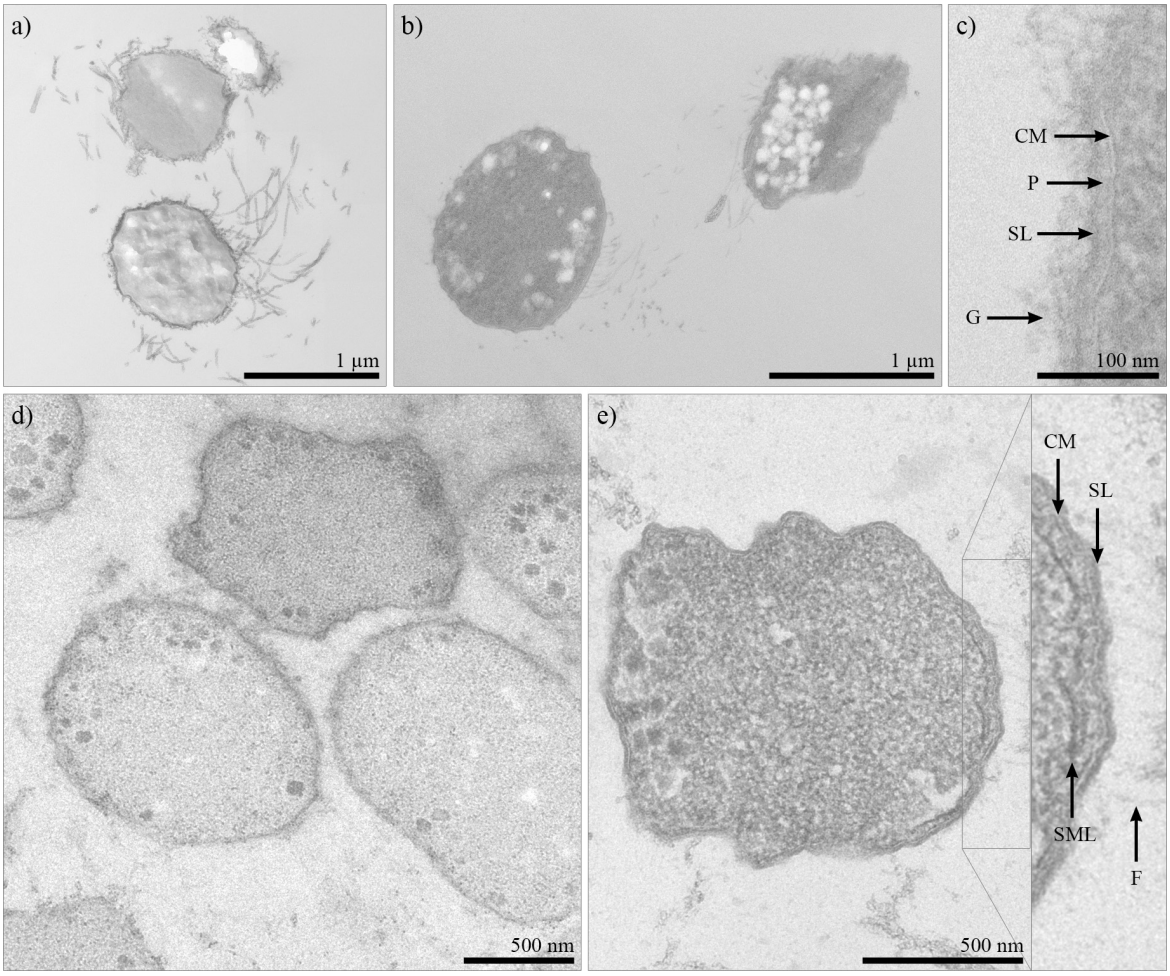

Figure 33: Ultrastructure of *M. villosus*. Transmission electron micrographs of *M. villosus* cells freeze-substituted either in a)-c) AOUH or in d) and e) EGFU. a) Cells coated with an unknown substance. b) Cells of the same sample without coating possessing multiple flagella and cytoplasmic globules. c) Cell envelope profile of *M. villosus* consisting of the cytoplasmic membrane (CM), the periplasm (P), the S-layer (SL) and a glycoprotein layer (G). d) Overview of cells exhibiting an inhomogeneous cytoplasm. e) Cell with truncated flagella. Arrows indicate flagella (F), the cytoplasmic membrane (CM), the S-layer (SL), and the submembraneous layer (SML).

Additionally to high-pressure freezing, cells of *M. villosus* were fixed chemically using glutardialdehyde, dehydrated at room temperature in acetone series and ultrathin sectioned after resin-embedding. Electron micrographs taken by Gerhard Wanner (LMU Munich, Germany) confirmed the aforementioned results of high-pressure frozen cells. The cytoplasm of *M. villosus* was tightly packed and densely contrasted, an observation that has rarely been reported for chemically fixed Archaea (Junglas et al., 2008). The region of flagella anchoring was preserved perfectly revealing a complex cytoplasmic assembly (Figure 34) that closely resembled bacterial chemoreceptor arrays (Briegel et al., 2008). The cytoplasmic complex consisted of a bended plate that followed exactly the curvature of the cell envelope and a series of thinner structures perpendicular to the plate, which were identified to span the distance of 20−25 nm to the cytoplasmic membrane. Another 20 nm below the plate, the submembraneous layer was detected, therewith located 40−45 nm beneath the cytoplasmic membrane instead of ~~2~~0 25 nm in chemoreceptor array-free parts. In all cells containing the array, flagella were truncated in close proximity, but never directly above the array. These data suggest a functional connection of the chemoreceptor array with flagella probably built by the submembraneous layer.

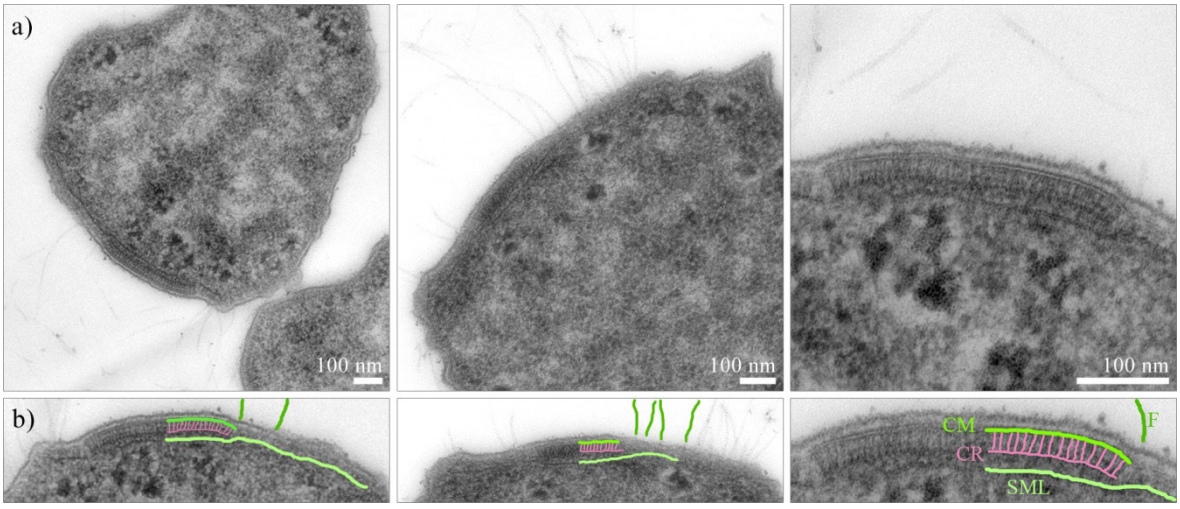

Figure 34: Submembraneous layer of *M. villosus*. 70 nm sections of chemically fixed cells. a) Cells. b) Detailed view of the images shown in a) visualizing the flagella (F), the cytoplasmic membrane (CM), the submembraneous layer (SML) and the chemoreceptor array (CR).

When analyzing the embedded *M. villosus* cells by FIB-SEM, the results of ultrathin sections were confirmed that both, the high-pressure frozen and the chemically fixed cells were structurally well-preserved. In the case that the microscope was perfectly adjusted, series of up to one thousand 5- or 10-nm slices were recorded (supporting material).

6 Discussion

In the last decades, various studies were set up to better understand the differences between Archaea and Bacteria. However, methods established for analysis of bacterial cells are often not applicable in Archaea, and thus, research is limited on few model organisms and focuses on (mostly) general aspects of the cell organization. What is missing in the present body of literature is a comprehensive study on the ultrastructure of archaeal flagellar filaments and cell architecture combined with a functional analysis of cell appendages in adhesion and biofilm formation. This thesis aims to contribute filling this gap by analyzing *Pyrococcus furiosus* and the newly described species *Methanocaldococcus villosus*.

1 Description of the novel species *Methanocaldococcus villosus*

In 2005, *M. villosus* was enriched from pulverized rocky material which was sampled from a northern-Icelandic active hydrothermal system, located in a depth of around 100 m. Phylogenetic analyses identified the new isolate to represent a deep branch within the genus *Methanocaldococcus*. Due to the large distance to other members of this genus, a description of a novel species and probably a novel genus was envisaged. *M. villosus* was isolated from a shallow marine habitat, whereas the other *Methanocaldococci* were obtained from deep sea hydrothermal systems (Whitman and Jeanthon, 2006). Consequently, specific adaptions to the different environmental conditions (e.g. pressure, composition of the hydrothermal fluids) could be expected.

Nevertheless, phenotypic analyses together with structural features of the S-layer and the G+C content attributed *M. villosus* to the genus *Methanocaldococcus*. The previous assumption that the requirement of selenium and tungsten can be used as a criterion for differentiation (Bellack, 2007) could not be confirmed in the present study. Whilst the growth of *Methanotorris igneus* was not affected in a medium prepared without trace mineral solution, *M. villosus* and *Methanocaldococcus jannaschii* required at least the addition of selenate for optimal growth. These data indicate that the literature is somewhat inaccurate stating the requirement of selenium and tungsten for the growth of the *Methanocaldococci* (e.g. Whitman et al., 2001). The species tested herein were indeed able to grow without these minerals, but growth was much slower.

Based on the results obtained in this study and earlier data (Bellack, 2007), *M. villosus* strain KIN24-T80 was described as new species (Bellack et al., 2011). The name refers to its multiple flagella and its unique striated surface structure observed in SEM preparations.

2 The adaption of *Pyrococcus furiosus* to continuous cultivation

P. furiosus was isolated from hot sediments at Vulcano Island, Italy, and then deposited to the DSMZ culture collection within one year after discovery (Fiala and Stetter, 1986). In 1991, an in-house culture collection was established at our institute for storage of (mostly) own isolated organisms. *P. furiosus* had been cultured already for six years in the lab until this strain was finally long-term stored in this. Interestingly, a few years later, Southern blotting analyses have revealed that parts of its genome related to sugar metabolism had been deleted during the cultivation procedure (personal communication, Winfried Hausner).

Once the investigation of archaeal cell appendages was started in the group of Reinhard Wirth in 2003, *P. furiosus* was chosen as one model organism and regenerated from our in-house culture collection. By analyzing various materials supplied to the cells during growth, flagella were demonstrated to mediate the contact to these surfaces and to other cells (Näther et al., 2006). In a comprehensive study on adhesion of Archaea, differences to the aforementioned study became evident, of which the detected adhesion to glass was the most obvious one (Janker, 2008). A further analysis confirmed these data and demonstrated morphological changes of the cells (Schopf, 2011). Based on its continuous cultivation in the lab, the strain was named *P. furiosus Laborstamm* (named *P. furiosus* LS in this study) and the *P. furiosus Typstamm* (*P. furiosus* Vc1 herein) was freshly regenerated from our in-house culture collection (Schopf, 2011). Testing the latter strain for adhesion on surfaces, no or only weak growth was detected except for two materials. From these results it was concluded that cultivation in the lab favored the selection to growth on surfaces (Schopf, 2011).

The adhesion studies performed in the present study, comparing *P. furiosus* LS and *P. furiosus* Vc1 to the wild type strain *P. furiosus* DSM 3638^T corroborated this theory. The type strain was shown to adhere weakly to carbon-coated gold grids, whereas *P. furiosus* Vc1 grew much denser on this surface. Further evidence for the selection towards an adhesive phenotype is finally given by the fact that *P. furiosus* LS and *P. furiosus* Vc1 originated from the same culture deposited in our in-house culture collection. On the basis of this unexpected result, *P. furiosus* Vc1 was freshly regenerated and compared to the Vc1 strain cultured for two years in the lab, but the analysis did not reveal any differences. A possible explanation for this might be that the period of two years was too short for establishing visible adaptions, particularly since serial transfer was kept to a minimum in this study. Additionally, fresh cultures were not inoculated from serum

bottles used for adhesion studies, and therefore the serum bottle itself was the only surface the cells had contact with.

In conclusion, these data demonstrate that the continuous cultivation of *P. furiosus* created two new phenotypes, which clearly differ from the wild type strain in morphology and adhesion behavior. Currently, it is unclear, on which level these modifications take place. However, since earlier studies reported some deletions in the genome, a dramatic change in the genomic information could be possible. A whole-genome sequencing approach of strains *P. furiosus* LS and *P. furiosus* Vc1 could reveal amazing insights into a fast-ongoing evolutionary process.

The dynamics of phenotype evolution were studied extensively during the last two decades using the example of *Escherichia coli*. Cells of this species were propagated for 10,000 generations in identical environment from a common ancestral clone by daily transfer into fresh medium. Analyzing the cell size and the mean fitness, both were shown to evolve rapidly for the first 2,000 generations, but were nearly static for the last 5,000 generations. The replicate populations differed significantly from another, the variance of which was consistent with theoretical expectations and revealed an increase of their mean fitness of about 37% (Lenski et al., 1991; Lenski and Travisano, 1994). Other studies examined the genomic variation among subclones, which were recovered from an *E. coli* stab culture stored for 30 years. Using restriction fragment length polymorphism analysis (RFLP) of eight intergenic spacer (IS) elements as molecular probes, a high level of genetic diversity was determined suggesting that genomic plasticity might play an adaptive role (Naas et al., 1994, 1995). Nowadays, state-of-the-art technologies can be utilized to measure changes in a population directly observing the basis of adaptive evolution. Whole-genome sequencing of an *E. coli* strain, which was adapted to L-lactate as carbon source by serial transfer for 60 days, revealed that the number and types of mutations not only vary with condition but even between replicates (Conrad et al., 2009).

All these observations indicate enormous dynamics in microbial genomes in a comparably very short evolutionary time. It is therefore likely that nutritional deprivation or other selective pressures as revealed in this study can lead to significant changes in the genetic information molecule.

3 (Putative) surface proteins of *P. furiosus*

Due to the morphological and behavioral alterations of *P. furiosus* observed at various stages in the course of this study, the results obtained cannot be directly compared with

each other. On the other hand, the differences in flagellation opened new possibilities to this study: Strain *P. furiosus* Vc1 provided access to a mutant deficient in flagella assembly thereby facilitating the identification of flagella-associated proteins if compared directly to *P. furiosus* LS. Therefore, the indirect method using different growth temperatures to modify flagellation could be omitted, particularly since it entailed cold-adaption of cells (Weinberg et al., 2005). Though, substantial differences were detected in cell envelope preparations between *P. furiosus* LS and *P. furiosus* Vc1 which were also reflected by mass spectrometry analysis of proteins. Of the four identified proteins PF0190, PF1399, PF1602, and PF1935, two referred to a dominant 200 kDa protein band that was suggested to be identical in both strains.

Of these two proteins, PF1399, a putative vanadate-sensitive ATPase displayed the lower Mascot score. A blastp database analysis identified an S-layer-like N- and C-terminus that showed great homologies to annotated S-layer proteins of the *Thermococcaceae*, and to those of the *Methanococcales*. The latter homology had already been demonstrated in a comparative study on S-layers of mesophilic, thermophilic, and hyperthermophilic species of the order *Methanococcales*. Therein, the primary structure of the S-layer proteins was determined by sequencing of the corresponding genes using primers constructed on the basis of conserved regions in presumptive S-layer genes of *Methanococcus voltae* and *M. jannaschii* (Akça et al., 2002). In the case of *M. voltae*, the postulated structural S-layer gene was identified by N-terminal sequencing of the isolated S-layer protein. The sequence matched perfectly in 20 residues the amino acid sequence derived from the gene sequence of a previously published vanadate-sensitive ATPase (Konisky et al., 1994). Based on these findings, it seems possible that the ATPase detected in cell envelope preparations of *P. furiosus* is the S-layer protein.

In contrast to these theoretical predictions, a previous study analyzing glycoproteins of *P. furiosus* succeeded in the isolation of its S-layer (Zach, 2009). The protein was identified by mass spectrometry to be the amylopullulanase PF1935, which was also detected in cell envelope analyses in this study. Interestingly, this enzyme has already been recombinantly expressed and proved to be extremely thermostable and highly resistant to chemical denaturing reagents (Dong et al., 1997). An S-layer formed by such a protein seems to be a very suitable outermost barrier for thermal and mechanical stabilization of the cells. Nevertheless, further analyses have to be performed to confirm that the amylopullulanase really forms the S-layer of *P. furiosus*. To address this question, two different methodological approaches can be conceived. Antibody-based immuno-

localization studies could prove the presence and abundance of this enzyme on the cell surface. On the other hand, the capability of the (recombinant) enzyme forming two-dimensional layered polymers *in vitro* could be tested. The results of such studies would greatly extend the current knowledge on S-layers of the *Thermococcaceae*, which is hitherto restricted to electron microscopic cell envelope analyses (e.g. Huber et al., 1995b; Kostyukova et al., 1999).

In accordance with the present study, the amylopullulanase, the putative vanadate-sensitive ATPase, and also the hypothetical protein PF0190 were identified in membrane fractions of *P. furiosus* (Holden et al., 2001). Previously, the hypothetical protein PF0190 was related to the cold stress response of *P. furiosus* (Weinberg et al., 2005). Two major proteins, accumulated in the membrane fraction of both, cold-shocked and cold-adapted cells, were identified as PF0190 and PF1408 and named CipA and CipB (for 'cold induced protein'). Compared to these up-regulated proteins, other glycoproteins were found with decreasing intensity in cold-adapted cells, most notably those with an apparent molecular mass of 18, 35, and 52 kDa (Weinberg et al., 2005). The 35 kDa protein band might well derive from the flagellins since the physiological studies reported herein demonstrated that cells grown at 72°C possessed no or only few flagella. In consistence with Weinberg et al. (2005), also in the present study a different protein pattern was observed in SDS-PAGE of cell envelopes isolated from cold-adapted cells.

Aside from the three membrane-associated proteins, a cytoplasmic enzyme, the glutamate dehydrogenase, was identified in the *P. furiosus* cell envelope preparations. Initially, it was assumed to be a contamination, particularly if taking into account that it was also assigned to the 200 kDa protein band.

Referring to the literature, this assumption, however, has to be discussed more critically. In a recent study, asking for the contribution of the glutamine-dependent regulator GlnR of *Streptococcus pneumoniae* to virulence, a deletion of the glutamate dehydrogenase gene *gdhA* resulted in a decrease of the *in vitro* adhesion of mutants to only 20% of the wild type level (Hendriksen et al., 2008). This result is not an exception, because various studies have demonstrated the ubiquity of housekeeping enzymes on the surface of microorganisms (e.g. reviewed by Pancholi and Chhatwal, 2003).

The first housekeeping enzyme found on the surface of Bacteria was the glyceraldehyde-3-phosphate dehydrogenase (GAPDH) of group A streptococci, described simultaneously by two independent studies (Lottenberg et al., 1992; Pancholi and Fischetti, 1992). Since GAPDH was shown to be a major surface protein displaying a binding capacity for a

variety of proteins such as fibronectin and cytoskeletal proteins, an active role of the enzyme in colonization was suggested (Pancholi and Fischetti, 1992). In further studies, GAPDH was reported to be located on the surface of various Gram-positive and Gram-negative bacteria, fungi, and parasitic Eukaryotes where it performs alternative and/or diverse functions besides its regular enzymatic activity. Moreover, other metabolic enzymes, mostly involved in glycolysis, were identified as virulence factors for many pathogens enabling the adhesion to and invasion of host cells (Pancholi and Chhatwal, 2003).

In contrast to the various bacterial and eukaryotic examples, similar reports for archaeal housekeeping enzymes are missing in the literature. The glutamate dehydrogenase of *P. furiosus* was therefore of interest and its role in adhesion was investigated in a binominal approach. On the one hand, immuno-localization studies were performed using antibodies generated against the recombinantly expressed enzyme; on the other hand, the enzyme should be knocked-out by transformation of *P. furiosus* with a shuttle vector containing a partial anti-sense sequence of the gene. Analyzing the derived mutants, it was found that within one culture cells contained vectors with and without insert; anyhow, serial transfers revealed the vector to be stably integrated for at least 100 generations (Schießl, 2010). Using the anti-Gdh Pfu antibodies in Western blotting analyses of the mutants, no differences to *P. furiosus* Vc1 were observed in the signal intensity of the cytoplasmic fraction, but in membrane fractions, the signal was weaker (personal communication, Yvonne Bilek). Adhesion studies on carbon-coated gold grids performed herein showed that the mutant can indeed grow on this surface in a similar way as it was described for *P. furiosus* Vc1 with the exception that the mutants possessed multiple flagella (Figure A2). From these data it can be concluded that the mutants did not exhibit a specific phenotype and, are consequently inappropriate for addressing functional studies of the glutamate dehydrogenase.

Further research focused on immuno-localization studies of the enzyme in both, planktonic and adherent cells. Epifluorescence microscopy of labeled cells revealed that the glutamate dehydrogenase is evenly distributed in the cell envelope of planktonic cells but clustered in those of adherent cells. These findings implicate that the function of the enzyme is somehow correlated with adhesion; the clustering might be a structural prerequisite for cell-cell communication or biofilm formation. This hypothesis, however, could not yet be confirmed by electron microscopic immuno-labeling studies. Although a strong antibody reaction within the cytoplasm of *P. furiosus* cells could be expected, almost no signal was

found in ultrathin sections. Since the secondary antibodies coupled to succinimidyl esters of fluorescent dyes were shown to bind unspecifically to the cells at the high concentration that had to be used, it can be speculated that the labeling of cells is attributed to unspecific binding. However, this would not explain the different staining behavior and the presence of clustered glutamate dehydrogenase signals in adherent cells.

All in all, this study gave preliminary evidence that the glutamate dehydrogenase of *P. furiosus* is located in the cell surface, but a role in adhesion was not finally proven yet. Further studies are highly recommended, since this would be, to the best of my knowledge, the first description of an archaeal housekeeping enzyme related to adhesion and moreover, the first analyzed enzyme of a non-pathogenic organism. Therefore, additional experiments are needed in order to study the subcellular distribution of the glutamate dehydrogenase in three dimensions. This technique is time-demanding but worth doing, and is established now in the electron microscopy center (Jennifer Flechsler and Thomas Heimerl, personal communication). For this purpose, another immunization attempt using either the enzyme purified from cell envelopes or a recombinantly expressed protein might be necessary as TEM investigations require highly sensitive antibodies. Furthermore, the ability of natural and recombinant glutamate dehydrogenase to bind to (a-)biotic surfaces should be determined. For this, a binding assay similar to enzyme-linked immunosorbent assays (ELISA) performed to recognize substrates of GAPDH could be used (Lama et al., 2009).

4 The role of flagella and pili in adhesion and biofilm formation

Another aspect of this thesis was to analyze the adhesion behavior of *M. villosus*, *M. igneus*, and different *P. furiosus* strains by electron microscopy. With exception of *P. furiosus* DSM 3638^T, all species effectively attached to the carbon-coated gold grids and formed (micro-) colonies and/or biofilms on the surface. Over time, the observed surface growth is, to some extent, comparable to the different stages of biofilm formation proposed for *Pseudomonas aeruginosa* (Sauer et al., 2002): In stage one, cells associate loosely or transiently with the surface, followed by irreversible attachment in stage two. Stages three and four are characterized by cellular aggregation into microcolonies and subsequent growth and maturation of biofilm structures including the production of EPS. In stage five, cells detach and disperse from the biofilm returning to the planktonic mode of growth (Sauer et al., 2002).

On the basis of this colonization model, it can be suggested that *P. furiosus* DSM 3638^T either is unable to form the initial contact to the surface or cannot switch from transient to

irreversible attachment. Instead, *P. furiosus* Vc1 and *P. furiosus* LS can form biofilms attended by the presence of β-glycosidic polysaccharides as shown by Calcofluor staining of monospecies (Schopf, 2006) and bispecies biofilms (Schopf et al., 2008).

Even for *M. villosus*, biofilm formation was found to be accompanied with the production of EPS as proven via Calcofluor staining and SR-FTIR. While no EPS signals were detectable along with single cells, the synthesis of EPS carbohydrates was linked to higher cell densities and growth into microcolonies. Only when biofilms were formed, also EPS protein signatures could be detected. These data represent, to the best of my knowledge, the first verification of EPS production by SR-FTIR (in combination with Calcofluor staining) in Archaea. However, more research on this topic needs to be undertaken to identify the extracellular proteins and polysaccharides of the *M. villosus* EPS matrix. Such data are highly requested by the scientific community since, up to know, surprisingly little information is available about archaeal EPS substances and the formation and maintenance of archaeal biofilms.

Contrary to the described stage five of bacterial biofilms, *M. villosus* cells did not detach but lysed on the surface. This result cannot be explained yet, especially since detachment was proven to occur for the *P. furiosus* strains and *M. igneus*. Nevertheless, all adhesion studies presented herein share that the different stages of biofilm development were completed within a single day. This consistency may be due to the short doubling time of less than one hour of all organisms tested. But this fact seems not to play a role, since for *P. aeruginosa*, the doubling time was 140 min and biofilm formation and maintenance was observed for up to twelve days (Sauer et al., 2002). Probably, the results for the Archaea can be explained by growth in serum bottles, where growth substrates are limited for methanogens or toxic hydrogen enriches in the case of the *P. furiosus* strains. This problem could be circumvented by (direct) analysis of continuous biofilm development but an assay system for anaerobic and hyperthermophilic organisms is not available yet.

Recently, an adapted microtiter plate assay gave first insights into the maturation of static crenarchaeal biofilms using the example of three *Sulfolobus* strains (Koerdt et al., 2010). Similar to the data obtained in the present study, the *Sulfolobus* cells started, after initial attachment, to form microcolonies, in which they were surrounded by an EPS matrix. In all three strains, biofilm formation was primarily detected as a response to physiological stress such as low temperatures or high pH enabling the cells to withstand unfavorable conditions in their natural habitat (Koerdt et al., 2010).

Additionally, Koerdt et al. (2010) demonstrated that *S. solfataricus* deletion mutants lacking the central ATPase necessary for pilus assembly (UpsE; Fröls et al., 2008) exhibited decreased static biofilm formation. By contrast, deletion of an accessory gene involved in flagellar biogenesis and motility (*flaJ*; Szabó et al., 2007a) resulted in no specific phenotype compared to the wild type (Koerdt et al., 2010). While flagella and pili do not seem to have a great impact on the formation of static *S. solfataricus* biofilms, the UpsE and FlaJ deletion mutants were unable to attach to different surfaces in shaken cultures (Zolghadr et al., 2010). A comparison of the gene expression level of selected genes between adherent and planktonic cells demonstrated that the UV-induced pilins, UpsA and UpsB, are up-regulated 5- and 2-fold in attached cells, respectively. However, the flagellin FlaB was repressed 12-fold and the authors therefore discussed that flagella are most probably required for initial attachment, but not for persistence of the biofilm (Zolghadr et al., 2010).

Contrary to those results, a recent study of *Haloferax volcanii* flagellin deletion mutants using an air-liquid interface assay has demonstrated that its flagella are not involved in surface adhesion regardless if the cells were shaken or not during cultivation (Tripepi et al., 2010). Instead, deletion of the type IV prepilin peptidase (TFPP)-like enzyme PibD resulted in mutants defective in processing of flagellins and pilins, and in adhesion to glass surfaces. Hence, it was concluded that non-flagellar cell appendages such as pili play a critical role in surface attachment of *H. volcanii* (Tripepi et al., 2010).

In consistence with this suggestion, detachment of *M. villosus* cells from surfaces using anti-Fla KIN antibodies was not observed indicating that adhesion of *M. villosus* is mediated not only by flagella. Presumably, the 6-nm filaments detected in flagella preparations of this organism have similar functions in adhesion as pili in *Sulfolobus* and *H. volcanii*. In addition, 5−7 nm thin filaments were found earlier in *Methanocaldococcus indicus*, *M. jannaschii*, and *M. vulcanius* (Bellack, 2007). An electron microscopic verification of an involvement of these cell appendages in adhesion failed due to the formation of a dense flagellar network entangling the cells grown on surfaces.

Aside from *M. villosus*, the induction of flagellar assembly in adherent cells was also demonstrated for the other five *Methanocaldococcus* species analyzed herein. It was shown that the number of cell-cell contacts formed by flagella increased when cells grow on surfaces. Similar results were obtained for the three *P. furiosus* strains except that a previous study identified the flagella to be functional adhesins (Näther et al., 2006). By contrast, the present study found that adherent *P. furiosus* Vc1 cells possess much more

thin filaments than planktonic cells but their correlation to adhesion is still highly speculative. Additionally, it cannot be excluded that the glutamate dehydrogenase (or another unknown surface protein) plays an important role as adhesive protein. It also has to be kept in mind that the adhesion behavior of *P. furiosus* was discussed as an adaptation mechanism to continuous cultivation, in which, most probably, existing surface structures were accommodated specifically for attachment.
Nevertheless, it can be concluded from the adhesion studies that flagella are important for biofilm formation and that their multifunctionality is a common feature among Archaea.

As a difference to *P. furiosus* and the *Methanocaldococcus* species, *M. igneus* was described to be non-motile (Burggraf et al., 1990). In consistence with earlier studies of *M. igneus*, filaments were hardly observed in planktonic cells (personal communication, Reinhard Rachel). Surprisingly, adherent cells exhibited a much higher number of cell appendages that also interconnected cells and that remained on the surface although the biofilm was already dispersed. From these data it can be surmised that their function is related to adhesion and the formation of cell-cell contacts, thus enabling the organism to stay in its habitat. Therewith, this study represents the first functional characterization of the *M. igneus* filaments and, in addition, gave some insights in their ultrastructure by identification of an anchor-like structure.
Because of the close relatedness of *M. igneus* to the genus *Methanocaldococcus* the question arose if the thin filaments, possessed by species of both genera, are homologous structures. Searching the genome of *M. igneus*, no pilins were annotated but two PilT protein domain-containing proteins were found. These proteins that were shown to be ATPases required for type IV pilus retraction associated with twitching motility in Bacteria (Merz et al., 2000), were also annotated in the five *Methanocaldococcus* genomes.
The existence of pili besides flagella as a second kind of cell appendages was already reported for the related genus *Methanococcus* (Jones et al., 1977; Koval and Jarrell, 1987; Ng et al., 2011). For *M. maripaludis*, the major structural pilin was identified recently to be MMP1685 (Ng et al., 2011). In a database search, MMP1685 homologues were found in the five annotated *Methanocaldococcus* genomes and the genome of *M. igneus*, mostly representing class III signal peptide-containing proteins or proteins of unknown function. The latter proteins contain a domain of unknown function (DUF361) that was described as conserved domain within the signal peptide of pilin-like proteins (Szabó et al., 2007b).
Based on genome data, it seems plausible that the *Methanocaldococci* and *M. igneus* possess pili that are homologous to those found in *M. maripaludis*. Further studies have to

prove if the identified genes are processed into pilins and assembled into the thin filaments identified in electron microscopic studies.

Whilst the thin filaments (most probably) represent the sole cell appendages of *M. igneus*, they are outnumbered by flagella in the species of the genus *Methanocaldococcus*. Therefore, the purification of these filaments is difficult, particularly since no genetic system is available as in *M. maripaludis*, whose pili were isolated from flagella-less mutants (Wang et al., 2008; Ng et al., 2011).

5 Ultrastructure of archaeal pili and flagella

The ultrastructure of *M. maripaludis* pili isolated from flagella-less mutants was shown by cryo-electron microscopy to be completely different from that of archaeal flagella and that of any of the known bacterial pili (Wang et al., 2008). Within a single filament, two different subunit packing arrangements were observed: One is a left-handed C_4 symmetry with a pitch of 4.4 nm, and the other is a right-handed one-start helix spaced by 3.0 nm. From the coexistence of different quaternary structures, it was concluded that subunits have the ability to switch between different contacts with the surrounding pilins (Wang et al., 2008).

In *M. villosus*, also two very different symmetries were shown to coexist within the same flagellum. The dominant helix is a left-handed 5.6-nm pitch three-start helix, while the other is a right-handed one-start helix. To the best of my knowledge, this result represents the first description of a dominant left-handed helix in archaeal flagellar filaments; other flagella described in literature are composed of right-handed helices (Alam and Oesterhelt, 1984; Szabó et al., 2007a; Cohen-Krausz and Trachtenberg, 2008). Unfortunately, flagella of *M. villosus* (and also those of *P. furiosus* DSM 3638^T) fell apart during preparation for cryo-electron microscopy; therefore, no three-dimensional reconstructions of the flagellar filaments were obtained. This problem was previously seen in the group of Edward H. Egelman with flagellar filaments of *Haloarcula marismortui*, and other groups experienced it, as well (personal communication, Edward H. Egelman).

Different subunit packing arrangement allowing the switch between different contacts seems to be common in Archaea since it was demonstrated also for flagellar filaments of *Halobacterium salinarum* (Trachtenberg et al., 2005) and *Sulfolobus shibatae* (Cohen-Krausz and Trachtenberg, 2008), and for fibers of *Ignicoccus hospitalis* (Meyer, 2010). These examples comprise different archaeal cell appendages made of either one or multiple subunits, whereby it seems unlikely that the mechanism of switching developed repeatedly

during evolution. More probably, it was already established in the most recent organism from which all Archaea descend. Interestingly, switching of conformation between two different stages was also demonstrated for bacterial flagellar filaments, in which it causes supercoiling of flagella and thus has an essential role in swimming (e.g. Kamiya and Asakuro, 1976; Samatey et al., 2001). Despite these similarities between packing interactions of the subunits, the arrangement of flagellins in the bacterial flagellum is completely different from that of archaeal flagella (Trachtenberg et al., 2005; Cohen-Krausz and Trachtenberg, 2008).
However, the role and regulation of polymorphic switches in archaeal filaments remains speculative because, up to now, the function and assembly of the different types of cell appendages is not fully understood.

In the last decade, deletion mutant analyses and immuno-localization studies gave first insights into the structure and assembly of archaeal flagella (Bardy et al., 2002; Beznosov et al., 2007; Chaban et al., 2007). From these studies, it seems that the hook region of the flagellum is formed by one of the flagellins, namely FlaB2 in *H. salinarum* (Beznosov et al., 2007), and FlaB3 in *M. maripaludis* (Chaban et al., 2007) and *M. voltae* (Bardy et al., 2002). Since the amino acid sequence of the *M. voltae* FlaB3 is very similar to the FlaB3 flagellin annotated in the genome of *M. jannaschii* (and the corresponding flagellin in the other four *Methanocaldococcus* genomes), it can be suggested that it also forms the hook of the flagella of the *Methanocaldococci*. A hook, however, was never observed in electron microscopic studies of the six *Methanocaldococcus* species analyzed in this thesis and only rarely in flagella preparations of *M. villosus*. It can therefore be assumed that the hook is barely visible in this genus and maybe also in other Archaea, and that it differentiates clearly from the well-defined bacterial hook.
While the ‘hook protein’ is located at the proximal end of the flagellum, the other flagellins of *M. voltae* were found throughout the entire flagellar filament (Kalmokoff and Jarrell, 1991; Bardy et al., 2002). By contrast, in immuno-localization studies performed with *P. furiosus* using the antibodies generated against recombinantly expressed parts of its flagellins, no labeling was detected on native flagella (Näther, 2007). Although the antibodies were shown to (partially) detach cells from surfaces (Näther, 2007), only the anti-FlaB1-MT Pfu and the anti-FlaB2-CT Pfu antibodies reacted positively with denaturated flagella in the present study. The two antibodies clearly labeled the surrounding of ultrathin-sectioned cells especially in close proximity to longitudinally sectioned flagella but not flagella itself. From these data it can be deduced that the epitopes

required for antibody binding are located inside the flagellum and hence only accessible in transverse sections. This explains also the results of the abovementioned study showing that immuno-labeling of flagella of planktonic *P. furiosus* cells was only achieved with anti-Fla Pfu antibodies but not with any of the flagellin specific antibodies (Näther, 2007).

For *M. villosus*, anti-Fla KIN antibodies were used for immuno-labeling analyses. A previous study has shown that these antibodies specifically bind to denaturated flagella of *M. villosus*, but not to flagellins of the other tested *Methanocaldococcus* species (Bellack, 2007). These findings indicate that the polyclonal antiserum recognizes structurally defined epitopes present only on the flagellar filaments of *M. villosus*. Database analyses performed herein revealed that single flagellins are more homologous to corresponding flagellins encoded in other *Methanocaldococci* than to those of the same genome. Since no cross-reactivity of the antibodies was detected, it can be assumed that they are directed against N-linked glycans. This hypothesis is supported by the fact that glycans were reported to be apparently different in the closely related *M. maripaludis* and *M. voltae* (Jarrell et al., 2010b). An effect of glycans seems even more likely as it is commonly accepted that antibodies are often directed against sugar moieties of glycoproteins.

In immuno-labeling studies, the antibodies not only labeled flagella of *M. villosus* but also clusters in the cytoplasm and the cell envelope. Labeling of the cytoplasm was also found in the aforementioned *P. furiosus* experiments and can be explained by the occurrence of preflagellins transported to the membrane for assembly. By contrast, it was somewhat surprising that the cell envelope was also labeled. This finding could result from the source of the antibodies: Antibodies against the flagellins of *P. furiosus* were generated from recombinantly expressed parts of the corresponding proteins, whereas in case of *M. villosus* sheared flagella were used for immunization. It might be possible that shearing broke the cells and that the flagellar preparation was contaminated with membrane proteins. Contrary to this, labeling of the cytoplasmic membrane (and of the outer membrane) was also detected in *I. hospitalis* using anti-Iho670 antibodies (Meyer, 2010). In this case, fibers precipitated from the culture supernatant and purified by differential centrifugation, dialysis, and gel filtration were applied for generation of antibodies (Meyer, 2010), which would exclude the contamination with membrane proteins. Another possible explanation is that labeling of the cell envelope could arise from a pool of flagellins stored in or at the membrane before being assembled into growing flagella. Moreover, a possible continuous rearrangement of flagella resembling mechanisms known for pili retraction in twitching motility (Merz et al., 2000; Skerker and Berg, 2001) could be envisaged. But for

both possibilities, it is more likely that labeling is restricted to the region of flagellar anchoring and not detectable spread over the entire membrane as observed here. Binding of antibodies to N-linked glycans discussed above is another explanation for the labeling of cell envelopes. It was proven earlier that the sugar residue structure of archaeal S-layer glycoproteins is indistinguishable from that found in flagellins of the same organism (Wieland et al., 1985; Voisin et al., 2005). This hypothesis is further supported by labeling of extracellular polymeric glycoprotein material detected in ultrathin sections of *M. villosus*.

6 Cell architecture of Archaea

Aside from the glycoprotein layer, it was shown for both, *M. villosus* and *P. furiosus* that the cell envelope profile consists of the cytoplasmic membrane, the 'periplasm', and the S-layer. For *M. villosus*, values for the various components are consistent with data found in the literature for *Methanococcales*, whereas the quasi-periplasmic space of *P. furiosus* was two- or three-fold as wide as the 10 nm published for members of the *Thermococcales* (König et al., 2007).

In the cytoplasm of *P. furiosus*, parallel filaments were occasionally found, whose function is yet unclear. Similar structures were already described for *Pyrodictium abyssi* (Rieger et al., 1995) and *I. hospitalis* (Junglas et al., 2008), both also prepared by high-pressure freezing for analysis. For *I. hospitalis*, it was discussed that the cytoplasmic filaments represent a bundle of an archaeal cytoskeleton resembling those found in Bacteria (Junglas et al., 2008). In *Caulobacter crescentus*, filament bundles detected in electron cryo-tomography were grouped in four major classes differing in shape and localization (Briegel et al., 2006). The overall arrangement of the filaments did not match *in vitro* data generated for either MreB, FtsZ, or crescentin cytoskeletal filaments suggesting that they are composed of a yet unknown protein (Briegel et al., 2006).

Like many other Archaea, the *P. furiosus* genome encodes different cytoskeletal/cell division proteins, namely FtsZ and the archaeal orthologue of SepF (Makarova et al., 2010). FtsZ was found in mostly all Euryarchaeota and mediates the cell division by formation of a constricting ring structure (Margolin, 2005). Its cytokinesis seems to be functionally substituted by SepF (Makarova et al., 2010).

These data suggest that the identified cytoplasmic filaments are indeed part of an archaeal cytoskeleton. To verify this hypothesis, further studies have to be performed including the isolation of these structures for identification of protein subunits and to analyze mechanisms of their assembly.

Moreover, a submembraneous layer, or second ‘membrane’, was repeatedly detected in electron microscopic studies of *P. furiosus* and *M. villosus*. Such a structure was found recently in micrographs of *P. furiosus* LS displaying ultrathin sectioned flagella, and an insertion of flagella in either the cytoplasmic membrane or in the layer was suggested (Schopf, 2011). The results obtained in the present study by ultrathin sections support the interpretation that flagella are anchored in the submembraneous layer. This suggestion is further corroborated by cell envelope preparations of *P. furiosus* LS, in which membrane patches with emerging flagella were detected. Interestingly, the size of the patches matched exactly with the granum-like body described previously (Fiala and Stetter, 1986; Näther, 2007).

An additional membrane beyond the cytoplasmic membrane was also described for *M. jannaschii* (Jones et al., 1983), *M. voltae* (Koval and Jarrell, 1987) and *H. salinarum*. But only for the latter case it was shown that flagella emerge from this membrane (Balch et al., 1979; Kupper et al., 1994). Since *M. villosus* and *P. furiosus* possess a thin kind of filament besides flagella, the question arises if these structures also anchor in the subcytoplasmic membrane.

Altogether, these data provide evidence that the presence of a submembraneous layer and the anchoring of flagella in it is prevalent among (Eury-)Archaea. Consequently, the question arises how flagella perforate the cytoplasmic membrane and how anchoring in such a layer allows the rotation of flagella required for swimming (Alam et al., 1984). To address these questions, high resolution models of archaeal flagellar filaments together with the motor/rotation system and of the cellular organization are needed. Future investigations should also comprise analysis of the biochemical composition of this ‘membrane’ (protein, lipids, or both) to better understand the evolutionary origin and the advantage of the submembraneous layer.

In chemically fixed and resin-embedded *M. villosus* cells, the submembraneous layer seems to form a functional connection of flagella with a plate-like cytoplasmic assembly similar to the bacterial chemoreceptor array. When comparing the macromolecular complex with (putative) chemoreceptors of the SM1 Euryarchaeon (Moissl, 2004), *C. crescentus* swarmer cells (Khursigara et al., 2008), or *Thermotoga maritima* (Briegel et al., 2009), notable similarities are found. All structures possess a base-plate located approximately 25–30 nm below the cytoplasmic membrane, whose space is spanned by thin, pillar-like structures. In Bacteria, it was shown that the distance of the base-plate to

the inner membrane correlates with the average sequence length of all topology type I methyl-accepting chemotaxis proteins (MCPs; Briegel et al., 2009).

Interestingly, no chemotaxis (*che*) genes were annotated in the genome of *M. jannaschii* (Bult et al., 1996) from which it can be assumed that *M. villosus* also lacks homologues of the known genes. Also in a recent study combining a homology search with cluster analysis, and genome region analysis, no *che* genes were found in *M. jannaschii* (and neither in *P. furiosus*; Schlesner et al., 2009). Nevertheless, it was demonstrated that *M. jannaschii* possessed only few or no flagella under hydrogen-excess conditions and that flagellar synthesis occurred when hydrogen became limiting (Mukhopadhyay et al., 2000). From these data it can be concluded that *M. jannaschii* is indeed chemotactic, but that its genes involved in chemotaxis are completely different from known annotated genes. This hypothesis is corroborated by the fact that previously unknown archaeal proteins were shown to be essential for taxis signaling to flagella (Schlesner et al., 2009). Therefore, one of the first questions addressed after release of the genome of *M. villosus* will be if any chemotaxis associated genes will have been annotated.

7 Conclusion

In summary, this thesis gave novel insights into the cell architecture of Archaea with focus on the ultrastructure and function of flagella.

By analysis of different euryarchaeal species it was demonstrated that their flagella are multifunctional organelles also involved in the formation of cell-cell contacts, adhesion, and biofilm formation. The different microscopic studies used herein allow the conclusion that flagella of (Eury-)Archaea are anchored in a submembraneous layer, which seems to be associated with a putative chemoreceptor array. Initial ultrastructural analyses of *M. villosus* flagella identified a dominant left-handed helix, a conformation previously not described in Archaea. Based on the results of this study, *M. villosus* is suggested to be an appropriate model organism for studies of the (eury-)archaeal cell architecture. With future availability of its annotated genome, the obtained ultrastructural data can be confirmed on the molecular level.

7 Summary

Earlier studies indicated that flagella might play a crucial role in motility, adhesion, and cell-cell contacts of Archaea. Thus, the ultrastructural and functional characterization of flagella and their anchoring in the cell are crucial for understanding the archaeal cell organization in general.

To address this topic, *Pyrococcus furiosus* was chosen as a suitable model organism. However, in the course of this study, morphological changes of this strain, cultured continuously for several years, were demonstrated. These changes resulted in decreased growth and less adhesion of cells. Comparing this strain to another continuous culture and to the wild type strain, it was shown that culturing in the laboratory caused the adaption of cells to an adhesive phenotype. Nevertheless, cell envelope analyses succeeded in the identification of the glutamate dehydrogenase in membrane fractions of *P. furiosus*. Immuno-localization studies provided evidence that the enzyme is located on the cell surface and a correlation with adhesion was suggested.

Besides the different *P. furiosus* strains, a newly isolated species, *Methanocaldococcus* sp. KIN24-T80 was analyzed. Results of characterization studies performed herein confirmed the affiliation of the strain to the genus *Methanocaldococcus*; the distinctiveness from any previously described species was proven by 16S rRNA gene sequence analysis. Ergo, the isolate was described as novel species named *Methanocaldococcus villosus* referring to its heavy flagellation and its unique striated surface pattern in SEM preparations.

Further following the scope of this study, a submembraneous layer below the cytoplasmic membrane was detected in *M. villosus* and *P. furiosus*. For both organisms, it was shown to be related to the anchoring of flagella. In the case of *M. villosus*, it was proven that the layer is associated with a (putative) chemoreceptor array.

Moreover, it was demonstrated for *P. furiosus*, *M. villosus*, and five other members of the genus *Methanocaldococcus* that assembly of flagella is induced as a response to surface associated growth, which helps the cells not only to get in tight contact with the solid support but also with each other. Flagella were identified as structural prerequisite for biofilm formation and other components such as pili or surface proteins were shown to be necessary for a more solid adhesion.

To sum up, analyses performed in this thesis extend the current knowledge on the cellular and flagellar ultrastructure of Archaea. Based on the data obtained, *M. villosus* is proposed as a model organism for studying the flagellation and adhesion of archaeal cells.

8 Zusammenfassung

Im Gegensatz zu bakteriellen Flagellen wurde für archaeelle Flagellen gezeigt, dass es sich um multifunktionelle Organelle handelt, die für die Adhäsion und die Ausbildung von Zell-Zell Kontakten benötigt werden.

Ziel dieser Studie war es, die Ultrastruktur und die Funktion der Flagellen verschiedener Archaeen in Hinblick auf ihre Verankerung zu untersuchen. Um Flagellen-assozierte Proteine analysieren zu können, wurden Zellhüllen von *Pyrococcus furiosus* isoliert. In der Membranfraktion konnte die Glutamatdehydrogenase identifiziert werden, die mit Hilfe von Immunlokalisationsstudien auf der Oberfläche von *P. furiosus* detektiert wurde und somit womöglich eine Adhäsionsstruktur darstellt. Jedoch zeigte sich im Verlauf der Analysen, dass die Zellform des Stammes sich stark veränderte und damit das Wachstum und die Adhäsion stark beeinträchtigt waren. Ein Vergleich mit dem Typstamm und einer weiteren Kultur, die über Jahre kontinuierlich im Labor untersucht wurde, machte deutlich, dass die Fähigkeit auf Oberflächen zu wachsen durch die Kultivierung erworben wurde.

In einem weiteren Teilprojekt dieser Arbeit wurde die Charakterisierung des Isolates *Methanocaldococcus* sp. KIN24-T80 abgeschlossen. Es konnte gezeigt werden, dass der Stamm phylogenetisch einen tiefen Zweig innerhalb der Gattung *Methanocaldococcus* darstellt. Physiologische Tests und elektronenmikroskopische Analysen bestätigten die Zuordnung zu dieser Gattung. Somit konnte das Isolat als neue Art beschrieben werden; es erhielt den Namen *Methanocaldococcus villosus* aufgrund der ungewöhnlichen Oberfläche in REM-Analysen und seiner vielen Flagellen.

Neben *M. villosus* konnte auch für andere *Methanocaldococci* und die verschiedene *P. furiosus* Stämme gezeigt werden, dass die Flagellen bei Oberflächenwachstum deutlich stärker expremiert sind als in planktonischen Zellen. Sie stellen somit eine wichtige Voraussetzung für die Bildung von Biofilmen dar, wobei aber gezeigt wurde, dass andere Strukturen wie zum Beispiel Pili für die Adhäsion benötigt werden.

Des Weiteren konnte im Rahmen dieser Arbeit gezeigt werden, dass *P. furiosus* und *M. villosus* eine ‚Membran' parallel unter der Cytoplasmamembran besitzen, in der die Flagellen inseriert sind und die in *M. villosus* auch mit (hypothetischen) Chemorezeptoren assoziiert ist.

Zusammenfassend konnten mit dieser Arbeit viele neue Einsichten in die Ultrastruktur und Funktionalität von Flagellen und den Zellaufbau von Archaeen gegeben werden. Für diese Untersuchungen stellt *M. villosus* einen interessanten Modellorganismus dar.

9 Appendix

The appendix contains useful tables, figures, and alignments sequences, which summarize or give details to the results gained during the course of this thesis.

1 Tables and figures

Table A1: Comparison of different *P. furiosus* strains. The three different *P. furiosus* strains used herein (*P. furiosus* LS, *P. furiosus* Vc1, and *P. furiosus* DSM 3638^T) were compared with respect to their growth rate, cell morphology, flagellation, and adhesion behavior to carbon-coated gold grids. For strain LS and Vc1, it is differentiated between the beginning and the end of this thesis.

	P. furiosus LS in 2007	in 2010/2011	*P. furiosus* Vc1 in 2008[a]	in 2010/2011	*P. furiosus* DSM 3638^T
Source	cultured in the lab since 2003 (regenerated from BBR 19/12/3 in 2003)		regenerated from BBR 19/12/3	cultured in the lab since 10/2008 (originally BBR 19/12/3)	DSMZ 12/2009 regenerated 01/2010
Depositon	cultured for six years in the lab prior to long-term storage		cultured for six years in the lab prior to long-term storage		immediately after isolation
Growth	normal growth	growth slower, 2–4-fold lower final cell density	normal growth	normal growth	in starch-medium as described by Fiala and Stetter, 1986
Cell shape	regular to irregular cocci	very diverse	regular cocci	regular cocci	regular cocci
Flagellation	multiple flagella		planktonic cells with hardly any flagella		heavily flagellated
Adhesion	very good adherence	decreased adhesion ; cell density comparable to *P. furiosus* Vc1	good adherence; cells possess much more flagella than planktonic cells		very weak adhesion; detachment of cells in stationary phase

BBR in-house culture collection, Institute of Microbiology and Archaea Center, University of Regensburg, Germany (Bakterienbank Regensburg)

[a] regenerated in November 2010 representing the appearance of the strain as in 10/2008 when originally regenerated from BBR 19/12/3

[b] compared to the original description by Fiala and Stetter, 1986

Table A2: Database analysis of flagella of the genus *Methanocaldococcus*. Flagellins annotated in the genomes of *M. fervens*, *M. jannaschii*, *M. infernus*, *M. vulcanius*, and *Methanocaldococcus* sp. FS406-22 were compared using different applications: Prediction on molecular masses with ProtParam. Possible N-glycosylation sites were predicted using NetNGlyc 1.0 Server. See next page and Figure A1 for multiple sequence alignment of selected flagellins.

species	flagellin ID	strand	with SP number of aa	Mr in kDa[a]	signal peptide	without SP number of aa	Mr in kDa[a]	N-glycosylation[b] Asn-Xaa-Ser/Thr sequons Nr	Position	glycosylated Asn Nr	
M. fervens	1208	-	151	16.3	nd			2	64, 127	1	127
Mefer	1209	-	138	15.5	nd			5	66, 72, 87, 95, 110	5	all
	1213	-	227	23.9	-MLLKYIKSRRG	216	22.5	4	72, 121, 149, 183	4	all
	1214	-	218	22.8	MKLLEFLKGKKG	206	21.5	8	38, 72, 73, 95, 129, 136, 156, 172	7	ex. 156
	1215	-	213	22.2	MKLLEFLKGKKG	201	20.9	3	38, 112, 131	3	all
M. infernus	1104	-	151	16.3	nd			2	123, 127	1	123
Metin	1105	-	137	15.3	nd			4	66, 72, 95, 116	4	ex. 95
	1109	-	219	23.3	---MKFFSSKKG	210	22.3	1	157	0	not any
	1110	-	217	22.6	MKLLAFLKGKKG	205	21.3	7	38, 72, 73, 95, 128, 135, 171	7	all
	1111	-	217	22.3	MKLLAFLKGKKG	205	21.1	2	38, 112	2	all
M. jannaschii	0891	+	217	22.7	MKVFEFLKGKRG	205	21.3	3	38, 113, 129	2	ex. 129
MJ	0892	+	217	22.6	MKVFEFLKGKRG	205	21.2	5	38, 95, 128, 135, 171	4	ex. 128
	0893	+	216	23.1	-MLLDYIKSRRG	205	21.7	5	75, 121, 128, 136, 154	3-4	ex. 128, 136=Pro
M. vulcanius	0092	+	213	22.4	MRVFEFLRGKKG	201	20.9	6	38, 72, 118, 121, 168, 174	4	ex. 118, 174
Metvu	0093	+	218	22.8	MRVFEFLRGKKG	206	21.3	6	38, 95, 120, 129, 136,172	6	all
	0094	+	216	22.8	MLMKYVGSRRG	205	21.6	5	75, 121, 128, 135, 154	4	ex. 128
	0098	+	138	15.7	nd			4	66, 72, 95, 116	3	ex. 95
	0099	+	146	15.8	nd			4	59, 81, 96, 122	1	59
M. sp. FS406-22	1260	-	146	15.6	nd			4	59, 81, 96, 122	1	122
MFS40622	1261	-	139	15.6	nd			4	66, 72, 95, 117	3	ex. 95
	1265	-	219	23.3	MLLLNYLKSRRG	207	21.9	5	72, 76, 124, 139, 157	4-5	all (ex. 139=Pro)
	1266	-	217	22.5	MKVLEFLKGKRG	205	21.1	6	38, 73, 95, 128, 135, 171	6	all
	1267	-	216	22.4	MKVLEFLKGKRG	204	21.0	4	38, 112, 128, 171	4	all

nd not determined, SP signal peptide

[a] Prediction of molecular masses of flagellins with ProtParam

[b] Prediction of N-glycosylation sites with NetNGlyc 1.0

Figure A1: ClustalW2 multiple sequence alignment of annotated *Methanocaldococcus* flagellins. First alignment of *M. jannaschii* FlaB1 with corresponding flagellins of the other species showing the homology between the proteins, second alignment of all flagellins.
fer *M. fervens*, inf *M. infernus*, jan *M. jannaschii*, vul *M. vulcanius*; protein numbers as given in Table A2.

```
SeqA Name        Len(aa)  SeqB Name        Len(aa)  Score
=========================================================
1    jan_0891    217      2    fer_1215    213      86
1    jan_0891    217      3    inf_1111    217      76
1    jan_0891    217      4    vul_0092    213      80
2    fer_1215    213      3    inf_1111    217      79
2    fer_1215    213      4    vul_0092    213      76
3    inf_1111    217      4    vul_0092    213      75
=========================================================

jan_0891         MKVFEFLKGKRGAMGIGTLIIFIAMVLVAAVAAAVLINTSGFLQQKAMATGKESTEQVAS 60
fer_1215         MKLLEFLKGKKGATGIGTLIVFIAMVLVAAVAAAVLINTSGFLQQKAMATGKESTEQVAS 60
vul_0092         MRVFEFLRGKKGAMGIGTLIIFIAMVLVAAVAAAVLINTSGFLQQKAMATGKESTEQVAS 60
inf_1111         MKLLAFLKGKKGAMGIGTLIVFIAMVLVAAVAAAVLINTSGFLQQKAMATGKESTEQVAS 60
                 *::: **:**:** ******:************************************

jan_0891         GLMCIGVTGHYDKTLGGIDKLAIYITPNAGSAPIDLKNAKLFLIYDGESHVLNYSTVTTA 120
fer_1215         GLMCMGVTGHYDGSNG-IDKLAIYIAPNAGSAPIDLKQAKLFLIYDGESHVLNYSTATTE 119
vul_0092         GLMCLGVTGHNN-GSG-IDQLAIYITPNAGSAPIDLKNTKLFLTYDGQSHVLTYGGYTEN 118
inf_1111         GLMCIGVTGHYDGTSG-IDRIAIFITPNAGSAPIDLKQCKVLLTYDGNTVVLNYSGYTSA 119
                 ****:***** :   * **::**:*:***********: *::* ***:: **.*.  *

jan_0891         TLGADDIFNSSAITDWSLADSSSYVVGVIQDADGSLSNG-VINKGDIAVLLVNANAVFNK 179
fer_1215         TLGATDIFS---VGNWSSADSSSYVVGVIQDADGSLSNG-VINKGDIAVLLVDVSQVFGN 175
vul_0092         TSNATNIFDYS--VGWSAANSKSYVVGIIQDADTSLKNG-VINKGDIAVLLVNASAVFNT 175
inf_1111         TAGASNIFDSATITAWSNADATSFVVGKIQDADGSLDNGQVINKGDIAVLLIDVSQVFGE 179
                 * .* :**.      ** *::.*:*** ***** **.** ***********::.. **.

jan_0891         AIPTRSEVSGQFQPEFGAPAVIQFTTPAAYTQTVIELQ 217
fer_1215         PIPTRKEVSGQYQPEFGAPAVIQFTTPAAYTQKVIELQ 213
vul_0092         TIPTRAEVSGEVQPEFGAPAVIDFTTPPAFTQTIIELQ 213
inf_1111         SIPDRKEVSGQVQPEFGAPAVIQFTTPAAFTSDIVELQ 217
                 .** * ****: **********:****.*:*. ::***


jan_0893         -MLLDYIKSRRGAIGIGTLIIFIALVLVAAVAAAVIINTAANLQHKAARVGEESTRQVAS 59
vul_0094         -MLMKYVGSRRGAIGIGTLIIFIALVLVAAVAAAVIINTAANLQHKAARVGEESTKQVAS 59
fer_1213         -MLLKYIKSRRGAVGIGTLIIFIALVLVAAVAAAVIINTAANLQHKAARVGQETTKQVAS 59
inf_1109         ---MKFFSSKKGAIGIGTLIIFIALVLVAAIAAAVIINTAANLQQKAARVGQESTKQVAS 57
jan_0891         MKVFEFLKGKRGAMGIGTLIIFIAMVLVAAVAAAVLINTSGFLQQKAMATGKESTEQVAS 60
fer_1215         MKLLEFLKGKKGATGIGTLIVFIAMVLVAAVAAAVLINTSGFLQQKAMATGKESTEQVAS 60
inf_1111         MKLLAFLKGKKGAMGIGTLIVFIAMVLVAAVAAAVLINTSGFLQQKAMATGKESTEQVAS 60
vul_0092         MRVFEFLRGKKGAMGIGTLIIFIAMVLVAAVAAAVLINTSGFLQQKAMATGKESTEQVAS 60
fer_1214         MKLLEFLKGKKGATGIGTLIVFIAMVLVAAVAAAVLINTSGFLQQKAMATGKESTEQVAS 60
inf_1110         MKLLAFLKGKKGAMGIGTLIVFIAMVLVAAVAAAVLINTSGFLQQKAMATGKESTEQVAS 60
jan_0892         MKVFEFLKGKRGAMGIGTLIIFIAMVLVAAVAAAVLINTSGFLQQKAMATGKESTEQVAS 60
vul_0093         MRVFEFLRGKKGAMGIGTLIIFIAMVLVAAVAAAVLINTSGFLQQKAMATGKESTEQVAS 60
fer_1208         ----------MASSALSEIIMFVAVLLIAAFVAGILTTSTYKISVNIGKKGDELSTKLSQ 50
vul_0099         ---------------MSEIIMFVAVLLIAAFVAGILTTSTYKISLNIDKKSDALSTKLSQ 45
inf_1104         ----------MASSALSEIILFVTVLIIAAFVAGVLLTSSYKISIGIGEKTDVLSEKLSQ 50
fer_1209         ---------MGFSSVVGATVMVIALLICGAYLYTTVDSHYETIYNAHESYYSHLNDKLHE 51
vul_0098         ---------MGFSSVVGTTVMVVALLICGAYLYTTMDNYYEDVNHAYSVYYEHMHNKLDE 51
inf_1105         ---------MGFSSVAGTVIMVISLLIVGAYLYTTIDSSYSILYKNYEAYQKHLENKINE 51
                                 .  ::.::::: .*     : .    :        .    :: .

jan_0893         GIQVLKITGYAV-NTKNITKLAILVSPNVG-DEIDLSSTIVTISNGDYKASLVYG--GQI 115
vul_0094         GIQVLKITGYAP-NSNNITKLAILVSPNIG-DEIDLSSTIITISNGQQKASLVYG--GVL 115
fer_1213         GLQVIKVVGYAP-NTSTIEDLVIFVSPNVG-DEVDLSSTIVVISNGNKKASLVYS--GLL 115
inf_1109         GIQVVKVVGYAP-NNNEITKLLIFVSPNIG-DEIDLSSTIVTLSNGEKKCSLVYDSAAYV 115
jan_0891         GLMCIGVTGHYDKTLGGIDKLAIYITPNAGSAPIDLKNAKLFLIYDGESHVLNYS-TVTT 119
fer_1215         GLMCMGVTGHYDGSNG-IDKLAIYIAPNAGSAPIDLKQAKLFLIYDGESHVLNYS-TATT 118
inf_1111         GLMCIGVTGHYDGTSG-IDRIAIFITPNAGSAPIDLKQCKVLLTYDGNTVVLNYS-GYTS 118
vul_0092         GLMCLGVTGHNN-GSG-IDQLAIYITPNAGSAPIDLKNTKLFLTYDGQSHVLTYG-GYTE 117
fer_1214         GLSTLQVIGIHN--NSTVNYLAIYITPNAGSAPIDLNQTKILITDGNKKAVLKYKGAAAW 118
inf_1110         GLQTLRVIGIHN--NTSINYLGIYITPNAGSAPIDLNQTKILISDGSRKAVLQYK-STAF 117
jan_0892         GLSTLQVIGIHD--NKAINYLAIYITPNAGSAAIDLNQTKILITDGEKKAVLRYN-SNAY 117
vul_0093         GLSALRVIGIHD--GSQINYLAIYISPNAGSAPIDLNQTKILITDGKEKAVLKYGGSDKY 118
fer_1208         DFEIINDPGSIP--RNSSAGITIIYIKNTGKDPIIFTDDSFTVIIDG-------------- 95
vul_0099         DFEIINDPGEII--RNPSAGVIYLYIKNTGKDPIVFTNTSFTVIVDG-------------- 90
inf_1104         DFEIVNDPSNIP--RDSNLGITTLYIKNTGNTQLPITKNSYTVIIDG-------------- 95
fer_1209         KLVITN--------VKSSASQTNITIYNNGS--VVVEPRKFSVLFNG-------------- 88
vul_0098         KLIITN--------VIATATQTNITIYNNGS--VVVEPDKFTILFDG-------------- 88
inf_1105         KLVITK--------VSSSATQTNITIYNNGS--VVVEPHKFTVLFDG-------------- 88
                  :                         * *   : .      :  .
```

```
jan_0893        TYVNTNGTRDIFNESWPNIA-----------NPTTEFGVIVLQDADGSMNNTEHPTMNFG 164
vul_0094        NHAETNGTKDIFNESWPKVN-----------DTSTEFGIIVLQDADGSMNNTEHPTMNFG 164
fer_1213        ADCGNNGTKDIFGTDNSNLNTFWNDLTTAQSNNNVSFGVIVLQDADGSASNVEHPTINFG 175
inf_1109        NDPAIQGTEDLFNGDNVQTAWT--------YSGGDRFGVIILQDADGSCNDSAHPTINFG 167
jan_0891        ATLGADDIFNSSAITDWSLAD----------SSSYVVGVIQDADGSLSNG---VINKG 164
fer_1215        ETLGATDIFS---VGNWSSAD----------SSSYVVGVIQDADGSLSNG---VINKG 160
inf_1111        ATAGASNIFDSATITAWSNAD----------ATSFVVGKIQDADGSLDNGQ--VINKG 164
vul_0092        NTSNATNIFDYS--VGWSAAN----------SKSYVVGIIQDADTSLKNG---VINKG 160
fer_1214        NDLDNGGEVTNTSLPAWNLS----------SGEFGIIVLQDADDSCKNITP-VINKG 164
inf_1110        TDLSTGGKVSNISKDAWNLS----------GGEFGIIVVQDADNSCTSNTP-VINKG 163
jan_0892        ADLTTGGEVTNTSLAAWNLS----------GGEFGIIVLQDADGSCKSTTP-VINKG 163
vul_0093        YNLSAGGEVTNLSLAAWNLS----------AGQFGIIVLQDADHSCQPSTP-VIDKG 164
fer_1208        ------------------------------------NIVEISDTKQLSNPESNTLYPG 117
vul_0099        ------------------------------------NIVGINNTYDLTDPGDNVLSPG 112
inf_1104        ------------------------------------LVVPIENVDNYNNPGSNVLYPG 117
fer_1209        ------------------------------------SVVPEENISYY--PQKDYLVPL 108
vul_0098        ------------------------------------TVVPEENISYY--PQKKYLVPL 108
inf_1105        ------------------------------------TIVPPQNISYS--PDVPYLLPL 108
                                                    .           :

jan_0893        DKAIIAINVGDVFGGIMP-RERIYGEVIPEFGASGIIEFRAPSTFS--EHVVTLQ 216
vul_0094        DKVLLTVDVGDVFGGIAP-REKVYGEVIPEFGSPGIIEFIAPSTFT--QHVVPLQ 216
fer_1213        DKVAIAINLSAIEMPISP-RDKVYGEVIPEYGASGIIEFIAPSVFT--ENVVPLQ 227
inf_1109        DKVALTVDLNAIGMPIKP-RDLIEGEVIPEYGSPGIIEFYAPSTFN--RRVIELQ 219
jan_0891        DIAVLLVNANAVFNKAIPTRSEVSGQFQPEFGAPAVIQFTTPAAYT--QTVIELQ 217
fer_1215        DIAVLLVDVSQVFGNPIPTRKEVSGQYQPEFGAPAVIQFTTPAAYT--QKVIELQ 213
inf_1111        DIAVLLIDVSQVFGESIPDRKEVSGQVQPEFGAPAVIQFTTPAAFT--SDIVELQ 217
vul_0092        DIAVLLVNASAVFNTTIPTRAEVSGEVQPEFGAPAVIDFTTPPAFT--QTIIELQ 213
fer_1214        DIVALTINASKISLDLKP-RTTVTGSVVPEFGAPAVIEFTTPATYLGDQEVIQLQ 218
inf_1110        DIVVLTINATANQFNLPP-RTTVTGSVVPEFGAPAVIQFTTPATYLGDQSVVTLQ 217
jan_0892        DIVALTINASAVGLNLVP-RTTVTGSVIPEFGAPAVIEFTTPAAYLSTQEVIQLQ 217
vul_0093        DIVALTINASAVGLDLAP-RTTVTGSVIPEFGAPAVIEFTTPASYLDTQKIIQLQ 218
fer_1208        DVGEIDVNYNETGY--------HKIKVVSDSGISRVIRGYIS-------------- 151
vul_0099        DVGEIVAKYNETGY--------HRIRVVSESGISRTIKGYIS-------------- 146
inf_1104        DVGIINVSYNNSGY--------HKIKVVLYSGLSREIIGYIP-------------- 151
fer_1209        DNITIIVNWPTP----------NRICIISDNGNKYFYSLS---------------- 138
vul_0098        DSITIVVNWTRP----------FRICVVSDNGNKYFYSVP---------------- 138
inf_1105        ESITLIVNWTQP----------TRICIVSNYGNKYFATT----------------- 137
                :   :  .                      *
```

Figure A2: Adhesion of the *P. furiosus* glutamate dehydrogenase knock-out strain. Cell were grown on carbon-coated gold grids

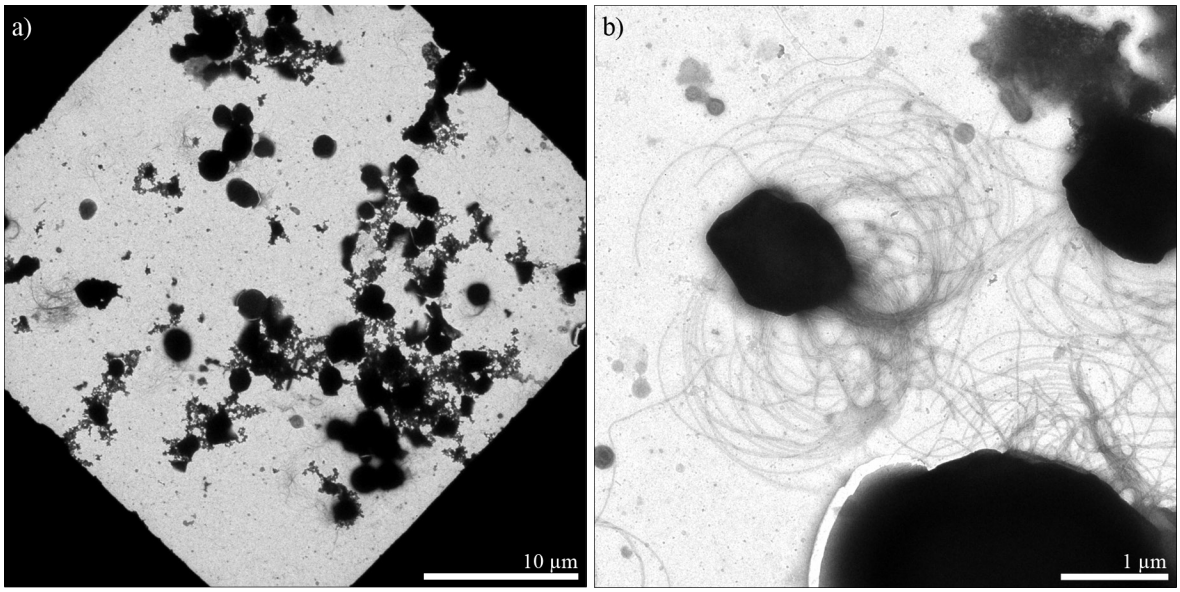

2 Supporting material provided on DVD

Please find attached a DVD containing short films that visualize the following structures:

CLSM Pfu GluDH	Animation supporting Figure 12 Localization of the glutamate dehydrogenase on the surface of *P. furiosus* DSM 3638^T was visualized using confocal sectioning. Two films are provided: AF shows track of anti-Gdh Pfu antibodies enhanced with Alexa Fluor® 488 labeled secondary antibodies, DIC shows the corresponding DIC images of the cells.
CLSM adhesion	Animation of Figure 29 Fluorescent staining of flagella of adherent *M. villosus* cells with anti-Fla KIN antibodies and signal enhancement using a secondary antibody coupled to Alexa Fluor® 488. Confocal sectioning reveals the three-dimensional growth of cells.
FIB-SEM	FIB-SEM analysis of high-pressure frozen and freeze-substituted *M. villosus* cells Series of ca. 200 8-nm slices
Amira	Reconstruction of *M. villosus* cells from FIB-SEM slices using Amira™

10 References

A

Abu-Qarn, M., Yurist-Doutsch, S., Giordano, A., Trauner, A., Morris, H.R., Hitchen, P., Medalia, O., Dell, A., and Eichler, J. (2007). *Haloferax volcanii* AglB and AglD are involved in N-glycosylation of the S-layer glycoprotein and proper assembly of the surface layer. *J Mol Biol* **374**, 1224−1236.

Akça, E., Claus, H., Schultz, N., Karbach, G., Schlott, B., Debaerdemaeker, T., Declercq, J.-P., and König, H. (2002). Genes and derived amino acid sequences of S-layer proteins from mesophilic, thermophilic, and extremely thermophilic methanococci. *Extremophiles* **6**, 351−358.

Alam, M., and Oesterhelt, D. (1984). Morphology, function and isolation of halobacterial flagella. *J Mol Biol* **176**, 459−475.

Albers, S.-V., Szabó, Z., and Driessen, A.J.M. (2003). Archaeal homolog of bacterial type IV prepilin signal peptidases with broad substrate specificity. *J Bacteriol* **185**, 3918−3925.

Altschul, S., Gish, W., Miller, W., Myers, E., and Lipman, D. (1990). Basic local alignment search tool. *J Mol Biol* **215**, 403−410.

Auernik, K.S., Maezato, Y., Blum, P.H., and Kelly, R.M. (2008). The genome sequence of the metal-mobilizing, extremely thermoacidophilic Archaeon *Metallosphaera sedula* provides insights into bioleaching-associated metabolism. *Appl Environ Microbiol* **74**, 682−692.

B

Balch, W.E., and Wolfe, R.S. (1976). New approach to the cultivation of methanogenic Bacteria: 2-mercaptoethanesulfonic acid (HS-CoM)-dependent growth of *Methanobacterium ruminantium* in a pressureized atmosphere. *Appl Environ Microbiol* **32**, 781−791.

Balch, W.E., Fox, G.E., Magrum, L.J., Woese, C.R., and Wolfe, R.S. (1979). Methanogens: Reevaluation of a unique biological group. *Microbiol Mol Biol Rev* **43**, 260−296.

Bardy, S.L., and Jarrell, K.F. (2002). FlaK of the archaeon *Methanococcus maripaludis* possesses preflagellin peptidase activity. *FEMS Microbiol Lett* **208**, 53−59.

Bardy, S.L., and Jarrell, K.F. (2003). Cleavage of preflagellins by an aspartic acid signal peptidase is essential for flagellation in the Archaeon *Methanococcus voltae. Mol Microbiol* **50**, 1339−1347.

Bardy, S.L., Eichler, J., and Jarrell, K.F. (2003). Archaeal signal peptides - A comparative survey at the genome level. *Protein Sci* **12**, 1833−1843.

Bardy, S.L., Mori, T., Komoriya, K., Aizawa, S.-I., and Jarrell, K.F. (2002). Identification and localization of flagellins FlaA and FlaB3 within flagella of *Methanococcus voltae. J Bacteriol* **184**, 5223−5233.

Barth, T. (2008). Untersuchungen zur Anheftung von *Pyrococcus furiosus* an feste Oberflächen über seine Flagellen. *Diploma thesis*. University of Regensburg. Regensburg, Germany.

Baumeister, W., and Lembcke, G. (1992). Structural features of archaebacterial cell envelopes. *J Bioenerg Biomembr* **24**, 567−575.

Bellack, A. (2007). Charakterisierung des methanogenen Isolates KIN24-T80. *Diploma thesis*. University of Regensburg. Regensburg, Germany.

Bellack, A., Huber, H., Rachel, R., Wanner, G., and Wirth, R. (2011). *Methanocaldococcus villosus* sp. nov., a heavily flagellated Archaeon that adheres to surfaces and forms cell–cell contacts. *Int J Syst Evol Microbiol* **61**, 1239−1245.

Beveridge, T., and Graham, L.L. (1991). Surface layers of Bacteria. *Microbiol Rev* **55**, 684−705.

Beznosov, S.N., Pyatibratov, M.G., and Fedorov, O.V. (2007). On the multicomponent nature of *Halobacterium salinarum* flagella. *Microbiology* **76**, 435−441.

Blum, H., Beier, H., and Gross, H.J. (1987). Improved silver staining of plant proteins, RNA and DNA in polyacrylamide gels. *Electrophoresis* **8**, 93−99.

Briegel, A., Dias, D.P., Li, Z., Jensen, R.B., Frangakis, A.S., and Jensen, G.J. (2006). Multiple large filament bundles observed in *Caulobacter crescentus* by electron cryotomography. *Mol Microbiol* **62**, 5−14.

Briegel, A., Ding, H.J., Li, Z., Werner, J., Gitai, Z., Dias, D.P., Jensen, R.B., and Jensen, G.J. (2008). Location and architecture of the *Caulobacter crescentus* chemoreceptor array. *Mol Microbiol* **69**, 30−41.

Briegel, A., Ortega, D.R., Tocheva, E.I., Wuichet, K., Li, Z., Chen, S., Müller, A., Iancu, C.V., Murphy, G.E., and Dobro, M.J., et al. (2009). Universal architecture of bacterial chemoreceptor arrays. *Proc Natl Acad Sci USA* **106**, 17181−17186.

Bult, C.J., White, O., Olsen, G.J., Zhou, L., Fleischmann, R.D., Sutton, G.G., Blake, J.A., FitzGerald, L.M., Clayton, R.A., and Gocayne, J.D., et al. (1996). Complete genome sequence of the methanogenic Archaeon, *Methanococcus jannaschii. Science* **273**, 1058−1073.

Burggraf, S., Fricke, H., Neuner, A., Kristjansson, J., Rouvier, P., Mandelco, L., Woese, C.R., and Stetter, K.O. (1990). *Methanococcus igneus* sp. nov., a novel hyperthermophilic methanogen from a shallow submarine hydrothermal system. *Syst Appl Microbiol* **13**, 263−269.

C

Chaban, B., Ng, S.Y.M., Kanbe, M., Saltzman, I., Nimmo, G., Aizawa, S.-I., and Jarrell, K.F. (2007). Systematic deletion analyses of the fla genes in the flagella operon identify several genes essential for proper assembly and function of flagella in the Archaeon, *Methanococcus maripaludis. Mol Microbiol* **66**, 596−609.

Chaban, B., Voisin, S., Kelly, J.F., Logan, S.M., and Jarrell, K.F. (2006). Identification of genes involved in the biosynthesis and attachment of *Methanococcus voltae* N-linked glycans: insight into N-linked glycosylation pathways in Archaea. *Mol Microbiol* **61**, 259−268.

Cohen-Krausz, S., and Trachtenberg, S. (2008). The flagellar filament structure of the extreme acidothermophile *Sulfolobus shibatae* B12 suggests that archaeabacterial flagella have a unique and common symmetry and design. *J Mol Biol* **375**, 1113−1124.

Conrad, T.M., Joyce, A.R., Applebee, M.K., Barrett, C.L., Xie, B., Gao, Y., and Palsson, B.Ø. (2009). Whole-genome resequencing of *Escherichia coli* K-12 MG1655 undergoing short-term laboratory evolution in lactate minimal media reveals flexible selection of adaptive mutations. *Genome Biol* **10**, R118.

Cruden, D., Sparling, R., and Markovetz, A.J. (1989). Isolation and ultrastructure of the flagella of *Methanococcus thermolithotrophicus* and *Methanospirillum hungatei. Appl Environ Microbiol* **55**, 1414−1419.

D

Doddema, H.J., Derksen, J.W.M., and Vogels, G.D. (1979). Fimbriae and flagella of methanogenic Bacteria. *FEMS Microbiol Lett* **5**, 135−138.

Dong, G., Vieille, C., and Zeikus, J.G. (1997). Cloning, sequencing, and expression of the gene encoding amylopullulanase from *Pyrococcus furiosus* and biochemical characterization of the recombinant enzyme. *Appl Environ Microbiol* **63**, 3577−3584.

E

Eder, W., Ludwig, W., and Huber, R. (1999). Novel 16S rRNA gene sequences retrieved from highly saline brine sediments of Kebrit Deep, Red Sea. *Arch Microbiol* **172**, 213−218.

Egelman, E.H. (2007). The iterative helical real space reconstruction method: Surmounting the problems posed by real polymers. Software tools for macromolecular microscopy. *J Struct Biol* **157**, 83−94.

Engelhardt, H. (2007). Are S-layers exoskeletons? The basic function of protein surface layers revisited. *J Struct Biol* **160**, 115−124.

F

Faguy, D.M., Koval, S.F., and Jarrell, K.F. (1992). Correlation between glycosylation of flagellin proteins and sensitivity of flagellar filaments to Triton X-100 in methanogens. *FEMS Microbiol Lett* **90**, 129−133.

Fiala, G., and Stetter, K.O. (1986). *Pyrococcus furiosus* sp. nov. represents a novel genus of marine heterotrophic archaebacteria growing optimally at 100°C. *Arch Microbiol* **145**, 56−61.

Flemming, H.-C., and Wingender, J. (2010). The biofilm matrix. *Nat Rev Micro* **8**, 623−633.

Fröls, S., Ajon, M., Wagner, M., Teichmann, D., Zolghadr, B., Folea, M., Boekema, E.J., Driessen, A.J.M., Schleper, C., and Albers, S.-V. (2008). UV-inducible cellular aggregation of the hyperthermophilic archaeon *Sulfolobus solfataricus* is mediated by pili formation. *Mol Microbiol* **70**, 938−952.

Fröls, S., Gordon, P.M.K., Panlilio, M.A., Duggin, I.G., Bell, S.D., Sensen, C.W., and Schleper, C. (2007). Response of the hyperthermophilic Archaeon *Sulfolobus solfataricus* to UV damage. *J Bacteriol* **189**, 8708−8718.

G

Gasteiger, E., Hoogland, C., Gattiker, A., Duvaud, S., Wilkins, M.R., Appel, R.D., and Bairoch, A. (2005). Protein identification and analysis tools on the ExPASy server. *In* The Proteomics Protocols Handbook. Humana Press: Totowa, pp. 571–607.

H

Häring, M. (2005). Isolierung und Charakterisierung neuer Viren von Hyperthermophilen. *PhD thesis.* University of Regensburg. Regensburg, Germany.

Haugland, R.P. (2005). The handbook: A guide to fluorescent probes and labeling technologies Karlsbad, CA, USA: Invitrogen Corp.

Hendriksen, W.T., Kloosterman, T.G., Bootsma, H.J., Estevao, S., de Groot, R., Kuipers, O.P., and Hermans, P.W.M. (2008). Site-specific contributions of glutamine-dependent regulator GlnR and GlnR-regulated genes to virulence of *Streptococcus pneumoniae. Infect Immun* **76**, 1230−1238.

Henneberger, R., Moissl, C., Amann, T., Rudolph, C., and Huber, R. (2006). New insights into the lifestyle of the cold-loving SM1 Euryarchaeon: Natural growth as a monospecies biofilm in the subsurface. *Appl Environ Microbiol* **72**, 192−199.

Herzog, B. (2009). Vergleichende Analyse des Schwimmverhaltens verschiedener Archaeen. University of Regensburg. Regensburg, Germany.

Holden, J.F., Poole II, F.L., Tollaksen, S.L., Giometti, C.S., Lim, H., Yates III, J.R., and Adams, M.W.W. (2001). Identification of membrane proteins in the hyperthermophilic archaeon *Pyrococcus furiosus* using proteomics and prediction programs. *Comp Funct Genomics* **2**, 275−288.

Holman, H.-Y.N., Bechtel, H.A., Hao, Z., and Martin, M.C. (2010). Synchrotron IR spectromicroscopy: Chemistry of living cells. *Anal Chem* **82**, 8757−8765.

Horn, C., Paulmann, B., Kerlen, G., Junker, N., and Huber, H. (1999). In vivo observation of cell division of anaerobic hyperthermophiles by using a high-intensity dark-field microscope. *J Bacteriol* **181**, 5114−5118.

Houwink, A.L. (1956). Flagella, gas vacuoles and cell-wall structure in *Halobacterium halobium*; an electron microscope study. *J Gen Microbiol* **15**, 146−150.

Huber, H., and Stetter, K.O. (2006). *Desulfurococcales*. *In* The Prokaryotes. A Handbook on the Biology of Bacteria 3, ed. M. Dworkin. Springer: New York, NY, pp. 52–68.

Huber, R., Burggraf, S., Mayer, T., Barns, S.M., Rossnagel, P., and Stetter, K.O. (1995a). Isolation of a hyperthermophilic Archaeum predicted by in situ RNA analysis. *Nature* **376**, 57−58.

Huber, R., Stöhr, J., Hohenhaus, S., Rachel, R., Burggraf, S., Jannasch, H.W., and Stetter, K.O. (1995b). *Thermococcus chitonophagus* sp. nov., a novel, chitin-degrading, hyperthermophilic archaeum from a deep-sea hydrothermal vent environment. *Arch Microbiol* **164**, 255−264.

Huet, J., Schnabel, R., Sentenac, A., and Zillig, W. (1983). Archaeabacteria and eukaryotes possess DNA-dependent RNA polymerases of a common type. *EMBO J* **2**, 1291−1294.

J

Janker, C. (2008). Anheftung ausgewählter Archaeen an unterschiedliche Oberflächen inkl. Literaturrecherche zu Zellanhängen von Bakterien und Archaeen. University of Regensburg. Regensburg, Germany.

Jarrell, K.F., and McBride, M.J. (2008). The surprisingly diverse ways that prokaryotes move. *Review. Nat Rev Micro* **6**, 466−476.

Jarrell, K.F., Bayley, D.P., and Kostyukova, A.S. (1996). The archaeal flagellum: a unique motility structure. *J Bacteriol* **178**, 5057−5064.

Jarrell, K.F., Jones, G.M., and Nair, D.B. (2010a). Biosynthesis and role of N-linked glycosylation in cell surface structures of Archaea with a focus on flagella and S layers. *Int J Microbiol* **2010**, 1−20.

Jarrell, K.F., Jones, G.M., Kandiba, L., Nair, D.B., and Eichler, J. (2010b). S-Layer glycoproteins and flagellins: Reporters of archaeal posttranslational modifications. *Archaea* **2010**, 1−13.

Jeanthon, C., L'Haridon, S., Reysenbach, A.L., Corre, E., Vernet, M., Messner, P., Sleytr, U.B., and Prieur, D. (1999). *Methanococcus vulcanius* sp. nov., a novel hyperthermophilic methanogen isolated from East Pacific Rise, and identification of *Methanococcus* sp. DSM 4213(T) as *Methanococcus fervens* sp. nov. *Int J Syst Bacteriol* **49**, 583−589.

Jeanthon, C., L'Haridon, S., Reysenbach, A.L., Vernet, M., Messner, P., Sleytr, U.B., and Prieur, D. (1998). *Methanococcus infernus* sp. nov., a novel hyperthermophilic lithotrophic methanogen isolated from a deep-sea hydrothermal vent. *Int J Syst Bacteriol* **48**, 913−919.

Jogler, C., Wanner, G., Kolinko, S., Niebler, M., Amann, R., Petersen, N., Kube, M., Reinhardt, R., and Schüler, D. (2011). Conservation of proteobacterial magnetosome genes and structures in an uncultivated member of the deep-branching *Nitrospira phylum. Proc Natl Acad Sci USA* **108**, 1134−1139.

Jones, J.B., Bowers, B., and Stadtman, T.C. (1977). *Methanococcus vannielii*: Ultrastructure and sensitivity to detergents and antibiotics. *J Bacteriol* **130**, 1357−1363.

Jones, W.J., Leigh, J.A., Mayer, F., Woese, C.R., and Wolfe, R.S. (1983). *Methanococcus jannaschii* sp. nov., an extremely thermophilic methanogen from a submarine hydrothermal vent. *Arch Microbiol* **136**, 254−261.

Junglas, J., Briegel, A., Burghardt, T., Walther, P., Wirth, R., Huber, H., and Rachel, R. (2008). *Ignicoccus hospitalis* and *Nanoarchaeum equitans*: ultrastructure, cell–cell interaction, and 3D reconstruction from serial sections of freeze-substituted cells and by electron cryotomography. *Arch Microbiol* **190**, 395−408.

K

Käll, L., Krogh, A., and Sonnhammer, E.L. (2007). Advantages of combined transmembrane topology and signal peptide prediction - the Phobius web server. *Nucleic Acids Res* **35**, W429.

Kalmokoff, M.L., and Jarrell, K.F. (1991). Cloning and sequencing of a multigene family encoding the flagellins of *Methanococcus voltae*. *J Bacteriol* **173**, 7113−7125.

Kalmokoff, M.L., Jarrell, K.F., and Koval, S.F. (1988). Isolation of flagella from the archaebacterium *Methanococcus voltae* by phase separation with Triton X-114. *J Bacteriol* **170**, 1752−1758.

Kalmokoff, M.L., Koval, S.F., and Jarrell, K.F. (1992). Relatedness of the flagellins from methanogens. *Arch Microbiol* **157**, 481−487.

Kamiya, R., and Asakuro, S. (1976). Helical transformations of *Salmonella* flagella in vitro. *J Mol Biol* **106**, 167−186.

Kandler, O., and Hippe, H. (1977). Lack of peptidoglycan in the cell walls of *Methanosarcina barkeri*. *Arch Microbiol* **113**, 57−60.

Kandler, O., and König, H. (1985). Cell envelopes of Archaebacteria. *In* The Bacteria. A treatise on structure and function VIII Archaebacteria, eds. C.R. Woese and R.S. Wolfe. Academic Press: New York, NY, pp. 413–457.

Khursigara, C.M., Wu, X., and Subramaniam, S. (2008). Chemoreceptors in *Caulobacter crescentus*: Trimers of receptor dimers in a partially ordered hexagonally packed array. *J Bacteriol* **190**, 6805−6810.

Kireev, I.I., Novikova, T.M., Sheval', E.V., and Metlina, A.L. (2006). Structure of the intracellular part of the motility apparatus of halobacteria. *Microbiology* **75**, 306−311.

Klingl, A. (2011). Charakterisierung der Surface Layer Pyrit-oxidierender Mikroorganismen: Struktur, Funktion und Notwendigkeit der S-Layer Proteine in *Acidithiobacillus ferrooxidans* SP5/1 und *Metallosphaera sedula* TH2. *PhD thesis*. University of Regensburg. Regensburg, Germany.

Koerdt, A., Gödeke, J., Berger, J., Thormann, K.M., and Albers, S.-V. (2010). Crenarchaeal biofilm formation under extreme conditions. *PLoS one* **5**, e14104.

König, H., Rachel, R., and Claus, H. (2007). Proteinaceous surface layers of Archaea: Ultrastructure and biochemistry. *In* Archaea. Molecular and cellular biology, ed. R. Cavicchioli. ASM Press: Washington, DC, pp. 315–340.

Konisky, J., Lynn, D., Hoppert, M., Mayer, F., and Haney, P. (1994). Identification of the *Methanococcus voltae* S-layer structural gene. *J Bacteriol* **176**, 1790−1792.

Kostyukova, A.S., Gongadze, G.M., Polosina, Y.Y., Bonch-Osmolovskaya, E.A., Miroshnichenko, M.L., Chernyh, N.A., Obraztsova, M.V., Svetlichny, V.A., Messner, P., and Sleytr, U.B., et al. (1999). Investigation of structure and antigenic capacities of *Thermococcales* cell envelopes and reclassification of "*Caldococcus litoralis*" Z-1301 as *Thermococcus litoralis* Z-1301. *Extremophiles* **3**, 239−246.

Koval, S.F., and Jarrell, K.F. (1987). Ultrastructure and biochemistry of the cell wall of *Methanococcus voltae*. *J Bacteriol* **169**, 1298−1306.

Krogh, A., Larsson, B., Heijne, G. von, and Sonnhammer, E.L. (2001). Predicting transmembrane protein topology with a hidden markov model: Application to complete genomes. *J Mol Biol* **305**, 567−580.

Kupper, J., Marwan, W., Typke, D., Grunberg, H., Uwer, U., Gluch, M., and Oesterhelt, D. (1994). The flagellar bundle of *Halobacterium salinarium* is inserted into a distinct polar cap structure. *J Bacteriol* **176**, 5184−5187.

L

Laemmli, U.K. (1970). Cleavage of structural proteins during the assembly of the head of bacteriophage T4. *Nature* **227**, 680−685.

Lama, A., Kucknoor, A., Mundodi, V., and Alderete, J.F. (2009). Glyceraldehyde-3-phosphate dehydrogenase is a surface-associated, fibronectin-binding protein of *Trichomonas vaginalis*. *Infect Immun* **77**, 2703−2711.

Lane, D.J. (1991). 16S/23S rRNA sequencing. *In* Nucleic acid techniques in bacterial systematics, eds. E. Stackebrandt and M. Goodfellow. Wiley: Chichester, pp. 115–175.

Lapaglia, C., and Hartzell, P.L. (1997). Stress-induced production of biofilm in the hyperthermophile *Archaeoglobus fulgidus*. *Appl Environ Microbiol* **63**, 3158−3163.

Larkin, M., Blackshields, G., Brown, N., Chenna, R., McGettigan, P., McWilliam, H., Valentin, F., Wallace, I.M., Wilm, A., and Lopez, R., et al. (2007). Clustal W and Clustal X version 2.0. *Bioinformatics* **23**, 2947−2948.

Lenski, R.E., and Travisano, M. (1994). Dynamics of adaptation and diversification: a 10,000-generation experiment with bacterial populations. *Proc Natl Acad Sci USA* **91**, 6808−6814.

Lenski, R.E., Rose, M., Simpson, S., and Tadler, S. (1991). Long-term experimental evolution in *Escherichia coli*. I. Adaptation and divergence during 2,000 generations. *Am Nat* **138**, 1315−1341.

L'Haridon, S., Reysenbach, A.L., Banta, A., Messner, P., Schumann, P., Stackebrandt, E., and Jeanthon, C. (2003). *Methanocaldococcus indicus* sp. nov., a novel hyperthermophilic methanogen isolated from the Central Indian Ridge. *Int J Syst Evol Microbiol* **53**, 1931−1935.

Loose, J. (2009). Expression der Glutamatdehydrogenase von *Pyrococcus furiosus*. *Bachelor thesis*. University of Regensburg. Regensburg, Germany.

Lottenberg, R., Broder, C.C., Boyle, M.D., Kain, S.J., Schroeder, B.L., and Curtiss, R.3. (1992). Cloning, sequence analysis, and expression in *Escherichia coli* of a streptococcal plasmin receptor. *J Bacteriol* **174**, 5204−5210.

Ludwig, W., Strunk, O., Westram, R., Richter, L., Meier, H., Yadhukumar, Buchner, A., Lai, T., Steppi, S., and Jobb, G., et al. (2004). ARB: A software environment for sequence data. *Nucleic Acids Res* **32**, 1363−1371.

M

Makarova, K.S., Yutin, N., Bell, S.D., and Koonin, E.V. (2010). Evolution of diverse cell division and vesicle formation systems in Archaea. *Nat Rev Micro* **8**, 731−741.

Margolin, W. (2005). FtsZ and the division of prokaryotic cells and organelles. *Nat Rev Mol Cell Biol* **6**, 862−871.

Marwan, W., Alam, M., and Oesterhelt, D. (1991). Rotation and switching of the flagellar motor assembly in *Halobacterium halobium*. *J Bacteriol* **173**, 1971−1977.

Mayr, E. (1998). Two empires or three? *Proc Natl Acad Sci USA* **95**, 9720−9723.

Merz, A.J., So, M., and Sheetz, M.P. (2000). Pilus retraction powers bacterial twitching motility. *Nature* **407**, 98−102.

Mescher, M.F., Strominger, J.L., and Watson, S.W. (1974). Protein and carbohydrate composition of the cell envelope of *Halobacterium salinarium*. *J Bacteriol* **120**, 945−954.

Meyer, C. (2010). Die Fibers von *Ignicoccus hospitalis*: Ultrastruktur, Verankerung und molekularbiologische Untersuchungen. *PhD thesis*. University of Regensburg. Regensburg, Germany.

Moissl, C. (2004). Molekularbiologische und strukturelle Untersuchungen zur Biologie des neuartigen, kälteliebenden SM1 Euryarchaeons und seiner verschiedenen Lebens-gemeinschaften. *PhD thesis*. University of Regensburg. Regensburg, Germany.

Moissl, C., Rachel, R., Briegel, A., Engelhardt, H., and Huber, R. (2005). The unique structure of archaeal 'hami', highly complex cell appendages with nano-grappling hooks. *Mol Microbiol* **56**, 361−370.

Moore, B.C., and Leigh, J.A. (2005). Markerless mutagenesis in *Methanococcus maripaludis* demonstrates roles for alanine dehydrogenase, alanine racemase, and alanine permease. *J Bacteriol* **187**, 972−979.

Mukhopadhyay, B., Johnson, E.F., and Wolfe, R.S. (2000). A novel p_{H2} control on the expression of flagella in the hyperthermophilic strictly hydrogenotrophic methanarchaeaon *Methanococcus jannaschii*. *Proc Natl Acad Sci* **97**, 11522−11527.

Müller, D.W., Meyer, C., Gürster, S., Küper, U., Huber, H., Rachel, R., Wanner, G., Wirth, R., and Bellack, A. (2009). The Iho670 fibers of *Ignicoccus hospitalis*: A new type of archaeal cell surface appendage. *J Bacteriol* **191**, 6465−6468.

Murray, B.E., Singh, K.V., Heath, J.D., Sharma, B.R., and Weinstock, G.M. (1990). Comparison of genomic DNAs of different enterococcal isolates using restriction endonucleases with infrequent recognition sites. *J Clin Microbiol* **28**, 2059−2063.

N

Naas, T., Blot, M., Fitch, W.M., and Arber, W. (1994). Insertion sequence-related genetic variation in resting *Escherichia coli* K-12. *Genetics* **136**, 721−730.

Naas, T., Blot, M., Fitch, W.M., and Arber, W. (1995). Dynamics of IS-related genetic rearrangements in resting *Escherichia coli* K-12. *Mol Biol Evol* **12**, 198−207.

Näther, D.J. (2007). Untersuchung der Flagellen von *Pyrococcus furiosus*. *Ph.D. thesis*. University of Regensburg. Regensburg, Germany.

Näther, D.J., Rachel, R., Wanner, G., and Wirth, R. (2006). Flagella of *Pyrococcus furiosus*: Multifunctional organelles, made for swimming, adhesion to various surfaces, and cell-cell contacts. *J Bacteriol* **188**, 6915−6923.

Naumann, D. (2000). Infrared spectroscopy in microbiology. *In* Encyclopedia of analytical chemistry, ed. R.A. Meyers. John Wiley & Sons, Ltd.: Chichester, U.K., pp. 102–131.

Ng, S.Y.M., and Jarrell, K.F. (2003). Cloning and characterization of archaeal type I signal peptidase from *Methanococcus voltae*. *J Bacteriol* **185**, 5936−5942.

Ng, S.Y.M., Chaban, B., and Jarrell, K.F. (2006). Archaeal flagella, bacterial flagella and type IV pili: A comparison of genes and posttranslational modifications. *J Mol Microbiol Biotechnol* **11**, 167−191.

Ng, S.Y.M., Chaban, B., VanDyke, D.J., and Jarrell, K.F. (2007). Archaeal signal peptidases. *Microbiology* **153**, 305−314.

Ng, S.Y.M., Wu, J., Nair, D.B., Logan, S.M., Robotham, A., Tessier, L., Kelly, J.F., Uchida, K., Aizawa, S.-I., and Jarrell, K.F. (2011). Genetic and mass spectrometry analyses of the unusual type IV-like pili of the Archaeon *Methanococcus maripaludis*. *J Bacteriol* **193**, 804−814.

Ng, S.Y.M., Zolghadr, B., Driessen, A.J.M., Albers, S.-V., and Jarrell, K.F. (2008). Cell surface structures of Archaea. *J Bacteriol* **190**, 6039−6047.

Nickell, S., Hegerl, R., Baumeister, W., and Rachel, R. (2003). *Pyrodictium cannulae* enter the periplasmic space but do not enter the cytoplasm, as revealed by cryo-electron tomography. *J Struct Biol* **141**, 34−42.

Nicolaus, B., Manca, M.C., Ramano, I., and Lama, L. (1993). Production of an exopolysaccharide from two thermophilic Archaea belonging to the genus *Sulfolobus*. *FEMS Microbiol Lett* **109**, 203−206.

P

Pancholi, V., and Chhatwal, G.S. (2003). Housekeeping enzymes as virulence factors for pathogens. *Int J Med Microbiol* **293**, 391−401.

Pancholi, V., and Fischetti, V. (1992). A major surface protein on group A streptococci is a glyceraldehyde-3-phosphate-dehydrogenase with multiple binding activity. *J Exp Med* **176**, 415−426.

Peters, J. (1995). Tetrabrachion: A filamentous archaebacterial surface protein assembly of unusual structure and extreme stability. *J Mol Biol* **245**, 385−401.

R

Rachel, R., Meyer, C., Klingl, A., Gürster, S., Heimerl, T., Wasserburger, N., Burghardt, T., Küper, U., Bellack, A., and Schopf, S., et al. (2010). Analysis of the ultrastructure of Archaea by electron microscopy. *In* Methods in cell biology: Electron microscopy of model systems 96, ed. T. Möller-Reichert. Academic Press: New York, NY, pp. 47–69.

Rachel, R., Wyschkony, I., Riehl, S., and Huber, H. (2002). The ultrastructure of *Ignicoccus*: Evidence for a novel outer membrane and for intracellular vesicle budding in an Archaeon. *Archaea* **1**, 9−18.

Rieger, G., Rachel, R., Hermann, R., and Stetter, K.O. (1995). Ultrastructure of the hyperthermophilic archaeon *Pyrodictium abyssi*. *J Struct Biol* **115**, 78−87.

Rinker, K.D., and Kelly, R.M. (1996). Growth physiology of the hyperthermophilic Archaeon *Thermococcus litoralis*: Development of a sulfur-free defined medium, characterization of an exopolysaccharide, and evidence of biofilm formation. *Appl Environ Microbiol* **62**, 4478−4485.

Rudolph, C., Wanner, G., and Huber, R. (2001). Natural communities of novel Archaea and Bacteria growing in cold sulfurous springs with a string-of-pearls-like morphology. *Appl Environ Microbiol* **67**, 2336−2344.

S

Samatey, F.A., Imada, K., Nagashima, S., Vonderviszt, F., Kumasaka, T., Yamamoto, M., and Namba, K. (2001). Structure of the bacterial flagellar protofilament and implications for a switch for supercoiling. *Nature* **410**, 331−337.

Sanger, F., Brownlee, G.G., and Barrell, B.G. (1965). A two-dimensional fractionation procedure for radioactive nucleotides. *J Mol Biol* **13**, 373−IN4.

Sauer, K., Camper, A.K., Ehrlich, G.D., Costerton, J.W., and Davies, D.G. (2002). *Pseudomonas aeruginosa* displays multiple phenotypes during development as a biofilm. *J Bacteriol* **184**, 1140−1154.

Schießl, K. (2010). Die Glutamatdehydrogenase in *Pyrococcus furiosus*. Erzeugung von Knock-out Mutanten und spezifischen Antikörpern. *Diploma thesis*. University of Regensburg. Regensburg, Germany.

Schlesner, M., Miller, A., Streif, S., Staudinger, W., Muller, J., Scheffer, B., Siedler, F., and Oesterhelt, D. (2009). Identification of archaea-specific chemotaxis proteins which interact with the flagellar apparatus. *BMC Microbiol* **9**, 56.

Schopf, S. (2006). Interaktionen von *Pyrococcus furiosus* mit biotischen und abiotischen Oberflächen. *Diploma thesis*. University of Regensburg. Regensburg, Germany.

Schopf, S. (2011). Untersuchungen der Flagellen von *Pyrococcus furiosus*: Flagellenvermittelte Interaktionen, Ultrastruktur und Molekularbiologie. University of Regensburg. Regensburg, Germany.

Schopf, S., Wanner, G., Rachel, R., and Wirth, R. (2008). An archaeal bi-species biofilm formed by *Pyrococcus furiosus* and *Methanopyrus kandleri*. *Arch Microbiol* **190**, 371−377.

Segrest, J.P., and Jackson, R.L. (2010). Molecular weight determination of glycoproteins by polyacrylamide gel electrophoresis in sodium dodecyl sulfate. *In* Methods in enzymology : Cryo-EM, part B: 3-D reconstruction Volume 28, ed. G.J. Jensen. Academic Press: New York, NY, pp. 54–63.

Skerker, J.M., and Berg, H. (2001). Direct observation of extension and retraction of type IV pili. *Proc Natl Acad Sci USA* **98**, 6901−6904.

Stetter, K.O. (2006). History of discovery of the first hyperthermophiles. *Extremophiles* **10**, 357−362.

Stetter, K.O., König, H., and Stackebrandt, E. (1983). *Pyrodictium* gen. nov., a new genus of submarine disc-shaped sulphur reducing Archaebacteria growing optimally at 105°C. *Syst Appl Microbiol* **4**, 535−551.

Stetter, K.O., Thomm, M., Winter, J., Wildgruber, G., Huber, H., Zillig, W., Janekovic, D., König, H., Palm, P., and Wunderl, S. (1981). *Methanothermus fervidus*, sp. nov., a novel extremely thermophilic methanogen isolated from an Icelandic hot spring. *Zbl Bakt Hyg I Abt Orig C* **2**, 166−178.

Szabó, Z., Sani, M., Groeneveld, M., Zolghadr, B., Schelert, J., Albers, S.-V., Blum, P., Boekema, E.J., and Driessen, A.J.M. (2007a). Flagellar motility and structure in the hyperthermoacidophilic Archaeon *Sulfolobus solfataricus*. *J Bacteriol* **189**, 4305−4309.

Szabó, Z., Stahl, A.O., Albers, S.-V., Kissinger, J.C., Driessen, A.J.M., and Pohlschröder, M. (2007b). Identification of diverse archaeal proteins with class III signal peptides cleaved by distinct archaeal prepilin peptidases. *J Bacteriol* **189**, 772−778.

T

Takai, K., Nealson, K.H., and Horikoshi, K. (2004). *Methanotorris formicicus* sp. nov., a novel extremely thermophilic, methane-producing Archaeon isolated from a black smoker chimney in the Central Indian Ridge. *Int J Syst Evol Microbiol* **54**, 1095−1100.

Thoma, C., Frank, M., Rachel, R., Schmid, S., Näther, D.J., Wanner, G., and Wirth, R. (2008). The Mth60 fimbriae of *Methanothermobacter thermoautotrophicus* are functional adhesins. *Environ Microbiol* **10**, 2785−2795.

Thomas, N.A., Bardy, S.L., and Jarrell, K.F. (2001). The archaeal flagellum: a different kind of prokaryotic motility structure. *FEMS Microbiol Rev* **25**, 147−174.

Towbin, H., Staehelin, T., and Gordon, J. (1979). Electrophoretic transfer of proteins from polyacrylamide gels to nitrocellulose sheets: Procedure and some applications. *Proc Natl Acad Sci USA* **76**, 4350−4354.

Trachtenberg, S., Galkin, V.E., and Egelman, E.H. (2005). Refining the structure of the *Halobacterium salinarum* flagellar filament using the iterative helical real space reconstruction method: Insights into polymorphism. *J Mol Biol* **346**, 665−676.

Tripepi, M., Imam, S., and Pohlschröder, M. (2010). *Haloferax volcanii* flagella are required for motility but are not involved in PibD-dependent surface adhesion. *J Bacteriol* **192**, 3093−3102.

Typke, D., Nitsch, M., Möhrle, A., Hegerl, R., Alam, M., Grogan, D., and Trent, J. (1988). Structural studies of the flagellar filaments of some Archaebacteria. *J Phys Conf Ser* **93**, 379−380.

V

Vestergaard, G., Häring, M., Peng, X., Rachel, R., Garrett, R.A., and Prangishvili, D. (2005). A novel rudivirus, ARV1, of the hyperthermophilic archaeal genus *Acidianus*. *Virology* **336**, 83−92.

Voisin, S., Houliston, R.S., Kelly, J.F., Brisson, J.-R., Watson, D., Bardy, S.L., Jarrell, K.F., and Logan, S.M. (2005). Identification and characterization of the unique N-Linked glycan common to the flagellins and S-layer glycoprotein of *Methanococcus voltae*. *J Biol Chem* **280**, 16586−16593.

W

Wang, Y.A., Yu, X., Ng, S.Y.M., Jarrell, K.F., and Egelman, E.H. (2008). The structure of an archaeal pilus. *J Mol Biol* **381**, 456−466.

Weinberg, M.V., Schut, G.J., Brehm, S., Datta, S., and Adams, M.W.W. (2005). Cold shock of a hyperthermophilic Archaeon: *Pyrococcus furiosus* exhibits multiple responses to a suboptimal growth temperature with a key role for membrane-bound glycoproteins. *J Bacteriol* **187**, 336−348.

Weiss, R.L. (1973). Attachment of Bacteria to sulphur in extreme environments. *J Gen Microbiol* **77**, 501−507.

Weiss, R.L. (1974). Subunit cell wall of *Sulfolobus acidocaldarius*. *J Bacteriol* **118**, 275−284.

Whitman, W.B., and Jeanthon, C. (2006). *Methanococcales. In* The Prokaryotes. A Handbook on the Biology of Bacteria 3, ed. M. Dworkin. Springer: New York, NY, pp. 257–273.

Whitman, W.B., Boone, D.R., and Koga, Y. (2001). Order *Methanococcales. In* Bergey's Manual of Systematic Bacteriology. Volume One : The Archaea and the Deeply Branching and Phototrophic Bacteria 1, ed. G.M. Garrity. Springer: New York, NY, pp. 236–246.

Wieland, F., Paul, G., and Sumper, M. (1985). Halobacterial flagellins are sulfated glycoproteins. *Journal of Biological Chemistry* **260**, 15180−15185.

Wimmer, N. (2007). Expression und funktionelle Charakterisierung von Teilbereichen des archaeellen Flagellins FlaB2 aus *Pyrococcus furiosus. Diploma thesis.* University of Regensburg. Regensburg, Germany.

Wirth, R., Bellack, A., Bertl, M., Bilek, Y., Heimerl, T., Herzog, B., Leisner, M., Probst, A., Rachel, R., and Sarbu, C., et al. (2011). The mode of cell wall growth in selected archaea follows the general mode of cell wall growth in bacteria - An analysis using fluorescent dyes. *Appl Environ Microbiol* **77**, 1556−1562.

Woese, C.R. (2004). The archaeal concept and the world it lives in: A retrospective. *Photosynth Res* **80**, 361−372.

Woese, C.R. (2007). The Archaea: An invitation to evolution. *In* Archaea. Molecular and cellular biology, ed. R. Cavicchioli. ASM Press: Washington, DC, pp. 1–13.

Woese, C.R., and Fox, G.E. (1977). Phylogenetic structure of the prokaryotic domain: The primary kingdoms. *Proc Natl Acad Sci USA* **74**, 5088−5090.

Woese, C.R., Kandler, O., and Wheelis, M.L. (1990). Towards a natural system of organisms: Proposal for the domains Archaea, Bacteria, and Eucarya. *Proc Natl Acad Sci USA* **87**, 4576−4579.

Woese, C.R., Magrum, L.J., and Fox, G.E. (1978). Archaebacteria. *J Mol Evol* **11**, 245−252.

Y

Yu, N.Y., Wagner, J.R., Laird, M.R., Melli, G., Rey, S., Lo, R., Dao, P., Sahinalp, S.C., Ester, M., and Foster, L.J., et al. (2010). PSORTb 3.0: Improved protein subcellular localization prediction with refined localization subcategories and predictive capabilities for all Prokaryotes. *Bioinformatics* **26**, 1608−1615.

Yurist-Doutsch, S., Chaban, B., VanDyke, D.J., Jarrell, K.F., and Eichler, J. (2008). Sweet to the extreme: Protein glycosylation in Archaea. *Mol Microbiol* **68**, 1079−1084.

Z

Zach, F. (2009). Analyse von Glykoproteinen von *Pyrococcus furiosus. Diploma thesis.* University of Regensburg. Regensburg, Germany.

Zillig, W., Stetter, K.O., Schäfer, W., Janekovic, D., Wunderl, S., Holz, I., and Palm, P. (1981a). *Thermoproteales*: A novel type of extremely thermoacidophilic anaerobic Archaebacteria isolated from Icelandic solfataras. *Zbl Bakt Hyg I Abt Orig C* **2**, 205−227.

Zillig, W., Tu, J., and Holz, I. (1981b). *Thermoproteales*: A third order of thermoacidophilic Archaebacteria. *Nature* **293**, 85−86.

Zolghadr, B., Klingl, A., Koerdt, A., Driessen, A.J.M., Rachel, R., and Albers, S.-V. (2010). Appendage-mediated surface adherence of *Sulfolobus solfataricus*. *J Bacteriol* **192**, 104−110.

Zum Gelingen dieser Arbeit haben viele tatkräftig beigetragen. Mein besonderer Dank gilt…

… **Prof. Dr. Reinhard Wirth**, meinem Doktorvater, für die produktive Zusammenarbeit, für die hilfreichen Anregungen und (wissenschaftlichen) Diskussionen und für das Vertrauen in mich und meine Arbeit. Vielen Dank, dass Sie mir immer tatkräftig zur Seite standen und mich durch alle Höhen und Tiefen dieser Arbeit begleitet haben. Danke auch für die ständige Versorgung mit (Knoblauch-)Oliven.

… **Prof. Dr. Reinhard Rachel** für die theoretische und praktische Hilfe am EM und die Begeisterung an so mancher Aufnahme, die ich total normal fand. Vielen Dank für das stetige Interesse am Fortgang dieser Arbeit und für (spontane) Besprechungen, auch wenn der Terminkalender es eigentlich nicht zugelassen hat.

… **Prof. Dr. Gerhard Wanner** für die vielen einfach genialen Aufnahmen und das kritische Hinterfragen von Ansätzen. Vielen Dank für die Einladungen nach München, für Ihre hilfreichen Tipps bei der Bildbearbeitung und Postererstellung, die ich nicht als ‚pingelig' empfand, und für das leckere Essen. Danke auch an **seine Arbeitsgruppe** für die Präparationen und die herzliche Aufnahme.

… **Prof. Dr. Michael Thomm** für die Möglichkeit, diese Arbeit an seinem Lehrstuhl durchführen zu können.

… **Dr. Harald Huber** für die Zusammenarbeit zur Artbeschreibung von meinem ‚Baby', für viele nützliche Tipps und hilfreiche Diskussionen.

… **dem Elektronenmikroskopie-Team** für die Möglichkeit selbstständig am EM arbeiten zu können und die Hilfe bei auftretenden (Bedienungs-)Problemen. **Carolin Meyer** für das Hochdruckgefrieren und die Einbettung der Zellen. **Andreas ‚Flash' Klingl** für die Einführung am Ultramikrotom und die Gefrierätzungen. **Cornelia Niemann** für die Anleitung am Ultramikrotom bzw. der Erstellung von Ultradünnschnitten. **Thomas Heimerl** für die Rekonstruktion von FIB-SEM Daten mit Amira™.

… **Prof. Edward H. Egelman** für die Zusammenarbeit zur Rekonstruktion der archaeellen Flagllen.

… **Prof. Dr. Rainer Deutzmann** und **Eduard Hochmuth** für die Durchführung und Auswertung der MALDI-TOF-Analysen.

… **Prof. Hoi-Ying N. Holman** für das Anfertigen der SR-FTIR Aufnahmen und die Auswertung der Daten.

… **Thomas Hader** und **Konrad Eichinger** für die Fermentationen und dafür, dass ich jeder Zeit auf einen Plausch und/oder Kaffee vorbei kommen konnte.

… **PD Dr. Hans-Peter Klenk** für die Zusammenarbeit bei der Antragstellung zur Gesamtgenomsequenzierung von *M. villous*. **Evelyne Brambilla** für die experimentellen Tipps.

… **den Mitgliedern der Arbeitsgruppen Reinhard Wirth und Christine Moissl-Eichinger**, den Kellerkindern, für das super Arbeitsklima und die stetige Unterstützung beim Voranschreiten dieser Arbeit vor allem in den letzen Wochen. **Yvonne Bilek** für die viele Hilfe im Laboralltag und hin und wieder auch bei der Durchführung von Versuchen. **Dr. Christine Moissl-Eichinger** für ein offenes Ohr bei (experimentellen) Fragen, für die Erstellung des Stammbaums, und für die viele Aufmunterung. Chaka! **Alexander Probst** für die Datenaufzeinung am CLSM, für die Abwechslung und Ablenkung nicht nur an schlechten Tagen und für so manches (nicht fachliche) Gespräch. **Jenni Loose**, meiner Bachelorette, **Anna Auerbach, AlexAnder Mahnert, Vroni Wirth, Simone Schopf, Christina Sarbu** und allen **ehemaligen Kellerkindern** für die schöne gemeinsame Zeit im und außerhalb des Labors.

… **den Korrekturlesern dieser Arbeit**, die beim Ausmerzen kleiner und großer sprachlicher Fehler geholfen haben und sich die Zeit genommen haben, auch wenn die Fristen knapp waren.

… **allen Mitgliedern des Lehrstuhls**, für ihre (wissenschaftliche) Unterstüzung und die gemeinsamen Feiern und Ausflüge. **Gabi Leichtl** und **Elisabeth Nagelfeld** für ihre schnelle und unkomplizierte Hilfe bei organisatorischen Fragen. **Wolfgang Forster** für die Hilfe bei Computerproblemen, deren Lösung meist einfacher war als gedacht.

… **meinen Freunden** für die schönen, unvergesslichen Jahre in Regensburg und für die Vermittlung des bayerischen Lebensgefühls an einen ‚Preiß'.

… und nicht zuletzt **meinen Eltern Regina** und **Michael Bellack**, die mich auf meinem Weg in jeglicher Art unterstützt haben. Vielen dank für euren Rückhalt und die liebevollen Aufmunterungen. Meiner **Schwerster Stephanie** dafür, dass sie immer für mich da ist, auch wenn sie tausende von Kilometern entfernt ist.